Open Water Evaporation Estimation Using Ground Measurements and Satellite Remote Sensing: a case study of Lake Tana, Ethiopia

Alebachew Abreham

March, 2009

Open Water Evaporation Estimation Using Ground Measurements and Satellite Remote Sensing: a case study of Lake Tana, Ethiopia

by

Alebachew Abreham

Thesis submitted to the International Institute for Geo-information Science and Earth Observation in partial fulfilment of the requirements for the degree of Master of Science in Geo-information Science and Earth Observation, Specialisation: Integrated Water Shed Modelling and Management

Thesis Assessment Board

Prof. Dr. Z. Su	(Chairman)	Head, WRS Dept. ITC Enschede
Prof. Dr. W.G.M. Bastiaanssen	(External examiner)	Civil Eng. Dept. (TU Delft)
Dr. A.S.M. Gieske	(First supervisor)	WRS Dept. ITC, Enschede
Dr. Ir. C. van der Tol	(Second supervisor)	WRS Dept. ITC, Enschede

INTERNATIONAL INSTITUTE FOR GEO-INFORMATION SCIENCE AND EARTH OBSERVATION
ENSCHEDE, THE NETHERLANDS

Disclaimer

This document describes work undertaken as part of a programme of study at the International Institute for Geo-information Science and Earth Observation. All views and opinions expressed therein remain the sole responsibility of the author, and do not necessarily represent those of the institute.

Abstract

Lake Tana is the largest natural reservoir of fresh water resources in Ethiopia. It is the source of Blue Nile River and is located in the north-western part of the country. It has a surface area of 3000 km^2 with an elevation of 1786m above sea level. Water resources management in Lake Tana and its surroundings is an issue of high significance because of great socio-cultural, ecological and economical values.

Evaporation is one of the main components of the water budget of lakes. Accurate estimates of lake evaporation are necessary for water and energy budget studies, lake level forecasts, water quality surveys, water management and planning of hydraulic constructions. Evaporation from open water remains a difficult process to measure or estimate. The major source of difficulty is the fact that the required meteorological parameters are rarely measured over the water surfaces, and the thermal lag between the water and land surfaces renders the land-based measurements less effective in the parameterization of open water evaporation. The use of remotely-sensed data provides a means of obtaining useful information about the evaporating water surface.

This study examines open water evaporation losses from the lake by different climatic methods and remotely sensed spectral data. The long-term daily meteorological (1995-2007) data from the nearby station of the lake is used as well as the annual cycle of albedo on a monthly time steps produced from Terra MODIS satellite image products. In situ measurements of instantaneous energy balance components was collected from the surface of the lake using 3D sonic anemometer and four channel radiometer and also the temperature profile of the water during the field campaign to calibrate and validate remote sensing data analysis.

A daily evaporation map is produced from combination of in situ measurements and satellite remote sensing data (Terra MODIS) using the evaporative fraction approach. The average daily evaporation from the lake calculated for a cloud free day of 27^{th} of September 2008 is obtained as 4.94 mm/day with standard deviation of 0.20 mm/day.

The surface temperature exhibits a strong diurnal variability that cannot be captured from polar orbiting satellites that sample each location approximately twice a day. Geostationary satellites provide diurnal coverage, and allow derivation of the surface temperature cycle. In this study four channels and split-window algorithms are used to retrieve the surface temperature of the lake from MSG/SEVIRI images. The four channel method gives slightly better results than the split window algorithm.

Key Words: Lake Tana, Evaporation, Energy balance, Remote sensing (RS), MODIS, MSG, Surface temperature

Acknowledgements

First of all I thank the almighty God whose grace and blessing have sustained me for all these years. The completion of this study has been made possible through the love, support, sacrifice and encouragement of many to whom I shall be eternally indebted.

First and foremost I would like to gratefully acknowledge the ITC capacity building programme for granting me the opportunity to study at ITC. I wish also to extend my gratitude to my government and my organization Bahir Dar University, Engineering Faculty for giving me long leave of absence.

I am deeply indebted to my first supervisor Dr. A.S.M. Gieske for the supervision, encouragement and guidance he has provided me throughout my research. His critical comments and helpful guidance gives me a chance to explore further. I have learned a lot from him. I have benefited not only from his academic advice and supervision but also he helped me to cope up with my family problem through advice and encouragement. He is unforgettable.

My deepest gratitude goes to my second supervisor Dr. Ir. C. van der Tol. His valuable comments, kind support and encouragement gave me strength right from the inception of the topic to the last minute of the research upon our discussions and meetings.

I like to extend my appreciation to the program director ir. Arno Van Lieshout for his kindness and understanding about my family problems to extend my stay beyond the course duration period.

I would like to thank my lecturers for giving me all the basics of science and their courage to help everybody. My sincere thanks also goes to every staff in the program and the institute.

I gratefully acknowledge to all offices and personalities who have given me data for my study. Ministry of water resources, Ethiopian Meteorological Services, Bahir Dar University, Engineering Faculty are some of them that I need to mention.

I would like to extend my appreciation to my course mates for their support, socialization and helping to each other. I will not forget the Ethiopian fellow friends for their support and encouragement in times of pressure and stress.

Special thanks to my beloved sister Alem (Titi) for your advice, encouragement and prayer. I owe a great deal for the spiritual support you gave me.

Last but not least, my everlasting gratitude goes to my loving mother, family, relatives and friends who always encourage me and wish my success.

Alexhydro81@gmail.com

Table of contents

List of figures

List of tables

1. Introduction

1.1. Background

The most accessible water available for human consumption and the ecosystems are contained in lakes and rivers. The volume in these water bodies corresponding to 0.27% of the global fresh water and only 0.008% of the earth water budget (Chow et al., 1988). Being a scarce resource strained by computing demands it has become crucial to develop and improve the techniques to serve the temporal and spatial variations in water volumes of lakes, rivers and wetlands. Quantification of hydrological fluxes, including evaporation, is very important to address issues related to water quality, recreations, and ecological processes.

Evaporation is one of the largest components of the water budget of lakes. Evaporation is also one of the main components of the energy budget of lakes and perhaps the most difficult (along with the sensible heat flux) to estimate. Accurate estimates of lake evaporation are necessary for water and energy budget studies, lake level forecasts, water quality surveys, water management and planning of hydraulic constructions. Moreover, with the recent changes in climate, and the relationship between variations in climate and lake size fluctuations, a method for estimating evaporation rates under different climate regimes is required.

For management of lake water volumes a proper assessment of different component of the hydrological cycle is very important. An accurate measurement of evaporation is required as part of a long-term study of hydrological and ecological processes on the lake. Therefore in this study one of the components of the water balance, evaporation from the lake is addressed.

1.2. Statement of the problem

Water resources management in Lake Tana and its surroundings is an issue of high significance because of great socio-cultural, ecological and economical values. Under Nile Basin Initiative, the Eastern Nile Committee of Ministers have agreed to initiate a number of projects in irrigation/drainage, watershed development, flood preparedness and early warning and power interconnection in a fast track mode. In addition the Ministers are also looking for opportunities for a large multi-purpose development. Some of the fast track projects in Ethiopia focus on the Lake Tana region and its surrounding environment. However the Lake Tana Water balance is not well understood. This is a source of uncertainty to the sustainable development and usage of the limited storages. Therefore it is very important to understand and study different components of the lake water balance.

Research on lake evaporation is needed because empirical methods to estimate evaporation are not necessarily correct. The uncertainty related to various empirical methods can be best evaluated by comparison with a physically based solution such as the energy balance method. On the other hand one of the most important parameters which control the physical and chemical processes in lake is

surface temperature of the water. However there are no any monitoring or continuous measurements of water temperature for Lake Tana.

1.3. Previous studies

Previous studies have been conducted to estimate evaporation from the land and water body of the Tana basin. However, due to lack of sufficient historical data and well established meteorological stations the figures published by different authors are not reliable. Abeyou (2008) estimated the evaporation from the lake using Penman open water approach, similarly Kebede et al. (2006) used the same approach to estimate the evaporation from the lake. However the data he took for shortwave radiation calculation is from Addis Ababa which is 565km far away from the lake. Remote sensing studies of Tana-Beles sub basins conducted by WaterWatch (2006) under Nile basin initiative project presented an annual and monthly evaporation of the lake. In the hydrological study of the Tana-Beles sub-basin by SMEC (2007) the evaporation from the lake estimated using Penman and energy balance approaches. However most of the previous studies on the lake were based on the meteorological data on the land surface but also the empirical formulas and constants were adopted without calibration. As a result there is uncertainty and inconsistency with regard to the estimation of lake evaporation.

1.4. Objectives and research questions

The main objective of the study is to estimate open water evaporation from the lake using satellite remote sensing data combined with in situ measurements.

The specific objectives are:

- To understand and estimate turbulent heat flux above the lake.
- To calculate the annual cycle of albedo on a monthly time step.
- To make a comparison between different methods for open water evaporation estimation.
- To retrieve surface temperature of the lake from remote sensing at high temporal scale and validate with in situ measurements.

In order to achieve the objectives of the study it is important to address the following questions:

- How large is the contribution of the water heat flux in the energy balance of the lake?
- How does the surface temperature of the lake change during day time?
- Is there spatio-temporal variability of albedo on the lake?
- How sensitive are the meteorological parameters on lake evaporation estimation?

1.5. Hypothesis

- The daytime sensible heat flux above the lake is less than 10% of the net radiation.

1.6. Thesis outline

The focus of this study is to make use of remote sensing observations combined with ground or in situ measurements for the estimation of open water evaporation.

Chapter two describes the literature review and discusses the principle of open water evaporation and the available methods for its estimation. The contributions of satellite remote sensing in hydrological studies as well as direct method of measuring turbulence heat flux are presented in this chapter.

Chapter three describes the characteristics of the study area with respect to its geographic location, climate, hydrological setting and drainage.

The fourth chapter discusses the instrumentation and data collected from the field work. The fifth chapter briefly describes the satellite imagery used and its pre-processing.

The methodology applied to fulfil the general and specific objectives of the study is discussed under chapter six.

Data processing, discussion and presentation of the result for microclimatological, in situ and remote sensing data are described in chapter seven and eight respectively.

Conclusions and recommendations are presented in chapter nine.

2. Literature review

2.1. Principles of evaporation processes

Evaporation is the primary process of water transfer in the hydrological cycle. Water is transformed into vapour and transported to the atmosphere. Evaporation plus transpiration from a vegetated surface with unlimited water supply is known as potential evaporation or potential evapotranspiration (PE) and it constitutes the maximum possible rate due to the prevailing meteorological conditions. Thus PE is the maximum value of the actual evaporation (E) and PE is equal to E when water supply is unlimited.

Actual daily evaporation is the amount of water which is evaporated on a normal day which means that if for instance the soil runs out of water, the actual evaporation is the amount of water which has been evaporated, and not the amount of water which could have been evaporated if the soil had had an infinite amount of water to evaporate. Because of the variability of region and seasons, water managers who are responsible for planning and adjudicating the distribution of water resources need to have a thorough understanding of the evapotranspiration process and knowledge about the spatial and temporal rates of evapotranspiration.

With respect to evaporation, open water bodies are quite different from land surfaces. According to the study in Lake Elephant Butte, USA (Eichinger et al., 2003), the solar energy penetrates the water to depths of as much as 30 m in clear water, somewhat less in turbid water, and is stored throughout the water column. The water column is mixed by surface motion and becomes the source of energy that drives evaporation. Because of the large heat storage capacity of water ($1x10^6$ Jm^{-3}), and the fact that water is approximately 1000 times more dense than air, the temperature of deep, clear, water bodies does not change considerably throughout the day when compared to the atmosphere.

The various methods for estimating evapotranspiration have been developed for specific surface and energy –exchange situation determined by the following conditions:

- Types of surface
- Availability of water
- Stored energy use
- Water advected energy use

Additional considerations in choosing a method for use in a given circumstance are:

- The purpose of the analysis (determination of the amount of evapotranspiration that has actually occurred in a given situations, incorporating in a hydrologic model, reservoir design, general water-resource assessment, etc.)
- The available data (particularly meteorological parameters measured and weather measurements were made at the area of interest or are estimated regional values)
- The time period of interest (hour, day month, year, climatic average).

2.2. Estimation of open water evaporation

In natural water bodies, water-advected heat and change in heat storage may play a substantial role in the energy balance. The magnitude of these components in a particular case depends in large part on the area, volume, and residence time of water in the lake relatively to the time period of the analysis. Because of available importance of these non-meteorological factors in the energy balance, it is not generally possible to develop equation for predicting the evaporation for a particular open water body such as a lake from meteorological data alone. In order to develop general methods for estimating evaporation from surface –water bodies, hydro-meteorologists have formulated the theoretical concepts of free-water evaporation: evaporation that would occur from an open water- surface in the absence of advection and changes in heat storage and which thus depends only on regionally continuous meteorological or climatic conditions. Lake evaporation is determined by adjusting mapped or computed free-water evaporation to account for advection and heat-storage effects in a given actual water body.

According to Dingman (2002), depending on the availability, accuracy and cost of the data it is possible to estimate open water evaporation using:

- Water-balance approach
- Mass-transfer approach
- Eddy- correlation approach
- Energy-balance approach
- Penman or combination approach.
- Pan-evaporation approach.

Yet evaporation from open water remains a difficult process to measure or estimate. The major source of difficulty is the fact that the required meteorological parameters are rarely measured over the water surfaces, and the thermal lag between the water and land surfaces renders the land-based measurements ineffective in the parameterization of open water evaporation. The use of remotely-sensed data provides a means of obtaining useful information about the evaporating water surface; however, an appropriate formulation of the transfer processes occurring in the advective boundary layer is required.

Granger and Hedstrom (2005) showed that lake evaporation is largely uncoupled from (or unsynchronized with) the land surface evapotranspiration. The land surface processes follow closely the pattern of energy supply, the partitioning of the net radiation is straightforward; the soil heat flux tends to be relatively small for most situations and the turbulent fluxes of sensible and latent heat, for the most part, behave in a similar manner. The partitioning of energy at a lake surface, on the other hand, is more complex. Because of radiation penetration, heat storage effects could be enormous (Mobley, 1994). The turbulent fluxes of sensible and latent heat are not necessarily in phase with the energy supply, but are governed by the gradients of temperature and humidity in the boundary layer. These gradients are controlled both by water surface temperatures (affected by radiation and intermittent mixing of the water) and by the processes occurring at the upwind land surface (heating of the air and evapotranspiration). For these reasons, land surface data alone are insufficient to parameterize the lake evaporation.

2.3. Application of remote sensing in hydrological studies

The extraction of data from remotely sensed images has tremendously increased in the last three decades. It has also increased our understanding of the temporal and spatial variation of the retrieved information. Retrieval of data like sea surface and land surface temperatures from radiances leaving the earth's surface (signatures from the thermal infrared regions of the electromagnetic radiation) and measured on sensors on board satellites are good examples of this aspect.

Remote sensing techniques provide a means of monitoring and measuring hydrological state variables over large areas. And it has become a powerful tool in its advantage of capturing spatial as well as temporal distribution of the variables within practical accuracy. Hydrologic variables such as rainfall and evaporation, which are used as major input components of hydrological analysis for water assessment can be estimated or measured directly or indirectly by the use of remote sensing systems and techniques, supplementing the already existing familiar method of estimation and measurements (Maidment, 1993)

Remote sensing is probably the only technique that can provide representative measurements of several relevant physical parameters at scales from a point to the whole globe. Techniques using remote sensing information to estimate atmospheric turbulent fluxes are therefore essential when dealing with processes that cannot be represented only by point measurements. In developing remote sensing algorithms for the estimation of atmospheric turbulent fluxes, two basic physical principles, the conservation of energy and turbulent transport, must be considered. The former is the basis of the energy balance approach, and the major challenge is the ability to determine the various physical quantities involved with the required accuracy. The rationale behind the energy balance approach is that evaporation is a change of state of water by demanding a supply of energy for vaporization. The whole problem then reduces to determine all other sources and sinks for energy such as to leave evaporation as the only unknown. The latter recognizes the importance of wind in transporting vapour away from the evaporating surface and, when successful, providing a direct estimate to evaporation. This is often called the aerodynamic approach and employs, typically, gradients of wind velocity, temperature, and water vapour density in the near-surface atmosphere where the measurements of these gradients are available. Since the energy budget (i.e., available energy to the surface less the soil or water heat flux) in the energy balance approach needs to be distributed between sensible heat and latent heat fluxes, which involves, again, the principle of turbulent transport, a complete treatment of both the conservation of energy and turbulent transport processes becomes necessary for developing relevant remote sensing algorithms for these fluxes. Currently there are many surface energy balance (SEB) algorithms which have been developed by different authors (Bastiaanssen et al., 1998a; Bastiaanssen et al., 1998b; Su, 2002) and others. Most of the algorithms make use of remote sensing data combined with ancillary ground measurements for estimation of surface energy balance components.

2.4. Eddy covariance system

Flux can be defined as an amount of a quantity that passes through a closed surface per unit of time and area. If net flux is away from the surface, the surface may be called a source. For example a lake surface is a source of water released into the atmosphere in the process of evaporation. If the opposite is true, the surface is called a sink. For example, a green canopy may be a sink of CO_2 during daytime, because green leaves would uptake CO_2 from the atmosphere in the process of photosynthesis.

Air flow can be imagined as flow of numerous rotating eddies. Each eddy has three 3D components, including vertical movement of the air. The situation looks chaotic at first, but these components can be measured from the tower. The physical meaning of the eddy covariance is that one physical point on the tower, at time1, eddy1 moves parcel of air c_1 down at the speed w_1. Then, at time2, eddy2 moves parcel c_2 up at the speed w_2. Each parcel has a concentration, temperature, and humidity. If these factors, along with the speed are known, we can determine the flux. For example, if one knew how many molecules of water went up with eddies at time1, and how many molecules went down with eddies at time2, at the same point, one could calculate the vertical flux of water at this point over this time. So, vertical flux can be presented as a covariance of the vertical wind velocity and the concentration of the quantity studied.

Eddy covariance method calculates only turbulent vertical flux, involves a lot of assumptions, and requires high-end instruments. On the other hand, it provides nearly direct flux measurements if the assumptions are satisfied. Some of these assumptions depend on the proper site selection and experimental setup (Gieske, 2006; Kaimal and Finnigan, 1994).

Major assumptions in eddy covariance techniques:

- Measurements at a point can represent footprint area
- Measurements are done inside the boundary layer of interest
- Fetch/footprint is adequate – fluxes are measured only at area of interest
- Flux is fully turbulent – most of the net vertical transfer is done by eddies
- Terrain is horizontal and uniform: average of fluctuations is zero; density fluctuations negligible; flow convergence & divergence negligible
- Instruments can detect very small changes at very high frequency

Measurements are of course never perfect, because of assumptions, instrumental problems, physical phenomena, and specifics of the particular terrain. As a result, there are a number of potential flux errors as explained by different authors (Schotanus et al., 1983; Twine et al., 2000) and presented as follows:

- Time response errors; occur because instruments may not be fast enough to catch all the rapid changes that result from the eddy transport.
- Sensor separation error; happens because of physical separation between the places where wind speed and concentration are measured, so covariance is computed for parameters that were not measured at the same point.

- Error due to spikes and noise; high frequency instantaneous data will have occasional spikes due to both electronic noise and some physical reasons (such as rainfall, birds or insects).
- Error due to unlevelled instrumentation: Sonic anemometers are used to determine the vertical fluxes of momentum and scalars in the atmospheric surface layers. In practice the coordinate systems of the sonic anemometers and the surface will not be perfectly aligned such that a tilt –correction for these small deviations of the anemometer coordinates is needed. These options are available; (i) to use known (e.g. measured) angles, (ii) to impose requirements on the means and stresses with an averaging period, (iii) to assume that the mean flow over a certain period, as observed by the sonic, is in a plane parallel to the surface (planner fit) method. The reader can refer more on coordinate rotation especially 2D coordinate transformation approach as explained by Gieske (2006)
- Error due to humidity fluctuations; sonic correction applies to a sensible heat flux measured with sonic anemometer - thermometers. It compensates for humidity fluctuations and momentum flux affecting sonic temperature measurements.

In the measurement of eddy fluxes it is generally recommended to sample at a rate twice the frequency of physical significance of the data to avoid aliasing. Sampling at a rate of 10 or 20 Hz is usually adequate for most land applications, while higher frequencies may be required for airborne applications and in special circumstances (e.g., at very low heights).

The minimum essential requirements for Eddy Covariance instruments include the following: instruments need to sample fast enough to cover all required frequency ranges, while at the same time, they need to be very sensitive to small changes in the quantities of interest; instruments should not break large eddies by having a bulky structure, and should be smooth enough to measure well at low heights; they also should not average small eddies by using large sensing volumes.

Flux data quality control

Removing bad data is an important part of the data quality control process. It ensures that results do not have a bias or errors due to some obvious or common reasons. As a first step, bad data are usually removed for one of the following causes: instrument malfunctions, processing/mathematical artefacts, ambient conditions not satisfying Eddy Covariance method, winds are not from the footprint of interest, and heavy precipitation. In general, however, the quality control procedure is very much a site-specific and instrument-specific activity (Foken and Wichura, 1996) , except for these common steps. Thus, it is important not to overdo bad data removal at one study site based on past experience with a different study site.

For example, the tolerance thresholds for sensible heat flux data will differ greatly between an open-water flux measurement, (which will have generally small sensible heat fluxes), and a desert measurement that has high heat fluxes. Thus, applying criteria developed for open water fluxes would probably eliminate many good data points if applied to measurements taken over the desert.

3. Description of the study area

3.1. General

Lake Tana sub-basin is part of the Blue Nile basin in Ethiopia. It comprises Lake Tana which has a surface area of 3000 km^2 with an elevation of 1786m above sea level and the surrounding sub-basins abutting the lake. The lake is fed by over 40 rivers and streams flowing from the Simien Mountains to the north, the large central plateau to the east and the gentler sloping land to the west. An important development to improve management of Lake Tana water resource includes the construction of the water level regulation weir at the outlet of the Lake in 1996. The weir enables to regulate the outflow of water for the Tis Abbay I and II hydroelectric power plant some 32km downstream of Lake Tana. Some details of Lake summarized as in table 2.1.

Table 3-1: Facts and figures of Lake Tana

No.	Description	Data
1	Location	12° 00'N, 37°15'E
2	Altitude	1786m amsl
3	Surface area	Approximately 3000 km^2
4	Catchment area	Approximately 15000 km^2
5	Depth	7.2m mean and 14m maximum
6	Volume	Approximately 28 km^3 at 1786m
7	Maximum length	84 km
8	Maximum width	64 km
9	Major influent rivers	Gilgel Abbay, Ribb, Kelti,Gumara and Megech
10	Effluent rivers	Abbay (Blue Nile) River

Lake Tana sub-basin is characterized by enormous potential for development of irrigated agriculture, hydropower, tourism, bio-diversity and recreations. For this reason, it is one of the richest sub-basin concerning water resource.

3.2. Location and accessibility

Lake Tana basin is found in North West part of Ethiopia in Amhara administrative region covering eight Woreda regions (smaller administrative units). Dembia and Gondar Zuria in the northern part of the sub-basin; Libo Kemkem, Fogera, Farta and Dera in the eastern part of the basin, Achefer and Alefa-Bechigne on the western part and with Bahir Dar Zuria on the southern part of the basin.

One major road originating from Addis Ababa passes across the basin connecting the major cities/towns namely Merowi, Wetet Abbay, Bahir Dar, Woreta, Addis Zemen and Gondar. This Sub-basin can also be accessed by another secondary road that originates from Weldiya passing through the towns Debre Tabor and Nefas Mewcha and joins the main road in Jiggna. Two International airports are located inside this basin, i.e. in Bahir Dar and Gondar Cities.

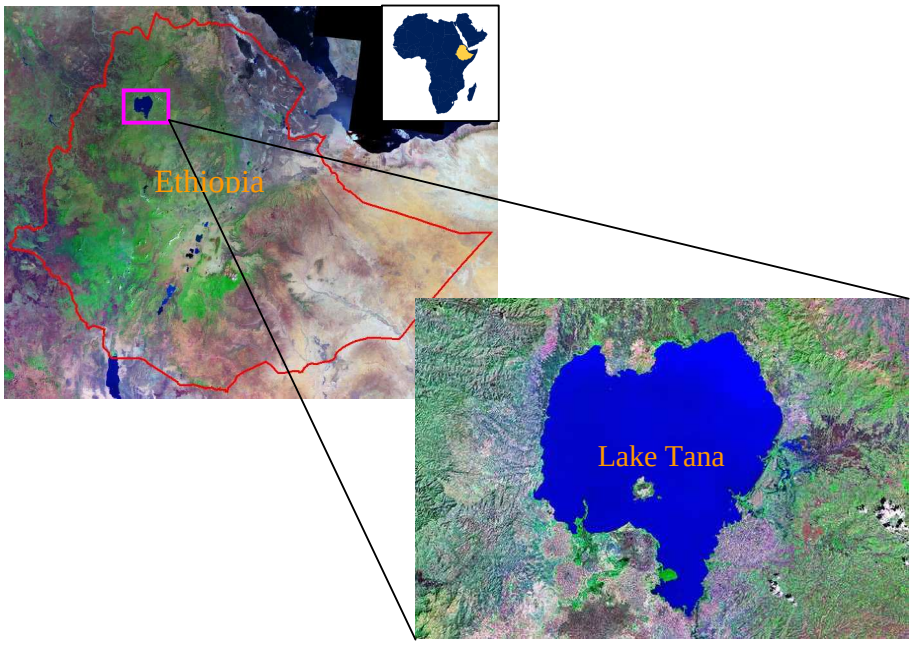

Figure 3-1: Location of the study area, Lake Tana (false colour composite of LANDSAT7 image, October 2003)

3.3. Climate of the study area

Based on the rainfall pattern, the year is divided into two seasons: a rainy season mainly centred on the months of June to September, and a dry season from October to March. In the southern parts of the basin the months of April and May are an intermediate season where minor rains often occur. Of the total annual rainfall, 70% to 90% occurs in the June to September rainy season. There is a high spatial variation of rainfall within the basin. The mean annual rainfall at Bahir Dar (south portion of the basin) is 1450mm and 1050 mm at Gondar Air Port meteorological station (northern portion). Rainfall distribution, both in time and space, decreases northwards in the basin. The weighted mean annual rainfall depth over the basin is estimated to be 1341.6 mm.

According to the study by Yohannes (2007) the spatial variation of temperature is fairly constant in the middle and upper part of the catchment which ranges within the limits of 19°C to 20°C. On the other hand, a small portion with about 10% by area at the lowest most part of the basin is observed to have a higher temperature record with average value of 23°C. Total weighted basin average temperature is estimated to 20°C. The average temporal variation ranges from 7.5°C down to 3°C within a year as we go to the southern portion of the sub-basin. The mean annual relative humidity (1994–2004) at Bahir Dar is 58% and Gondar is 52.7% therefore the sub-basin is characterized as humid climate.

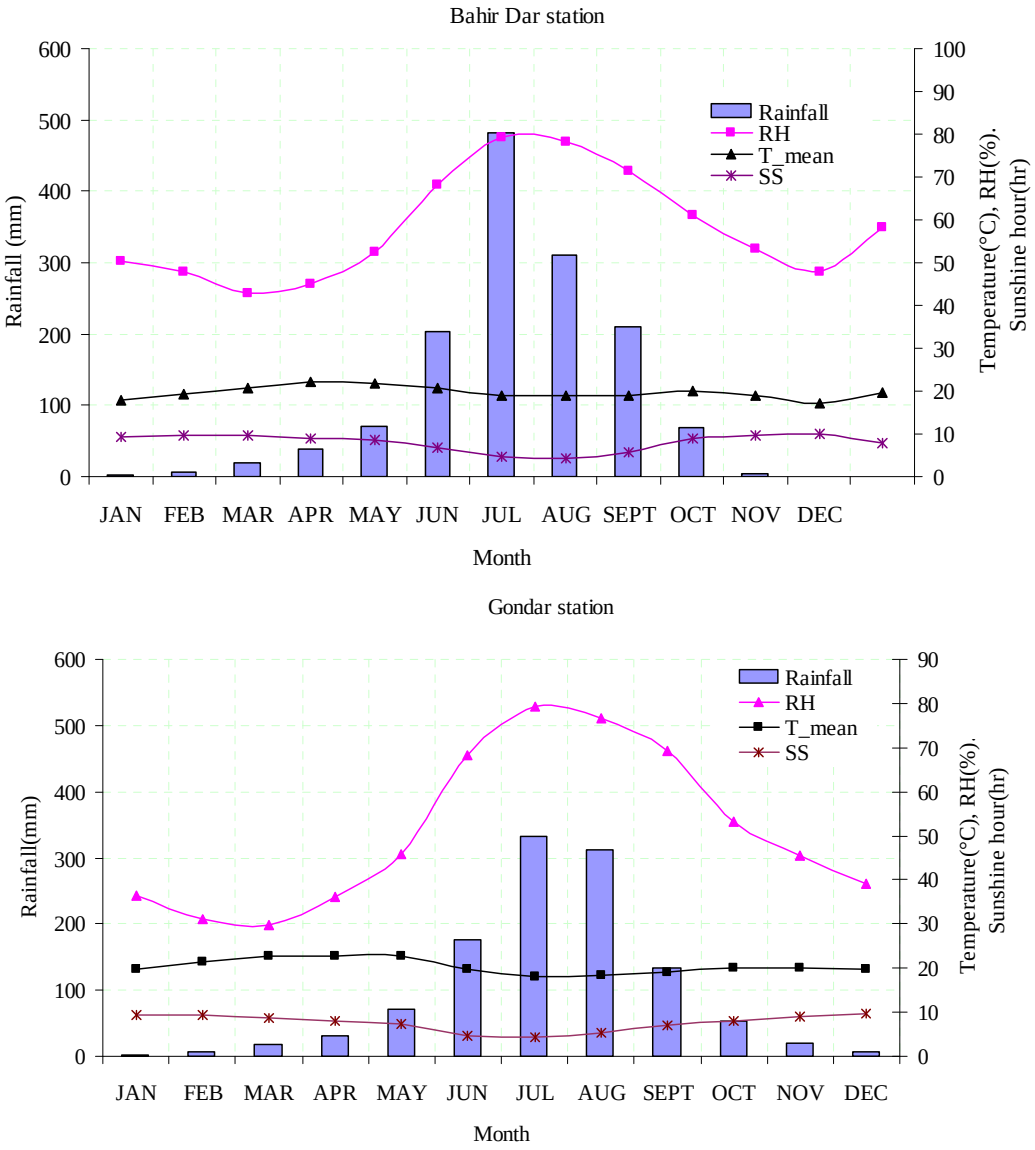

Figure 3-2: Long-term average meteorological observations at Bahir Dar and Gondar stations

3.4. Hydrological setting of the area

The lake has more than 40 tributary rivers, but the major rivers feeding the lake are Gilgel Abbay from the south, Ribb and Gumara from the east and Megetch river from the north, while there are no large rivers that flows from the western side of the Lake. According to Kebede et al.(2006) those four major rivers contribute 93% of the lake inflow. The water level of the lake rises gradually during the rainy season to reach its maximum level in September at the end of rainy season, after which it slowly falls to reach its minimum water level in June. The annual water level variation is approximately 1.6m, while the historical maximum water level was 1788 amsl (September 21, 1998) and minimum water level 1784 amsl (June 30, 2003) as reported by Yohannes (2007). The outflow from the lake joins the head of the Blue Nile. The natural annual outflow from the lake ranges from a minimum of 1075Mm^3 (in 1984) to maximum of 6181Mm^3 (in 1964) with an average of 3732 Mm^3 (from 1976-2006).

Figure 3-3: Lake Tana basin (source: Ethiopian ministry of water recourses)

3.5. Lake bathymetry

Bathymetry is the measure of the depth of water bodies from the water surface. Early techniques used pre-measured heavy ropes or cable lowered over a ship's side. The data to make bathymetric maps this days typically comes from an echo-sounder mounted beneath or over the side of boat, sending a beam of sound downward at the seafloor or from remote sensing systems. The amount of time it takes for the sound or light to travel trough the water, bounce off the seafloor, and return to the sounder makes it possible to determine the depth to the lake's bottom. The first bathymetric survey of the lake was made in 1937 by Italian researchers (Morandini, 1940) and the lake area was estimated to be 3156 km^2 and its elevation was quoted as 1829m amsl. In 2006 a bathymetry survey was conducted by Kaba (2007) and later Abeyou (2008) has modified the bathymetry survey of Kaba by using some additional control points and found out the surface area of the lake varies between 3000-3150 km^2.

4. Instrumentation and data availability

4.1. General

Hydro-meteorological data are the main input to study the water resources potential of an area for operational and planning purposes. As part of my research work a field campaign was carried out from September 04 to October 02/2008. The field work and its associated activities can be explained in two phases. The first phase was historical data collection from different ministries and offices. The second phase mainly consisted of in situ measurements of different parameters and variables.

4.2. Historical data

Hydro-meteorological data was collected from the Ministry of Water Resources and National Meteorological Service. The stream flow data consists of all gauged catchments in Lake Tana basin. Two stations (Bahir Dar and Gondar) were selected to collect the meteorological data. These stations are near the lake and are also class I stations. The data collected are:

- Rainfall
- Maximum and minimum temperature
- Relative humidity
- Wind speed
- Sunshine hours
- Piche evaporation

The description of those data are shown in appendix D

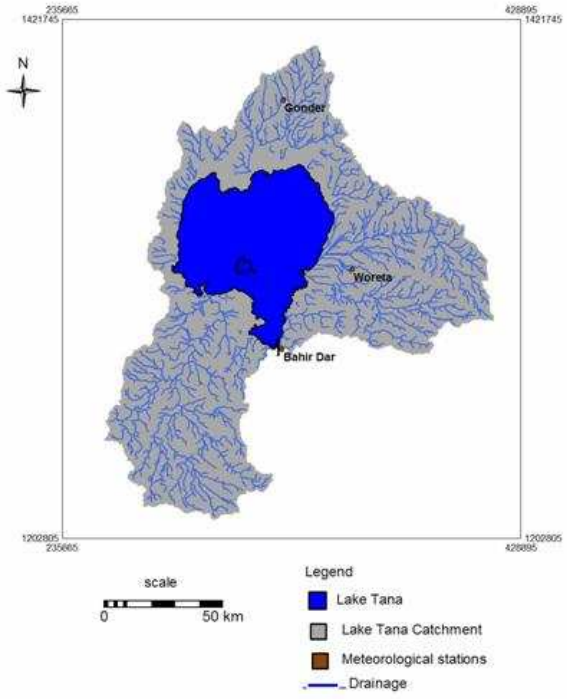

Figure 4-1: Meteorological stations around Lake Tana

4.3. Automatic weather data

Recently an automatic weather station was installed near Woreta about 20 km to the shore of the lake by Dr. A.S.M. Gieske and Dr.Ing. T.H.M. Rientjes (ITC) in June 2008 (Temesgen, 2009). This favourable condition encourages the ongoing research in the basin. The parameters that are measured on the weather station are:

- Air temperature
- Relative humidity
- Wind speed
- Water content and temperature profile of the soil at three depth
- Solar radiation

The description of those data are shown in appendix D

4.4. In situ measurement

Instantaneous measurements of eddy flux and radiation were carried out on the land surface as well as on the lake during the field campaign. But also air temperature, relative humidity and temperature profile on the lake was collected.

4.4.1. Instruments used

In situ measurements on the land and water surface were collected with different equipments. The description of the instruments is presented as follows:

i. Radiation sensors:

The radiation sensor used during data collection was CNR1. The CNR1 (Kipp and Zonen, Delft, Holland) net radiometer is intended for the analysis of the radiation of solar and far infrared radiation. The most common application is the measurement of net (total) radiation at the earth's surface. The CNR1 design is such that both the upward-facing and downward facing instrument measure the energy that is received from the whole hemisphere (180 degrees field of view). The output is expressed in Wm^{-2}. The spectral range that is measured is roughly from 0.3 to 50 μm. This spectral range covers both the solar Radiation, 0.3 to 3 μm, and the far infrared radiation, 5 to 50 μm.

The design of CNR1 is such that solar radiation and far infrared radiation are measured separately. Solar radiation is measured by two CM3 pyranometers, one for measuring incoming solar radiation from the sky, and the other, which faces downward, for measuring the reflected solar radiation. From these two pyranometers, albedo, the ratio of reflected and incoming radiation, can also be determined. Far infrared radiation is measured by two CG3 pyrgeometers, one for measuring the far infrared radiation from the sky, the other from the earth's surface.

Figure 4-2: CNR1 net radiometer sensor (source: Campbell scientific users manual)

ii. Eddy Flux sensors:

Eddy flux measurements require very sophisticated instrumentation, because turbulent fluctuations happen very quickly; changes in concentration, density or temperature are small, and need to be measured very fast and with great accuracy. The instrument used during the field campaign was CSAT3.

The CSAT3 is a three-dimensional sonic anemometer. It measures wind speed and the speed of sound on three non-orthogonal axes. From these measurements, orthogonal wind speed and sonic temperature can be computed. Errors caused by wind blowing normal to the sonic path have to be corrected before the wind speed is transformed into orthogonal coordinates. The three wind components are defined by a right handed orthogonal coordinate system. In general, point the anemometer into the prevailing wind to minimize the amount of data that is contaminated by the anemometer's arms and other supporting structures.

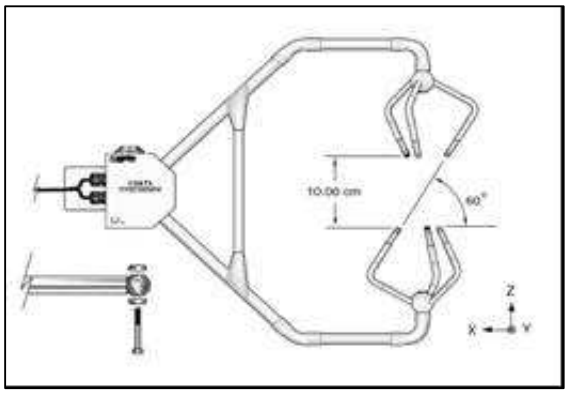

Figure 4-3: CSAT, 3-D sonic anemometer (source: Campbell scientific users manual)

The measurements of wind speed and air temperature using the CSAT3 underlie some limitations. These limitations can be summarized as follows:

- Operating temperature range: -30°C to +50°C
- Speed of sound: 300 to 366 ms^{-1}; least significant bit is 1 mms^{-1}
- No data can be recorded during rain.

During the field campaign using 3D sonic anemometer the three directional wind speed (U_x, U_y, U_z) at height of 2.60m above the water surface was measured with a temporal resolution of 20 Hz .

iii. Air temperature and relative humidity sensor:

During the field campaign air temperature and relative humidity was measured by two different sensors operates by Campbell Scientific and Hobo Ware data loggers. The HMP45C, relative humidity/ temperature probe combines a high accuracy humidity sensor and temperature sensors into one compact units produced by Campbell Scientific. The probe must be housed inside a radiation shield when used in the field. The 41003-5 radiation shield is used to block direct and reflected solar radiation, yet permits easy passage of air and can be attached with tripod/mast/tower leg. The range of measurement is from -50 °C to 50 °C and from 0 to 100 % for temperature and relative humidity probes respectively. The accuracy of the measurement is ± 0.3 °C for temperature and ± 2% for relative humidity.

iv. Temperature probe:

The TMC6–HOBO temperature probe with 1.8m lead was used for temperatures profile measurements at four depths in the water. Temperature sensors for use with HOBO external –channel data loggers, this model measures temperature in the air, water, or soil.

Before an intensive measurement of water temperature profiles it very important to calibrate the sensors for offset and response times. During the field campaign calibration of sensors was done at Bahir Dar University, Engineering faculty. In order to calibrate the temperature probe for offset (correction) and response time, we have used a standard thermometer from the water quality laboratory of Bahir Dar University. To determine the response time we have modelled the measured temperature (T_m) as:

$$T_m = T + (T_0 - T)\, e^{-\alpha t} \qquad 4\text{-}1$$

Where: T = Temperature at any time t
T_o = Initial temperature
α = Alfa (Decaying parameter)
t = Time in sec

Table 4-1: Response time and offset of temperature probe

Temperature sensor	T_average (°C)	Standard dev. (°C)	Offset (°C)	Alfa (sec^{-1})	Response time(1/alfa)
H1	22.5	0.07	-0.027	0.23	4.44
H2	22.6	0.06	-0.056	0.29	3.47
H3	22.5	0.06	-0.024	0.13	8.03
H4	22.5	0.04	0.035	0.12	8.19

4.4.2. Data Collection on land

Radiation and 3D sonic anemometer measurements were taken near to the Woreta weather station from September 22/2008 to September 29/2008. Figure 4-4 (a and b) shows installation of the instruments on the field and downloading the data from the logger to the laptop.

(a) (b)

Figure 4-4: Setting up of instruments for data collection at Woreta (22/09/08)

4.4.3. Data collection on the Lake

The in situ measurements on the lake were made by using fast and slow response sensors for two days. As shown in figure 4-5 the two sensors were fixed at height of 2.6 m above the water (H_1 = 0.85 and H_2 =1.75). The first day of measurements was on 27/09/2008 from 7:46 to 18:20 local time and the second day of measurements on 30/09/208 from 7:25 to 16:59 local time. Description of the data measured by these two sensors is given in Appendix C:

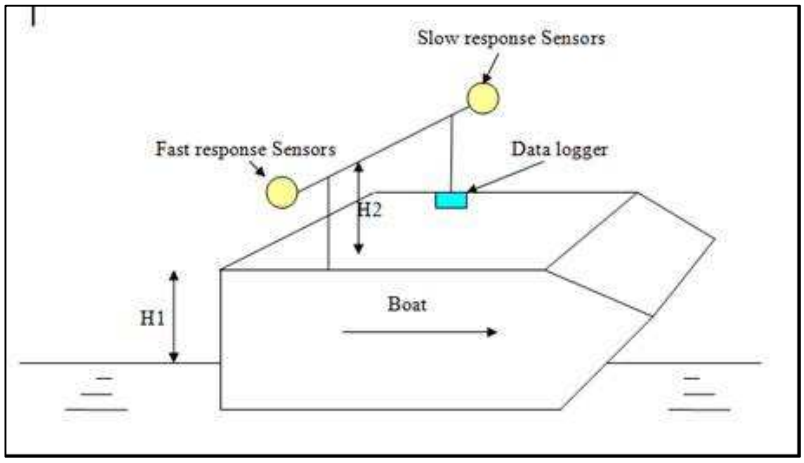

Figure 4-5: Schematic representation of instrument (sensors) mounted on the boat

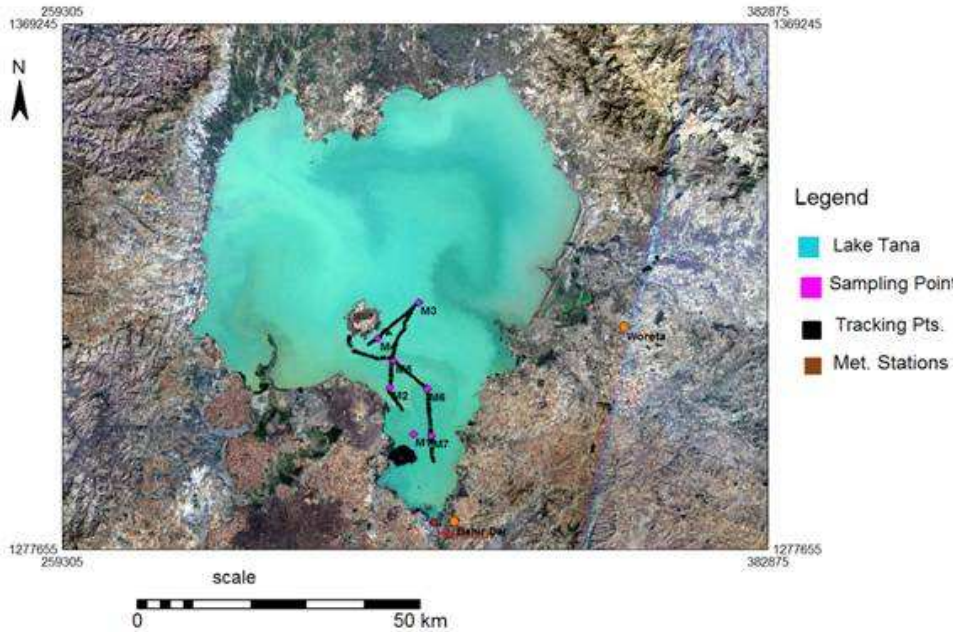

Figure 4-6: Sampling points on the lake (LANDSAT7 image, December 2003)

(a): Radiation measurements (4 component)

(b): 3D-sonic anemometer measurements

(c) Temperature profile measurements

(d) Temperature profile measurements

Figure 4-7: Measurements of different parameters on the lake (27/09/08)

5. Satellite Imagery

In addition to the data collected during the field campaign, satellite imagery from Terra/MODIS and MSG/SEVIRI are used for this study.

5.1. Terra/MODIS

MODIS (or Moderate Resolution Imaging Spectroradiometer) is a key instrument onboard of the Terra (EOS AM) and Aqua (EOS PM) satellites. Terra is at an altitude of 705km and has a cross track and along track swath of 2330 and 10km, respectively. Terra's orbit around the Earth is timed so that it passes from north to south across the equator in the morning (10:30 local time), while Aqua passes south to north over the equator in the afternoon (13:30 local time). Terra MODIS and Aqua MODIS are viewing the entire Earth's surface every 1 to 2 days, acquiring data in 36 spectral bands, or groups of wavelengths (see MODIS Technical Specifications). These data will improve our understanding of global dynamics and processes occurring on the land, in the oceans, and in the lower atmosphere (King et al., 1992; Running et al., 1994; Salomonson et al., 1989). MODIS is playing a vital role in the development of validated, global, interactive Earth system models able to predict global change accurately enough to assist policy makers in making sound decisions concerning the protection of our environment.

Table 5-1: MODIS visible and thermal infrared bands used in this study

Bands	Band width(µm)		IFOV/m
1	0.620	0.670	250
2	0.841	0.876	250
3	0.459	0.479	500
4	0.545	0.565	500
5	1.230	1.250	500
7	2.105	2.155	500
31	10.780	11.280	1000
32	11.770	12.270	1000

MODIS data is available free of charge and can be accessed from NASA website. In order to download level1 use the link: http://ladsweb.nascom.nasa.gov/data/search.html. Atmospheric products can also obtain from the same site. ModisSwath and ModisTool are software that can be used to pre-process raw and products of MODIS images respectively. The MODIS products also can be accessed from https://lpdaac.usgs.gov/lpdaac/products. Most products from level 1b up are in HDF format either in "swath" or integrated sinusoidal projection so that we can use the MODIS reprojection tool to convert to the required format and to create the spatial subset of the area.

5.2. MSG/SEVIRI

The first satellite of a new series of European geostationary meteorological satellites, Meteosat Second Generation (MSG-1), launched on 28 August 2002 and followed by the launch of MSG-2 on 21 December 2005. The twelve channel imager, called SEVIRI (Spinning Enhanced Visible and Infrared Imager) observes the full disk of the Earth with an unprecedented repeat cycle of 15 minutes. SEVIRI has eight channels in the thermal infrared (IR) at 3.9, 6.2, 7.3, 8.7, 9.7, 10.8, 12.0 and 13.4 μm, three channels in the solar spectrum at 0.6, 0.8, 1.6 μm and a broad-band high resolution visible. The high resolution visible channel has a spatial resolution of 1.67 km at nadir; pixels are over sampled with a factor of 1.67 corresponding to a sampling distance of 1 km at nadir. The corresponding values for the eight thermal IR and the other three solar channels are 4.8 km spatial resolution at nadir and an over sampling factor of 1.6, which corresponds to a sampling distance of 3 km at nadir.

Table 5-2: Spectral channel characteristics of SEVIRI

Channel no.		Characteristics of spectral Band(μm)			Main gaseous absorber or window
		λ_{cen}	λ_{min}	λ_{max}	
1	VIS0.6	0.64	0.56	0.71	Window
2	VIS0.8	0.81	0.74	0.88	Window
3	NIR1.6	1.64	1.50	1.78	Window
4	IR3.9	3.90	3.48	4.36	Window
5	WV6.2	6.25	5.35	7.15	Water Vapor
6	WV7.3	7.35	6.85	7.85	Water vapor
7	IR8.7	8.70	8.30	9.10	Window
8	IR9.7	9.66	9.38	9.94	Ozone
9	IR10.8	10.80	9.80	11.80	Window
10	IR12.0	12.00	11.00	13.00	Window
11	IR13.4	13.40	12.40	14.40	Carbon dioxide
12	HRV	Broadband (about 0.4-1.1)			Window/water vapor

The Spinning Enhance Visible and Infrared Imager (SEVIRI) sensor onboard MSG satellite provides data to EUMETSAT at Darmstadt (Germany) which is processed and then uplink to HOTBIRD-6 in wavelet compressed format (Gieske et al., 2005). The images are received and archived at ITC in compressed form on external drivers which are linked to the ITC network and hence accessed trough ordinary personal computers. The images are geocoded and radiometrically calibrated. The data is not atmospherically corrected. Therefore direct ground observation(s) can only be related to the satellite observation(s) (at the required resolution) after atmospheric correction of images.

The retrieval of MSG data is straightforward using import utilities developed. External batch files were created using the MSG data Retriever software developed and available at ITC. Figure 5.1 shows data Retriever window with the command line indicating all parameters that are to be retrieved from MSG images.

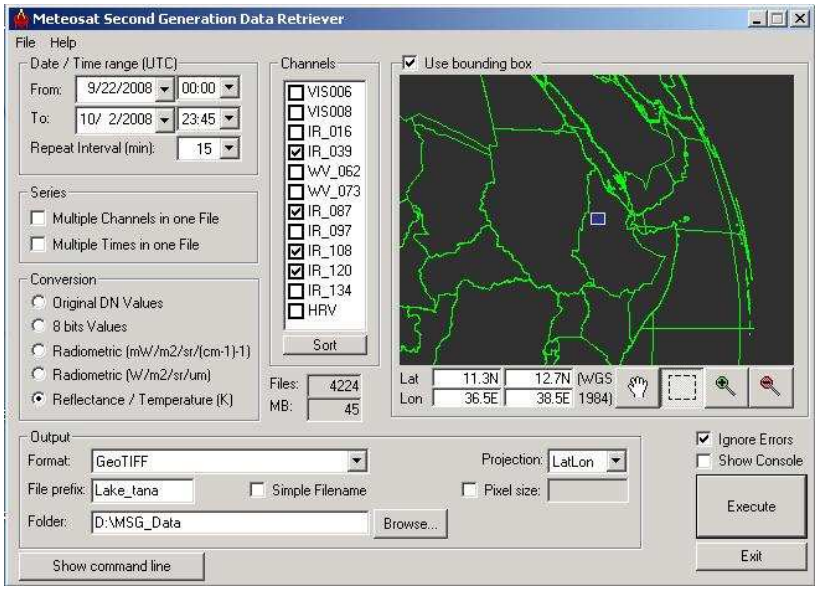

Figure 5-1: MSG Data Retriever window (courtesy of ITC)

While using MSG data Retriever the executed commands can be saved as a text file and therefore any time a different image is required the changes are only done using a text editor saved as a batch file in ILWIS software. In this study, only bands 4, 7, 9 and 10 (3.90µm, 8.70µm, 10.80µm and 12.0µm respectively) were used in surface temperature retrieval.

In order to retrieve the required information from remote sensing data we should keep in mind that the area of interest necessarily be near to the centre of the scene to reduce geometric distortion as well as free of cloud cover to avoid contamination of radiance measurement on the sensor.

Table 5-3: Satellite imagery used for the study

Satellite/Sensor	Date of acquisition	Satellite overpass time	Temporal resolution	Cloud conditions of the area
TERRA/MODIS	27/09/08	11:15	daily	clear sky during day time and cloudy during the night
MSG/SEVIRI	27/09/08	geostationary	every 15 minute	clear sky during day time and cloudy during the night

5.3. Image pre-processing

In order to get the required surface parameters from remote sensing data for evaporation estimation requires the routine processing of images. Image pre-processing commonly comprises a series of sequential operations, including atmospheric correction or normalization, image registration,

geometric correction, and masking (e.g., for clouds, water, irrelevant features). Geometric rectifications of the imagery resample or change the pixel grid to fit that of a map projection or another reference image. This becomes especially important when scene to scene comparisons of individual pixels in applications such as change detections are being sought.

5.3.1. Solar and Satellite zenith angles for MSG data processing

For many applications corrections to the pixels have to be applied based on satellite or sun azimuth and zenith angles. A Java applet has been used which allows computation of MSG satellite and sun azimuth and zenith angles based on date and time. Generating MSG satellite and sun angles was done by creating a batch file which could be adopted for any date and time in case new angles were required. This particular applet, which can be executed into an active directory, works in a java environment which must be installed in the system. Generated angles were imported into ILWIS for further processing. Figure 5.2 shows the flow chart for generating the satellite and solar angles.

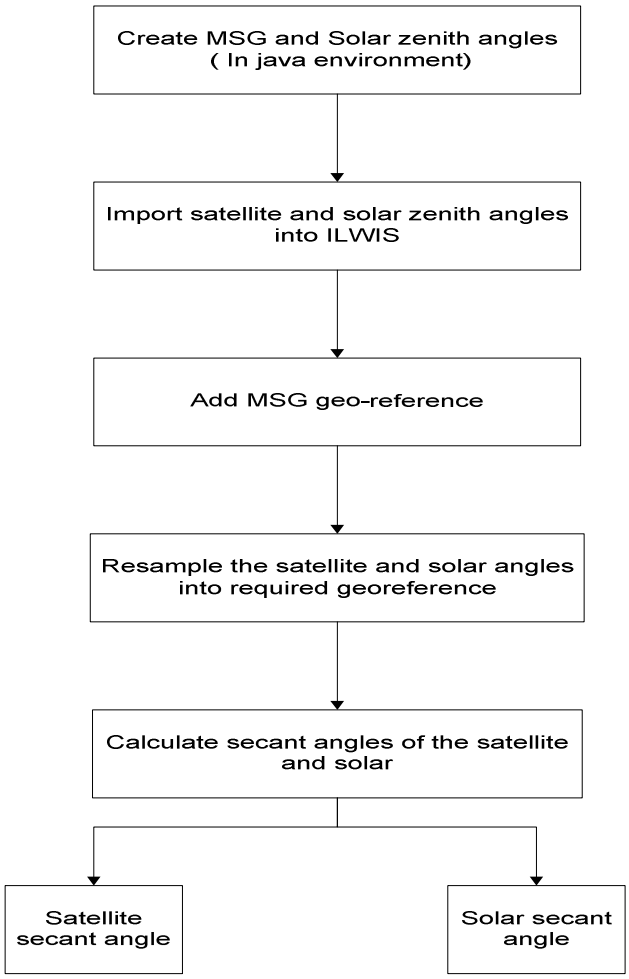

Figure 5-2: Generation of MSG satellite and solar angles

5.3.2. MODIS products

A large number of products are available for land and atmospheric parameters. In this study I make use of 8 days composite reflectance for monthly albedo calculation and daily surface temperature for the estimation of long wave radiation.

Table 5-4: MODIS land surface products used in the study

Product name	Band used	Spatial resolution	Temporal resolution	Name /coding
Surface reflectance	Band1 to band7	500 m	8 days-composite	MOD09A1
Surface temperature and emissivity	Band 31 and 32	1000 m	daily	MOD11A1

The MODIS surface reflectance products provide an estimate of the surface spectral reflectance as it would be measured at ground level in the absence of atmospheric scattering or absorption. Low-level data are corrected for atmospheric gases and aerosols, yielding a level-2 basis for several higher-order gridded level-2 (L2G) and level-3 products. MOD09A1 provides Bands 1–7 at 500-meter resolution in an 8-day gridded level-3 product in the Sinusoidal projection. Each MOD09A1 pixel contains the best possible L2G observation during an 8-day period as selected on the basis of high observation coverage, low view angle, the absence of clouds or cloud shadow, and aerosol loading. Science data sets provided for this product include reflectance values for bands 1–7, quality assessment, and the day of the year for the pixel along with solar, view, and zenith angles.

The level-3 MODIS global Land Surface Temperature (LST) and emissivity daily data include values generated in a Sinusoidal projected tile by mapping the level-2 LST product on 1-kilometer (actual 0.928-km) grids. MYD11A1 is comprised of daytime and night-time LSTs, quality assessment, observation times, view angles, clear sky coverage and emissivities estimated in Bands 31 and 32 from land cover types.

Most products from level 1b up are in HDF format either in "swath" or integrated sinusoidal projection. One of the tools which use to process these products is MODIS Reprojection Tool available in public domain. The MODIS Reprojection Tool (MRT) is software designed to help individuals work with MODIS data by reprojecting MODIS images (Level-2G, Level-3, and Level-4 land data products) into more standard map projections. If desired, the user may reproject only selected portions of the image (spatial subsetting) and only selected image bands (spectral subsetting). The software produces MODIS data in file formats that are supported by existing software packages (raw binary and GeoTIFF) as well as HDF-EOS.

5.3.3. MODIS level-1B data conversion

The MODIS level-1b and geolocation files are available through the GSFC DAAC as the MOD02 and MOD03, for Terra, MYD02 and MYD03 for Aqua products respectively. From these data we can

select the required bands as well as band height, solar zenith, solar azimuth, sensor zenith, sensor azimuth.
The MODIS Swath Reprojection Tool (MRTSwath) provides the capability to transform MODIS Level-1B and Level-2 land products from HDF-EOS swath format to a uniformly gridded image that is geographically referenced according to user-specified projection and resampling parameters and then we can import to ILWIS as Geotiff format for further pre-processing.

5.3.4. Calibration and atmospheric correction of MODIS data

Pre-processing of MODIS images was done by tools built on ILWIS software for SEBS operation. The step by step procedure of these pre-processing presented as follows.

1. Digital number (DN) to radiance/reflectance: It provides the tool to convert the imported MODIS Channels in digital number into radiance or reflectance, which is done by applying the proper calibration coefficients. The calibration coefficients consist of a scale and offset and are provided in the HDF header file of the raw data. The coefficients can be read by using of HDFView software.
2. Brightness temperature computation: This procedure provides the options to convert the bands 31 and 32 of MODIS from radiance to blackbody temperatures. This conversion is done by applying the well-known Planck equation.

$$T_c = \frac{c_2}{\lambda_c \log\left(\frac{c_1}{\lambda_c^5 \pi L_s} + 1\right)} \tag{5.1}$$

Where:

T_c	=	Brightness temperature, from a central wavelength (K)
λ_c	=	the sensor's central wavelength (µm)
Ls	=	the sensor's radiance ($Wm^{-2}Sr^{-1}\ \mu m^{-1}$)
c_1	=	first radiation constant ($3.741775\times10\text{-}22\ Wm^3\mu m^{-1}$)
c_2	=	second radiation constant (0.0143877 µmK)

3. Atmospheric Correction (AC): The accurate retrieval of surface reflectance and temperature is very important in deriving land surface biophysical parameters and in determination of fluxes. In mapping of the surface physical properties from remotely sensed spectral data, the surface information is highly affected by atmospheric interference.

   The atmospheric effects include scattering by aerosols and absorption by gases, such as water vapour, ozone, and oxygen. The AC method is an essential part to improve the analysis of the remote sensing data in many ways:

   - Multi-temporal scenes recorded under different atmospheric conditions can better be compared after atmospheric correction. Changes observed will be due to changes on the earth's surface and not due to different atmospheric conditions.

- For comparison of vegetation condition and surface brightness between and among years of selected time periods.
- For quantitative remote sensing applications like surface vegetation atmosphere transfer (SVAT) modelling.

Therefore, methods of atmospheric correction (AC) are needed to correct the radiances for the atmospheric disturbances, in order to allow the retrieval of pure ground radiance from target. The correction methods can be grouped according to the final product required by the application. Generally the methods are grouped into two:

i Relative atmospheric methods: These methods include invariant object, histogram matching, and dark object analysis. For details of the discussion of these methods the reader is referred to Liang (2001b).

ii Absolute atmospheric correction methods: These methods require a description of the components in the atmospheric profile. Detailed atmospheric information can only be obtained through atmospheric sounding procedures, consisting of a series of instruments able to sample the atmosphere at fixed intervals while transported vertically by a balloon. This kind of profiling is carried out daily at the some atmospheric centres at fixed times, regardless of the satellite overpass time. The output of these methods is an image that matches the reflectance of the ground pixels with a maximum estimated error of 10%, if atmospheric profiling is adequate enough (Kerle et al., 2004). Some typical examples of radiative transfer models used for absolute atmospheric correction are: MODTRAN and SMAC (Simplified Method for Atmospheric Correction). These methods are producing some accurate results but they need the acquisition of atmospheric parameters like aerosol properties, ozone and water vapour content.

Due to lack of direct measurement of atmospheric profile variables for the study area and also its simplicity I applied the SMAC atmospheric correction method in this study. SMAC is a simplified version of Code 5S and 6S. It was originally designed for NOAA AVHRR imagery, and has been extended to include some high resolution satellites. The main advantage of the method is that it is several hundred times faster than more detailed radiative transfer models like 5S and that it does not require pre-calculated look-up tables. The method is especially useful for correcting the huge amounts of data acquired by large-field-of-view high-repetitively sensors, like the ones on board polar orbiting and geostationary meteorological satellites. It still requires information of ozone, aerosol and water vapour, but adapted to total amounts in vertical columns of atmosphere, while detailed profile are not necessary. This information is extracted from MODIS atmospheric products (http://ladsweb.nascom.nasa.gov/data/search.html). The table below shows the atmospheric data obtained from MODIS product for day 27/09/2008.

Table 5-5: Atmospheric correction data for SMAC (day 271, year 2008)

Atmospheric correction data	Value
Optical thickness (Aerosol) (nm)	0.2
Water vapour (gcm^{-2})	2.8
Ozone content (atm.cm)	0.268
Surface pressure (hpa)	Raster map produced from height information of geolocation file.

6. Methodology

6.1. Evaporation estimates using climate data

Most of the methods proposed to estimate lake evaporation when available meteorological observations are limited, derive evaporation either from the aerodynamic principle, the energy balance, or a combination of both (Cahoon et al., 1991; Morton, 1983; Rosenberry et al., 1993; Vardavas and Fountoulakis, 1996). In this research the two widely used methods, i.e. the energy balance and Penman open water approach are applied at a daily time steps for annual evaporation estimates.

6.1.1. The lake energy balance

The lake energy balance method is one of the best methods for inferring evaporation (Ashfaque, 1999; Assouline and Mahrer, 1993; Gianniou and Antonopoulos, 2007; Keijman, 1974; Vallet-Coulomb et al., 2001; Yin and Nicholson, 1998). It does not require wind speed data. A general expression of the energy balance is:

$$R_n = H + \lambda E + \Delta S \qquad 6\text{-}1$$

Where R_n is the net radiation, λE the latent heat flux (λ the latent heat of vaporization in J kg^{-1}, and E the evaporation rate in kg s^{-1} m^{-2}), H the sensible heat flux, and ΔS the change of energy storage in the lake fluxes (all terms expressed in Wm^{-2}).
The net radiation (R_n) results from the balance between short wave and long wave radiation:

$$R_n = R_s(1-\alpha) + R_l \qquad 6\text{-}2$$

Where R_s is the incoming short wave radiation, R_l is the net long wave radiation (Wm^{-2}) and α is the surface albedo.
In the absence of direct radiation measurements, daily incoming shortwave radiation can be calculated with the Angstrom formula, which relates solar radiation to extraterrestrial radiation and relative sunshine durations:

$$R_s = (a_s + b_s \frac{n}{N}) R_a \qquad 6\text{-}3$$

Where n is actual duration of sunshine [hour], N is the maximum possible duration of sunshine or daylight hours [hour], R_a extraterrestrial radiation [Wm^{-2}], a_s and b_s are regression constants.

Depending on the atmospheric conditions (humidity, dust) and solar declination (latitude and month), the Angstrom constants will vary. Where no actual solar radiation data are available and no calibration has been carried out for improved a_s and b_s parameters, the values a_s= 0.25 and b_s= 0.50 are usually recommended.

Land surface broadband albedo is one of the most important physical parameters for climate models in determination of net short wave radiation as shown in Equation 6-2, because it governs the exchange of radiation between the land surface and the atmosphere. It depends on the atmospheric conditions through downward fluxes. Satellite remote sensing techniques provide a more accurate pixel-level estimation of surface albedo than traditional field measurements. However, the accurate determination of land surface broadband albedo from top-of atmosphere (TOA) observations requires the knowledge of the atmospheric conditions and surface characteristics, which can be monitored effectively only by multispectral sensors.

In this study attempt has made to estimate the spatial as well as temporal map of lake surface albedo from TERRA/MODIS reflectance product which is freely available and downloaded from https://lpdaac.usgs.gov/lpdaac/products.

The surface albedo can be computed from visible and near IR bands of MODIS sensor. The formula developed by Liang et al. (2001a) has used.

$$\alpha = 0.160\,r_1 + 0.291\,r_2 + 0.243\,r_3 + 0.116\,r_4 + 0.112\,r_5 + 0.018\,r_7 - 0.0015 \qquad 6\text{-}4$$

Where r_1, r_2, r_3, r_4, r_5, r_7 are surface reflectance derived from MODIS band of 1, 2,3,4,5 and 7 respectively.
The daily net long wave radiation as recommended in FAO 56 manual (Allen et al., 1998) as follows:

$$R_{nl} = \sigma\left[\frac{T_{\max}^4 + T_{\min}^4}{2}\right](0.34 - 0.14\sqrt{e_a})(1.35\frac{R_s}{R_{so}} - 0.35) \qquad 6\text{-}5$$

Where

σ	=	Stefan-Boltzmann's constant [$4.903\ 10^{-9}$ MJ K^{-4} m^{-2} day^{-1}]
T_{max}	=	maximum temperature during the 24-hour period
T_{min}	=	minimum absolute temperature during the 24-hour period
e_a	=	actual vapour pressure [kPa]
R_s/R_{so}	=	relative shortwave radiation (limited to$\leq$ 1)
R_s	=	measured or calculated solar radiation
R_{so}	=	calculated clear-sky radiation

The changes in stored energy (ΔS) may be important in deep lakes subject to large seasonal variations in air temperature (Hostetler and Bartlein, 1990; Tasumi, 2005; Vassiljev et al., 1995). In this study owing to the shallowness of the lake and to the weak seasonal variation in air temperature, this term could be neglected without introducing a considerable error in the annual evaporation estimate. Equation 6-1 further can be simplified by introducing Bowen ratio, i.e. the ratio of sensible to latent heat flux.

$$E = \frac{R_n}{\lambda(\beta + 1)} \qquad 6\text{-}6$$

Considering the transport coefficients (inverse of aerodynamic resistance) are equal for H and λE, β can be expressed as:

$$\beta = \frac{H}{\lambda E} = \gamma \frac{[T_2 - T_1 + \Gamma(z_2 - z_1)]}{e_2 - e_1} \qquad 6\text{-}7$$

Where T_1 [K] and e_1 [mbar] are air temperature and vapour pressure at height z_1 [m] and T_2 [K] and e_2 [mbar] are air temperature and vapour pressure at height z_2 [m], γ is the psychometric constant [mbar.K^{-1}] and Γ is the adiabatic lapse rate, generally taken as 0.0065 Km^{-1}. Γ can be neglected if the distance between the Bowen ratio measurement heights is less than 2m. So the final equation used for interpolation of field measurements is:

$$\beta = \frac{H}{\lambda E} = \gamma \frac{[T_2 - T_1]}{e_2 - e_1} \qquad 6\text{-}8$$

For a lake surface, the Bowen ratio is generally estimated from measurement of air temperature, air humidity and water –surface temperature at a time step, which can vary from less than an hour to a month. Due to lake of long term recorded of water-surface temperature in this case we can estimate from a comparable environment. For example, an annual average Bowen ratio of 0.2 was taken in water and energy balance models developed for Lake Victoria (Yin and Nicholson, 1998) and most recently a research on Lake Ziway of Ethiopia (Vallet-Coulomb et al., 2001) have used a value of 0.15.

6.1.2. Penman open water approach

In 1948, Penman combined the energy balance with the mass transfer method and derived an equation to compare the evaporation from an open water surface from standard climatic records of daily sunshine hours, temperature, humidity, altitude and wind speed. This so-called combination method was further developed and modified by many researchers (Allen et al., 1998; Maidment, 1993; Vallet-Coulomb et al., 2001).

The Penman combination equation for open water equation given by:

$$E = \frac{\Delta(R_n - G) + \rho_a c_p (e_s - e_a)/r_a}{\Delta + \gamma} \qquad \text{(Allen et al., 1998)} \qquad 6\text{-}9$$

$$E = (R_n - G)\frac{\Delta}{\Delta + \gamma} + E_a \frac{\gamma}{\Delta + \gamma} \qquad \text{(Vallet-Coulomb et al., 2001)} \qquad 6\text{-}10$$

$$E = \frac{\Delta}{\Delta + \gamma}(R_n - G + A_h) + \frac{\gamma}{\Delta + \gamma}\frac{6.43(1 + 0.536U_2)D}{\lambda} \qquad \text{(Maidment, 1993)} \qquad 6\text{-}11$$

Where:

E	=	is evaporation that occurs from free water evaporation [mmday^{-1}]
R_n	=	is the radiation exchange for the free water surface [mmday^{-1}]
A_h	=	is energy advected to the water body [mm per day]
U_2	=	is wind speed measured at 2 m [ms^{-1}]
D	=	is average vapour pressure deficit, [KPa]
λ	=	is the latent heat of vaporization [MJKg^{-1}]
γ	=	is psychometric constant [KPa°C^{-1}]
r_a	=	is aerodynamic resistance
Δ	=	is slope of saturation vapour pressure curve at air temperature [KPa°C^{-1}]
E_a	=	is the drying power of air and given by:

$$E_a = 0.26(1+0.54U)(e_s - e) \quad \text{6-12}$$

6.2. Turbulent heat flux estimation

The eddy-covariance technique (EC) is broadly considered to be today's reference method for the estimation of turbulent heat fluxes (Kaimal and Finnigan, 1994). The technique is also used extensively for verification and tuning of global climate models, mesoscale and weather models, complex biogeochemical and ecological models, and remote sensing estimates from satellites and aircraft. The technique is mathematically complex, and requires considerable care in setting up and processing data. To date, there is no uniform terminology or a single methodology for the eddy covariance technique, but much effort is being made by flux measurement networks.

The fluxes that can be directly measured using eddy covariance principles are:

1. Sensible heat flux: estimated as mean air density multiplied by the covariance between deviations in instantaneous vertical wind speed and temperature, and converted to energy units using the specific heat.

$$H = \rho_a C_p \overline{w'T'} \quad \text{6-13}$$

Where H [Wm^{-2}] is the sensible heat flux, ρ_a [kgm^{-3}] is the mean air density, C_p is the heat capacity of air, w [ms^{-1}] the vertical wind speed and T is the sonic temperature [K]

2. Latent heat flux: computed in a similar manner using water vapour, and later also converted to energy units.

$$\lambda E = \lambda \frac{M_w / M_a}{P} \rho_a \overline{w'e'} \quad \text{6-14}$$

Where λE [Wm^{-2}] is the latent heat flux, λ [ ] heat of vaporization of water, ρ_a [kgm^{-3}] is the mean air density, M_w is molecular weight of water, w [ms^{-1}] the vertical wind speed, e[mbar] water vapour.

3. Carbon dioxide flux: presented as the mean covariance between deviations in instantaneous vertical wind speed and density of the CO_2 in the air

$$F_c = \overline{w'\rho_c'} \qquad 6\text{-}15$$

Where F_c [Wm^{-2}] is the carbon dioxide flux, w [m/s] the vertical wind speed, ρ_c [Kgm^{-3}] is the mean density of carbon dioxide in the air.

In general the software requirement in eddy covariance measurement can be grouped into data collection (e.g. loggernet) and data processing. Eventhough researchers often write their own software to process specific data, recently, comprehensive data processing packages have became available from flux networks, research groups and instrument manufacturers (Mauder and Foken, 2004). One example of such a package is ECPack. It is an open source FORTRAN library developed by the Meteorology and Air Quality group, Wageningen University, containing all relevant EC-routines and an interface to raw measurements stored in NetCDF-format. ECPack can be downloaded for free from the JEP-site http://www.met.wau.nl/projects/JEP/index.html, together with the report that explains the theory and all practical steps. The library has been split into functionally different groups of routines (mathematics, corrections, general physics, IO, NetCDF). From the name of a routine one can see to which group it belongs. With a set of integrated routines one can take collections of steps in the data processing in one call. The separate routines can easily be added by people to their existing programs to incorporate new functionality. The integrated routines, with a sample program, give an efficient tool for the processing of EC-data.

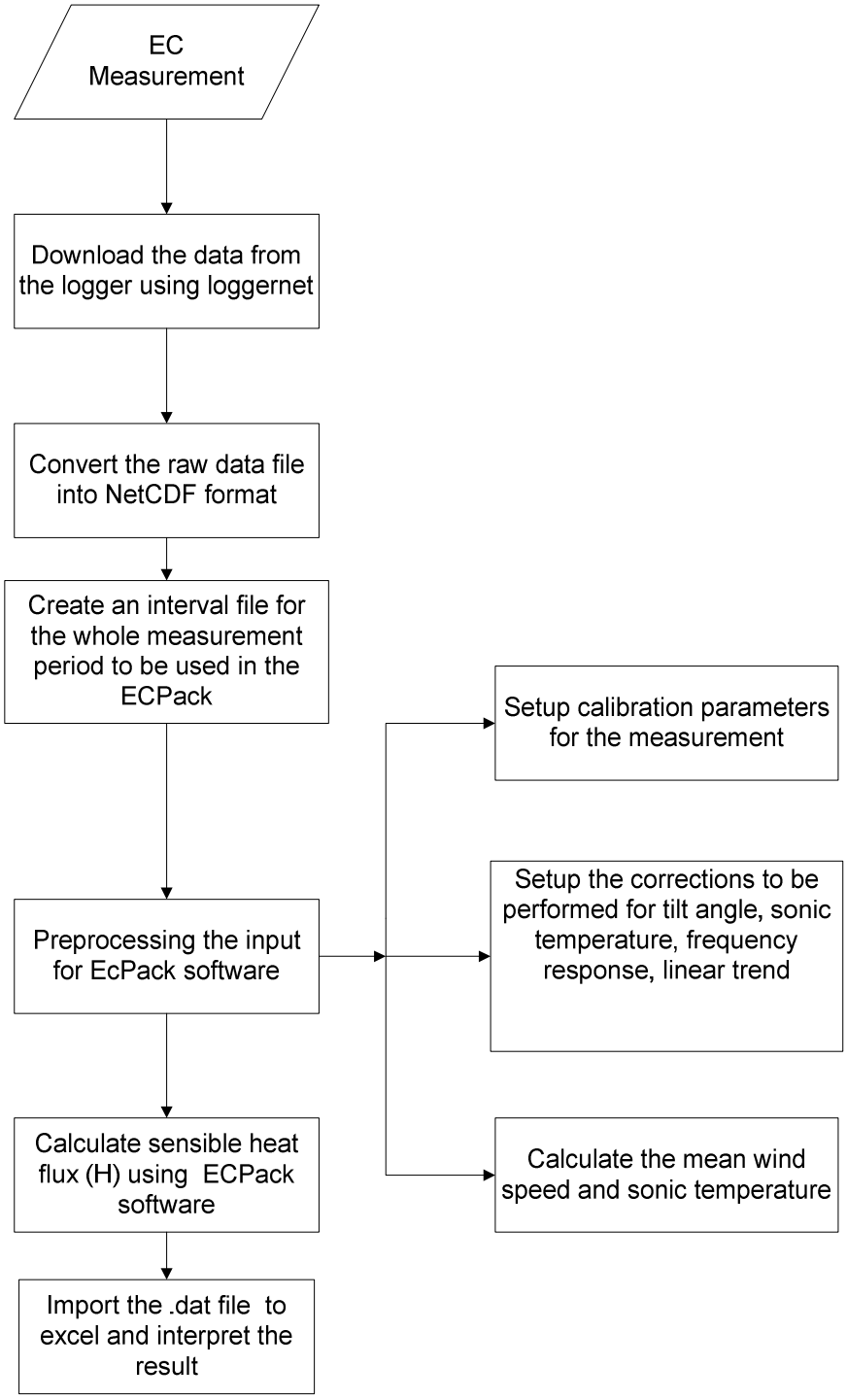

Figure 6-1: Flowchart showing how to calculate sensible flux using ECPack Software

6.3. Satellite Remote sensing for evaporation estimation

Remote sensing-based evapotranspiration (ET) estimations using the surface energy budget equation are proving to be one of the most recently accepted techniques for aerial ET estimation covering larger areas. The energy balance method for estimating evaporation from the Lake and reservoirs is considered by many to be the most accurate method (Delclaux et al., 2007; dos Reis and Dias, 1998; Gianniou and Antonopoulos, 2007; Vallet-Coulomb et al., 2001; Winter et al., 2003) .

The latent heat flux can be computed as residual of surface energy balance equation given as:

$$\lambda E = R_n - G - H \qquad 6\text{-}16$$

Where λE is the latent heat flux [Wm^{-2}], E is evaporation and λ is the latent heat of vaporization, R_n is net radiation flux [Wm^{-2}] at the water surface, G is water heat flux [Wm^{-2}] (positive if the water surface is warmer than the lower part and via versa) and H is sensible heat flux [Wm^{-2}] from water surface to air (positive if air is warmer than water and via versa). The net radiation (R_n), the water heats flux (G) and the sensible heat flux (H) can be calculated as follows:

6.3.1. Net radiation from MODIS

The amount of radiation received at the Earth's surface influences the latent heat flux of vaporization, the energy balance, the level of soil moisture status, the water available for plants, the air, surface and soil temperature, and also affects the suppression of phytoplankton productivity (Hurtado and Sobrino, 2001; Wang et al., 2000). Therefore, knowledge on net radiation flux is of great interest in agriculture, hydrology, climatology and ecosystems. Turbulent exchanges at the surface are governed by the net radiation, so it is necessary that this parameter is accurate. The net radiation can be expressed as the sum of the four major components, i.e.

$$R_n = R_s \downarrow - R_s \uparrow + R_l \downarrow - R_l \uparrow \qquad 6\text{-}17$$

Where $R_s\downarrow$ is the downward shortwave radiation from the Sun and atmosphere, $R_s\uparrow$ is the reflected shortwave radiation by the surface, $R_l\downarrow$ is the long wave radiation emitted from the atmosphere toward the surface and $R_l\uparrow$ is the long wave radiation emitted from the surface into the atmosphere. To get the net radiation, the net long wave radiation and shortwave radiation should first be obtained.

The methods span a range of complexity from simple statistical, empirical to theoretical and physical. Xue et al.(2000) calculated shortwave net radiation from ATSR data in three different ways. Combining Landsat-5 TM and digital elevation models, Wang et al.(2000) estimated surface net solar radiation over an experimental site which covers a 17 by 17 km area near Manhattan, Kansas. Hurtado and Sobrino (2001) obtained shortwave radiation flux from the solar global radiation flux and the albedo map.

Long wave radiation

The difference between the earth's surface emission and the counter radiation of the atmosphere is the net long wave radiation neglecting incoming long wave radiation from the Sun. The value of the net long wave radiation depends on air temperature, humidity, cloudiness, and the vertical gradients of temperature and moisture in the atmosphere. In acquiring the long wave radiation, Berliand (1960) proposed an expression for the dependence of clear sky net long wave radiation upon the temperature and humidity of air. Besides the temperature and humidity of the air, net long wave radiation is considerably influenced by cloudiness and by air and surface temperatures. For a cloudless sky, the net long wave radiation R_{nl} can be expressed as:

$$R_{nl} = R_l \downarrow - R_l \uparrow \qquad 6\text{-}18$$

Where Rl↓ is the long wave radiation emitted from the atmosphere toward the surface, Rl↑ is the long wave radiation emitted from the surface into the atmosphere. The incoming and outgoing long wave radiations are interdependent. Xue et al. (1998) developed a relation ship between these two terms as:

$$R_{nl} = \varepsilon\sigma T_a^4 (0.39 - 0.05\sqrt{e(T_a)/100}) + 4\varepsilon\sigma T_a^3 (T_s - T_a) \qquad 6\text{-}19$$

Where ε is the surface emissivity, σ is the Stefan-Boltzmann constant ($5.67 \times 10^{-8} Wm^{-2}K^{-4}$) and e ($T_a$) is the vapour pressure (Pa) of the air.

Oberhuber (1988) gave an expression for e(T_a), which is,

$$e(T_a) = 611 \times 10^{7.5(T_a - 273.16)/(T_a - 35.86)} \qquad 6\text{-}20$$

T_a can be obtained from local meteorological station. So, to obtain the net long wave radiation, the retrieval accuracy of surface temperature T_s and emissivity ε from remotely sensed data is very important. The linear formula to convert from narrow to broad band emissivity using channel 31 and 32 of MODIS given by Shunlin (2004) as:

$$\varepsilon = 0.261 + 0.314\varepsilon_{31} + 0.411\varepsilon_{32} \qquad 6\text{-}21$$

Shortwave radiation

The sun emits the shortwave radiation within the wave length of interval of 0.3 and 3 μm. When measured at the earth surface, solar radiation includes both direct and diffused shortwave radiation and their sum may be called global radiation. The amount of incoming solar radiation ($R_l\downarrow$) which reaches the earth's surface can be determined from extraterrestrial solar radiation, atmospheric conditions or cloudiness factor and by earth surface configuration. The outgoing shortwave radiation $R_l\uparrow$, is the portion of the visible energy, which is reflected back to the atmosphere. The difference

between the downward shortwave radiation from the Sun and atmosphere and the reflected shortwave radiation by the surface is shortwave net radiation. As early as several decades ago a high correlation between satellite observations of reflected shortwave fluxes at the top of the atmosphere and ground measurements of shortwave fluxes was reported (Pinker et al., 1995). In the following decade the first quantitative estimates of these fluxes were derived, and eventually improved methodologies that allowed global-scale implementation were developed. Based on equations from Xue and Cracknell (1995), the net shortwave radiation can be expressed as:

$$R_S = (1-\alpha)S_0 C_t \cos\theta = R_s \downarrow - R_s \uparrow \qquad 6\text{-}22$$

Where α is the Earth surface albedo, S_0 is the solar constant ($1367 Wm^{-2}$), C_t is the atmospheric transmittance in the visible spectrum (typically 0.75), and the solar zenith angle ($\cos\theta$) can be obtained from MODIS product or calculated as:

$$\cos\theta = \sin\delta\sin\phi + \cos\delta\cos\phi\cos(\omega t) \qquad 6\text{-}23$$

Where δ is the solar declination and ω is the angular velocity of rotation of the Earth. ϕ is the local latitude which can be obtained from MODIS data. So, to obtain shortwave radiation, the Earth surface albedo α is a key issue. The surface albedo can be obtained by combining the narrow band spectral reflectance.

6.3.2. Water heat flux, G

The water heat flux, G, is the energy that is utilized in heating the water. G is positive when the water is warming and negative when the water is cooling. The involvement of G in the energy balance of water bodies has to be considered from shorter (instantaneous) to larger (seasonal) time sale. On daily basis many studies inferred that G can be neglected because the energy gained during day time is lost at night. However it is very important to analyze the periodic change of water temperature to understand the contribution of G on seasonal basis. Using MSG-2 data analysis Gieske (2008) reported that minimum change in water temperature occurs around December-January on Lake Tana.

When we want to use remote sensing data in the energy balance equation, all components of energy balance has to be acquired at the instantaneous time scale. Hence, there should be a way to calculate instantaneous G from ground observations. Most of the available mathematical expressions are developed for soil heat fluxes estimation, therefore care has to taken when we want to apply for water surfaces because the energy balance dynamics of water bodies and soil are different (Anthony et al., 2000). The instantaneous rate of heat storage or release at any depth z can be expressed by:

$$G = \lambda_w \frac{dT_w}{dz} \qquad 6\text{-}24$$

Where, λ_w is the thermal conductivity of water which is 0.607 $Wm^{-1}K^{-1}$(at 25° C), dT_w/dz is the gradient of temperature in the water, T_w is the temperature of water [K], z in meter. The limitation of

this method is that the thermal conductivity of water is very difficult to estimate because every time it can be affected by mixing due to turbulence action. Hence this method is mainly recommended for stagnant water body.
G can be also estimated from the change in temperature profile with respect to time, mathematical written as:

$$G = \rho C_p \int_{z=0}^{z} \Delta T / \Delta t \, dz \qquad 6\text{-}25$$

Where ρ is the density of water [kgm^{-3}], C_p is the specific heat capacity of water [$Jkg^{-1}K^{-1}$], $\Delta T / \Delta t$ is the change in temperature with two consecutive measurements [Ks^{-1}]. The limitation of this method is the measurements have to be done on specific location to track the change in water temperature with time.
In the presence of all measurements of energy balance components the water heat flux can also estimated as a residual of energy balance equation as:

$$G = R_n - H - \lambda E \qquad 6\text{-}26$$

Where H is the sensible heat flux estimated from temperature gradient, λE is the sensible heat flux and related with sensible heat flux using Bowen ratio (β). Then the above equation simplified as:

$$G = R_n - H(1 + \frac{1}{\beta}) \qquad 6\text{-}27$$

6.3.3. Sensible heat flux, H

Studies addressing the scientific issues of climate change and variability have discussed the need to quantitatively measure and better understand surface–atmosphere exchange processes. In addition, having reliable measurements of the magnitude and variability of surface sensible and latent heat fluxes is important for the development of regional climate models and the verification of regional climate simulations because of the significance of local processes on the kind and intensity of weather experienced in a region.

Sensible heat is heat energy transferred between the surface and air when there is a difference in temperature between them. A change in temperature over distance is called a "temperature gradient". In this case, it is a vertical temperature gradient, i.e., between the surface and the air above. We feel the transfer of sensible heat as a rise or fall in the temperature of the air. Heat is initially transferred into the air by conduction as air molecules collide with those of the surface. As the air warms it circulates upwards via convection. Thus the transfer of sensible heat is accomplished in a two-step process. Because air is such a poor conductor of heat, it is convection that is the most efficient way of transferring sensible heat into the air. Mathematically the sensible heat flux can be expressed as:

$$H = \frac{\rho_a c_p}{r_{ah}} (T_o - T_a) \qquad 6\text{-}28$$

Where: ρ_a is air density [kgm^{-3}], c_p is specific heat of moist air, 1004 [$Jkg^{-1}K^{-1}$] , r_{ah} is aerodynamic resistance to heat transport [sm^{-1}], to is water surface temperature [K], and T_a is the air temperature at observation height [K].

The calculation of r_{ah} can not obtained without difficulty. It varies with wind speed and the intensity and the direction of H itself. The aerodynamic resistance to heat transport between the surface and the reference height z can be estimated by:

$$r_{ah} = \frac{1}{k_2 u}\left[\ln\left(\frac{z-d}{z_{om}}\right) - \psi_{sm}\right]\left[\ln\left(\frac{z-d}{z_{oh}}\right) - \psi_{sh}\right] \qquad 6\text{-}29$$

Where, d is zero plane displacement, k is Von Karman's constant (=0.41), u is velocity of air [ms^{-1}], z is observation height, z_{om} is surface roughness length for momentum transfer [m], z_{oh} is the surface roughness length for sensible heat transfer [m], ψ_{sh} and ψ_{sm} are the integrated stability functions for describing effect of buoyancy or stability between the surface and height z on the sensible heat and momentum transfer. For neutral conditions (T_0=T_a, hence H=0), ψ_{sh} = ψ_{sm}= 0 and for simplicity one can assume z_{oh}= z_{om} = z_0. This assumptions gives comparatively small errors in combination formula (Thom, 1972) . So the above equation can be simplified as:

$$r_{ah} = \frac{1}{k^2 u}[\ln(\frac{z}{z_0})]^2 \qquad 6\text{-}30$$

For water surface, d=0, z_{om}=0.0001m (Allen et al., 1996; Brutsaert, 1982) suggested a value for z_{0h} = 0.00023m over typical water surface whereas Penman assumes a roughness length z_0=0.0013m. As Penman equation was developed to estimate open water evaporation, I took roughness length z_0=0.0013 for calculation or r_{ah}.

6.3.4. Daily Total from instantaneous evaporation

In order to calculate the daily total evaporation from instantaneous latent heat flux, Brutsaert and Sugita(1992) used evaporative fraction approach. The evaporative fraction Λ is computed from the instantaneous surface energy balance at satellite overpass on a pixel-by-pixel basis. The instantaneous latent heat flux, λE, is the calculated residual term of the energy budget, and it is then used to compute the instantaneous evaporative fractionΛ:

$$\Lambda_{inst} = \frac{\lambda E}{\lambda E + H} = \frac{\lambda E}{R_n - G} \qquad 6\text{-}31$$

Although the sensible heat and latent heat fluxes are fluctuating strongly on daily basis, evaporation fraction behaves steadily during daytime (Bastiaanssen et al., 1998a; Crago, 1996) as result instantaneous and the integrated daily evaporative fraction can be hold similar.

$$\Lambda_{24hours} = \Lambda_{inst} \quad 6\text{-}32$$

The difference between the instantaneous evaporative fraction at satellite overpass and the evaporative fraction derived from the 24-hour integrated energy balance is marginal and may be neglected. At daily timescales, E_{24} (mmday^{-1}) can be computed as:

$$E_{24} = \frac{86400 \times 10^3}{\lambda \rho_w} \Lambda_{24} (R_{n24} - G_{24}) \quad 6\text{-}33$$

Where: R_{n24} (Wm^{-2}) is the 24-h averaged net radiation, λ [Jkg^{-1}] is the latent heat of vaporization, and ρ_w [kgm^{-3}] is the density of water, G_{24} is the net 24 hour water heat flux (Wm^{-2}).

6.4. Surface temperature retrieval from MSG

6.4.1. Background

One of the most important parameters in all surface-atmosphere interactions and energy fluxes between the ground and the atmosphere is land surface temperature (LST). It is also a good indicator of the energy balance at the Earth's surface. As such, LST is used as a parameter for a wide variety of scientific studies and agricultural applications (Caselles and Sobrino, 1989; Kimura and Shimizu, 1994; Vining and Blad, 1992). On the other hand water surface temperature is the result of the energy balance at the water surface and heat transport mechanisms within the water body. Therefore, knowledge of it is required to characterize processes at the water surface. Water surface temperature is an important water quality parameter related to biodiversity in the marine, coastal, and lake environments. Moreover, water temperatures are a key climatologic parameter. Nowadays thanks to the advancement in remote sensing observation it is possible to track this parameter at the required accuracy.

Experiments in retrieving LST have been carried out using different sensors. Most studies focus on the use of polar orbiting satellites because of their high spatial resolution (about 1 km). Examples are the National Oceanic and Atmospheric Administration Advanced Very High-Resolution Radiometer (NOAA-AVHRR) (Coll et al., 1994; Price, 1983), the Along-Track Scanning Radiometer (ATSR) (Sobrino et al., 1996), and the Moderate Resolution Imaging Spectroradiometer (MODIS) (Liang, 2001b; Wan and Dozier, 1996).

LST exhibits a strong diurnal variability that cannot be captured from polar orbiting satellites that sample each location approximately twice a day. Geostationary satellites provide diurnal coverage, and allow derivation of the LST diurnal (LSTD) cycle. Hence MSG/SEVIRI having spatial resolution of 3 km for the visible and infrared channels and temporal resolution of 15 min is an improvement.

6.4.2. Method and material used

In estimation of LST from satellite thermal data, the digital number (N_D) of image pixels needs to be converted into spectral radiance using the sensor calibration data. However, the radiance converted from digital number does not represent a true surface temperature but a mixed signal or the sum of different fractions of energy. These fractions include the energy emitted from the ground, upwelling

radiance from the atmosphere, as well as the downwelling radiance from the sky integrated over the hemisphere above the surface. Therefore, the effect of both surface emissivity and atmosphere must be corrected in the accurate estimation of LST.

Methods used to correct radiometric surface temperature for atmospheric interference fall basically into two categories as discussed in AHAS (AVHRR Hydrological Analysis System) by Parodi (2002).

- Direct methods use radiation transfer models, such as LOWTRAN and MODTRAN together with atmospheric radio soundings, satellite vertical sounders, and climatologically data.
- Indirect methods are based on split-window or in situ temperature observations.

i Split window technique

When two channels, or more, corresponding to different atmospheric transmission, are available, it is possible to use the differential absorption to estimate the atmospheric contribution to the signal. This method is known the split window technique (SWT). It has the advantage of being suitable for global applications and can be run operationally with out sophisticated ancillary data hence the method used by many researchers. The SWT relies on the different absorption characteristics of the atmosphere with two different but close wavelengths. The algorithm consists simply of a linear combination of the thermal channels, which gives a surface temperature pseudo-corrected for the atmospheric contribution. A typical split-window algorithm can be written as:

$$T_s = a_0 + a_1 T_1 + a_2 T_2 \qquad 6\text{-}34$$

Where T_1 and T_2 are the brightness temperatures at the top of the atmosphere in the two adjacent infrared bands (in the region of 10.5-12.5 μm). The coefficients a_i are suggested by different authors. The main difference between the top of atmosphere temperatures is directly linked to the difference in water vapour absorption, assuming the surface emissivities in the two channels are really identical. If these assumptions are correct, extracting surface temperature is rather straightforward. The problem is usually much more complicated as land surface characteristics are often not the same in the two bands. For water surface many studies showed that emissivity is not wavelength dependent in the thermal region hence we can apply the method without incurring considerable error. The emissivity of the surface can be calibrated from in situ measurements.

Becker and Li (1990) applied a substantial effort to determine the split window coefficients from the actual emissivity values of the two channels and these are given in the following equations.

$$a_0 = 1.276$$

$$a_1 = 3.63 + 2.068\frac{(1-\varepsilon)}{\varepsilon} + 18.924\frac{\Delta\varepsilon}{\varepsilon^2} \qquad 6\text{-}35$$

$$a_2 = -2.63 - 1.912\frac{(1-\varepsilon)}{\varepsilon} - 19.406\frac{\Delta\varepsilon}{\varepsilon^2} \qquad 6\text{-}36$$

Where $\varepsilon_{10.8}$ and $\varepsilon_{12,}$ are emissivity at channel 10.8 and 12 of SEVIRI/MSG respectively.

$$\varepsilon = (\varepsilon_{10.8}+\varepsilon_{12})/2 \quad and \quad \Delta\varepsilon = \varepsilon_{10.8} - \varepsilon_{12} \qquad 6\text{-}37$$

ii **Four channel algorithm**

The conventional SWT use two adjacent channels to account the effect of atmospheric interference in the retrieval of surface temperature. The theoretical background behind four channel algorithm is that because of the middle infrared (MIR) 3.9μm channel has low atmospheric absorption and attenuation; it can be used to improve the atmospheric correction. Sun and Pinker (2003) clearly explained that to fully utilize this characteristics, under the hypothesis adding another pair of brightness temperature difference between the 3.9 and 8.7 μm window channels ($T_{3.9}$-$T_{8.7}$) could further correct the atmospheric effects, in addition to the use of the traditional brightness temperature difference between the 10.8 and 12 μm split window channels ($T_{10.8}$-T_{12}). In this study the equation formulated by Sun and Pinker (2007) using four thermal channel of MSG has been applied and then validated with in situ measurements.

$$T_s = a_0 + a_1 T_{10.8} + a_2 (T_{10.8} - T_{12.0}) + a_3 (T_{3.9} - T_{8.7}) + a_4 (T_{10.8} - T12.0)^2 + a_5 (\sec\ \theta - 1) \qquad 6\text{-}38$$

Where T_s is the surface temperature, T is the brightness temperature, Subscripts 3.9, 8.7, 10.8, and 12.0 represent SEVIRI IR window channels 3.9, 8.7, 10.8, and 12.0 μm, respectively a_i are the regression coefficients dependent on surface types, sec θ is the secant of satellite viewing angle. While using the (MIR) 3.9 mm channel care has to be taken because it contains solar signals during the daytime, which need to be accounted for. Therefore a solar zenith angle correction (θ_s) for the MIR 3.9 mm channel during the daytime has to be incorporated and the above equation modified as:

$$T_s = a_0 + a_1 T_{10.8} + a_2 (T_{10.8} - T_{12.0}) + a_3 (T_{3.9} - T_{8.7}) + a_4 (T_{10.8} - T12.0)^2 + a_5 (\sec\ \theta - 1) + a_6 T_{3.9} \cos\ \theta_s \qquad 6\text{-}39$$

The regression coefficients, a_0, a_1, a_2, a_3, a_4, a_5 and a_6 in the above equations are calibrated based on the land cover type (Sun and Pinker, 2007). The emissivity effects are now considered through the surface type. The coefficients for water surface given as below:

Table 6-1: Coefficients for four channel algorithm

Coefficients	Day time	Night Time
a_0	-29.2629	-20.8035
a_1	1.1054	1.0907
a_2	2.2502	1.8823
a_3	0.1322	0.3357
a_4	0.1889	0.2987
a_5	464.1204	350.8949
a_6	5.75E-05	-

7. Microclimatology and in situ data analysis

7.1. In situ data analysis

A field campaign has been carried out to collect different microclimatological data and in situ measurements in and around the lake. The analysis, result and discussion of the measurements are presented as follows:

7.1.1. Radiation budget

The incoming and outgoing short wave radiation was measured by using net radiometer and from this measurement we can calculate the surface albedo as well as net short wave radiation. As shown from the graph (see Figure 7-2) the first day was clear sky. However the second day was very cloudy. For validation of remote sensing analysis the first day of measurements was a golden day. For the sake of comparison between two sensors, the incoming solar radiation was also measured on the land surface near the lake at Woreta weather stations. The solar radiations measured by the two sensors have good correlation (see Appendix E, Figure E-3)

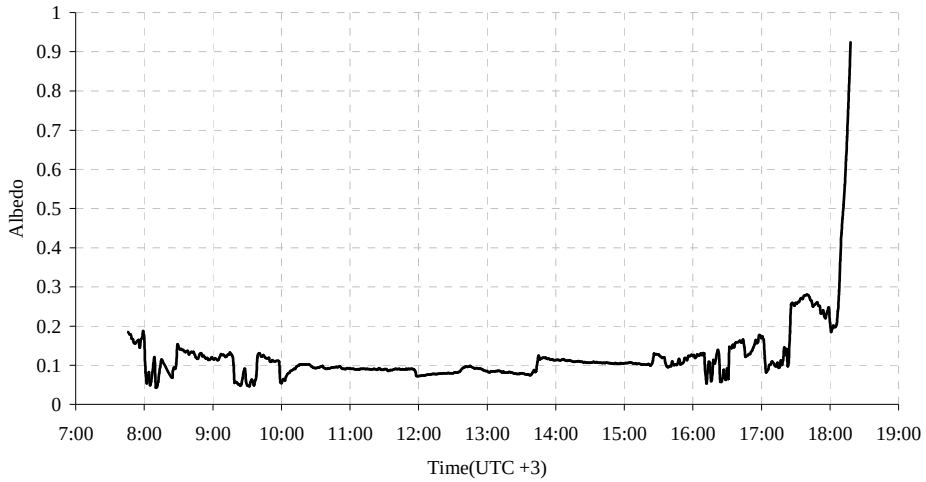

Figure 7-1: Albedo of Lake Tana on 27th of September 2008

The albedo of the water surface is estimated from the incoming and outgoing short wave radiation. Generally the albedo of a surface depends on both the reflective properties of that surface and on atmospheric parameters which can alter the spectral distribution of incident irradiance. As can be noted from the graph (Figure 7-1) the albedo of the water surface is not constant. In particular it depends upon the angle at which the direct beam strikes the surface. With cloudless skies and higher solar altitude, water is one of the most absorbing surfaces. When the sun is close near sunrise or sunset the reflection is specular. Under cloudy skies the diffused solar radiation forms a large portion of incoming solar radiation and the effect of solar elevation angle is completely damped. The altitude dependence is also modified by the roughness of the water surface (wave action)

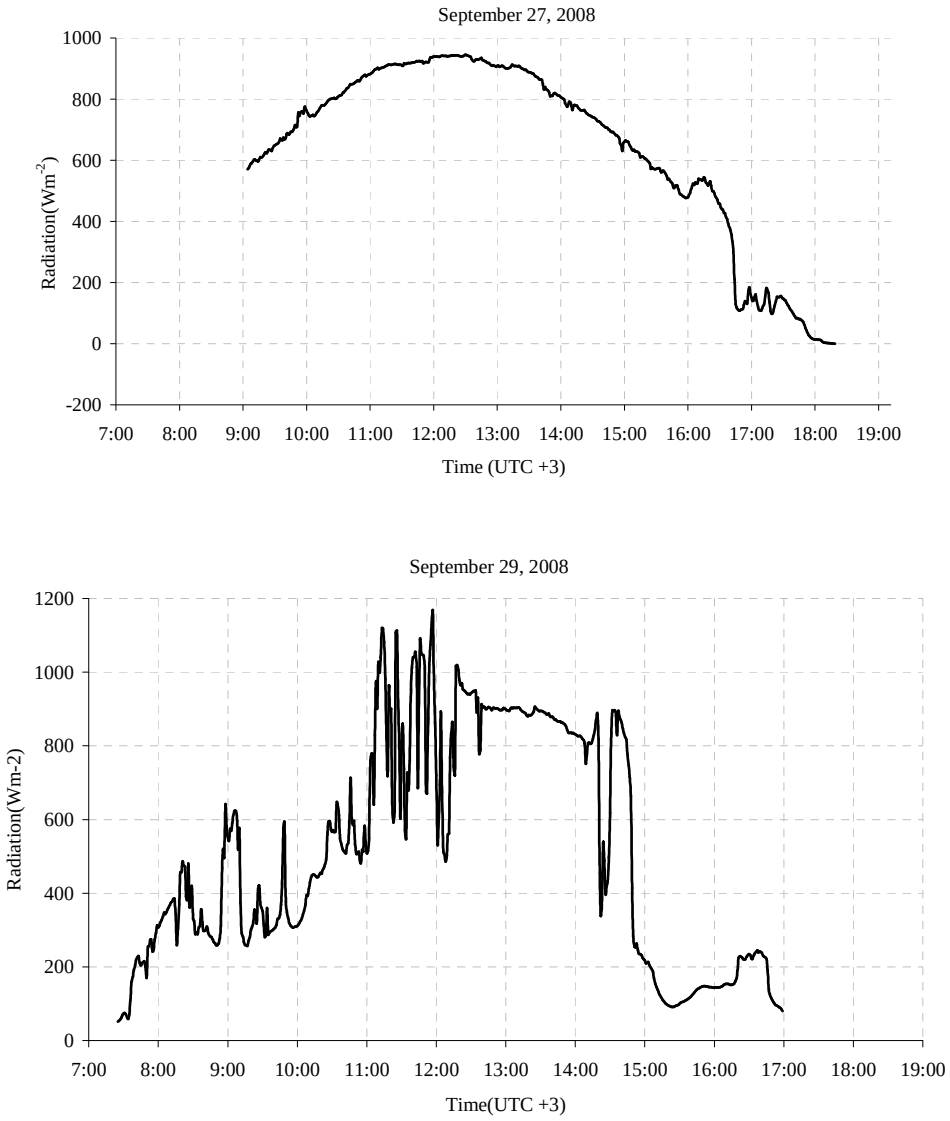

Figure 7-2: Net shortwave radiation measured on 27th and 29th of September 2008

Net radiative flux is dominated by incident solar radiation, modulated by surface albedo and cloud cover. It is also dependent on downward long wave radiation as a function of atmospheric temperature, humidity, and cloud cover, and on surface temperature-dependent upward long wave radiation. As we can see clearly from Figure 7-3 the net radiation is dominated by net shortwave radiation. The net long wave radiation for the two days as shown in the figure below is more or less constant throughout the day which implies the surface temperature of the lake does not vary considerably. The satellite overpass time for Terra/MODIS is at 11:15 local time indicated in the figure below on September 27, 2008.

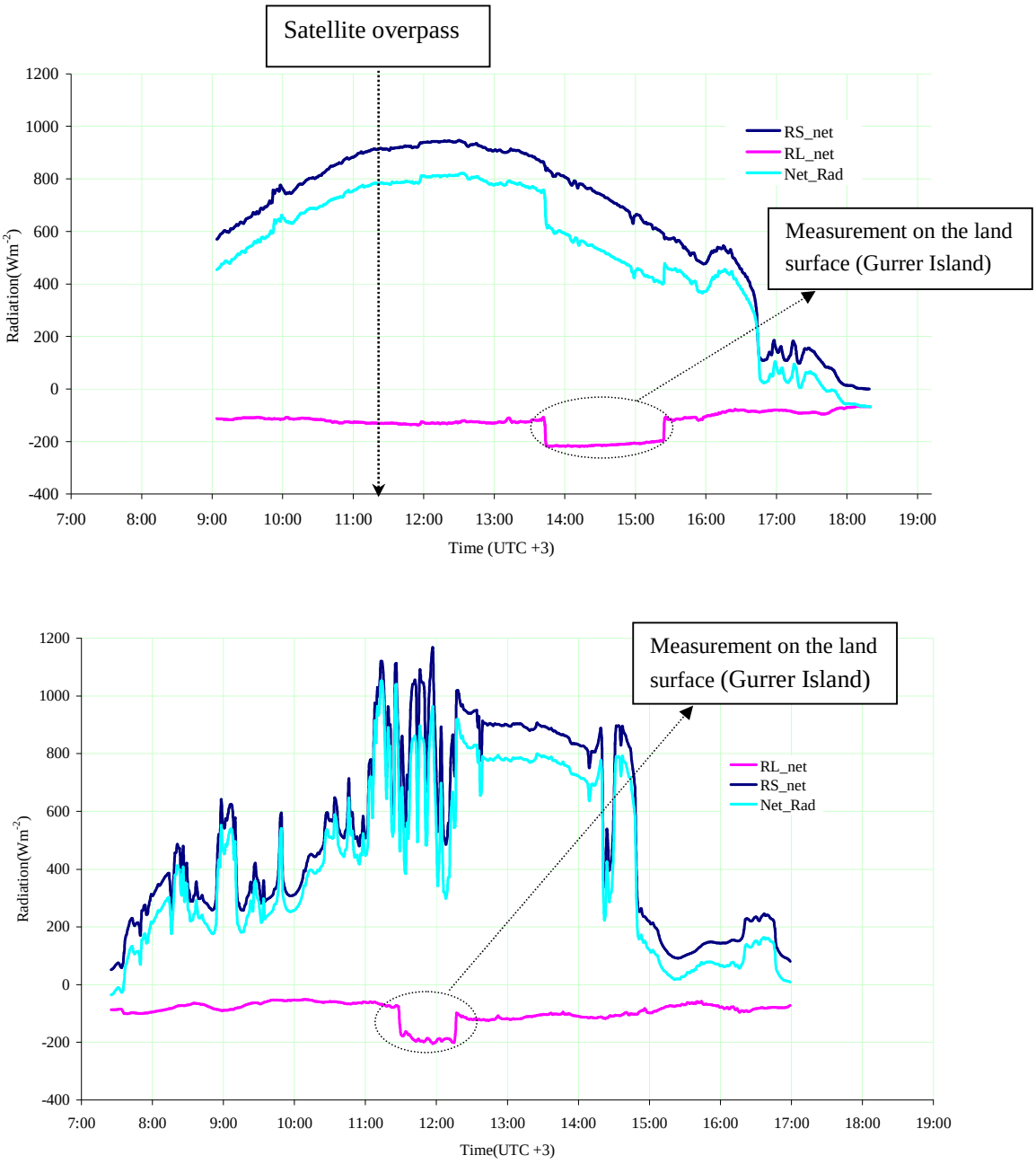

Figure 7-3: Net radiation measured on September 27 (up) and 29 (down), 2008

Figure 7-4 shows the relative humidity and air temperature measurement on the lake using HMP45C sensor. Relative humidity is usually high at midnight and early in the morning, drops rapidly after the sun rises, until it is lowest just after midday. However the temperature behaves the other way round. The reason behind inverse relation between RH and air temperature is that warm air has the potential to hold more water vapour than cool air. By definition RH is the ratio of amount of moisture to maximum amount that could be contained hence if the moisture in the air remains unchanged and temperature rises, the maximum amount of moisture that the air could hold increases. However the

absolute humidity calculated using Equation shown in Appendix B is directly proportional to the air temperature and it does not fluctuate too much.

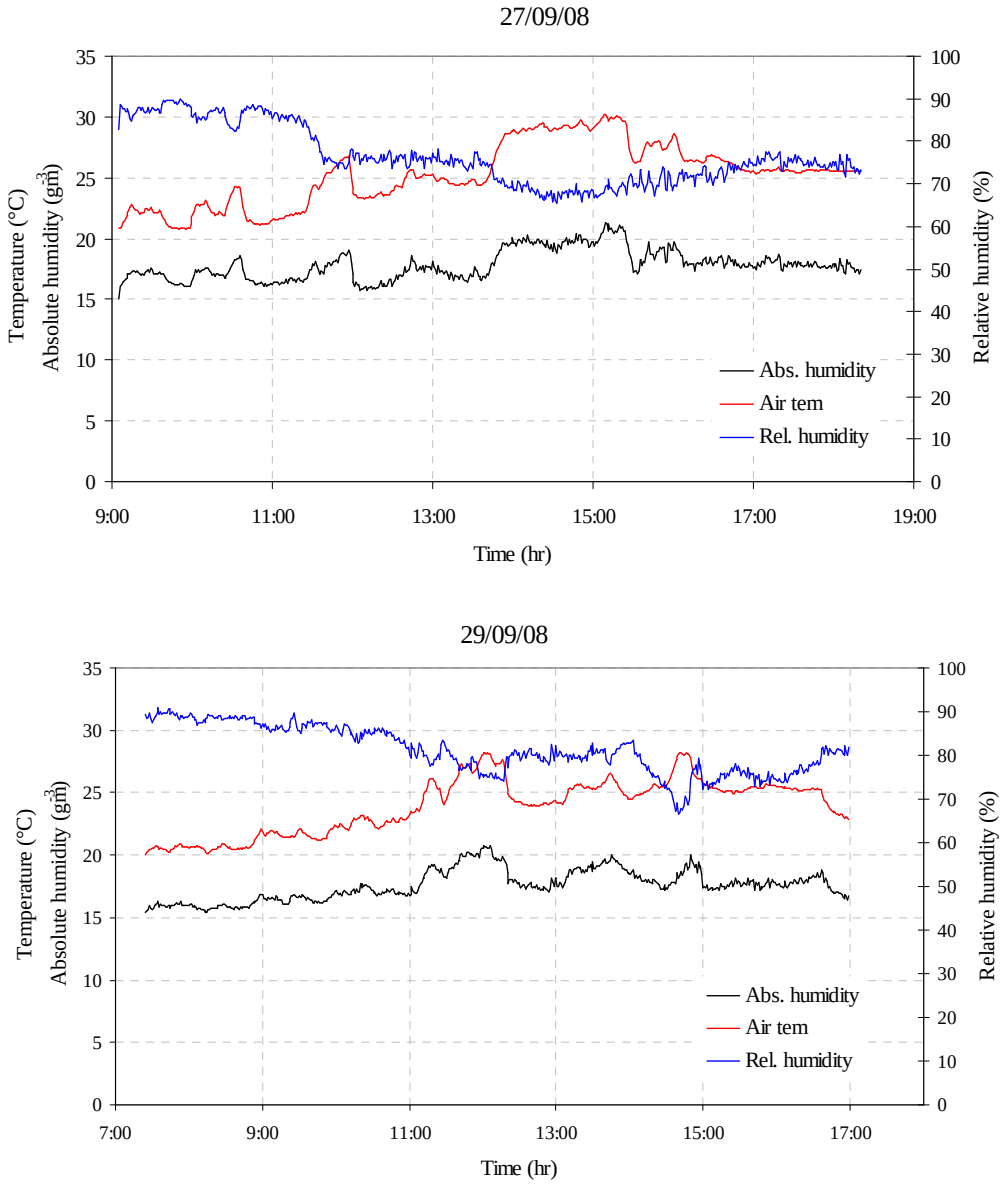

Figure 7-4: Relative humidity and air temperature measurements using HMP45C

7.1.2. Bowen ratio

A Bowen ratio is a dimensionless quantity which measures the ratio of the turbulent flux densities of sensible heat to latent heat. Such a quantity is important to understand because knowledge of this variable quantifies the relative magnitudes of surface energy expenditure to heat the air and to evaporate water, and has been widely used in evaporation estimation. In this study the Bowen ratio is calculated for day time periods from in situ measurements of air temperature, surface temperature, and vapour pressure deficit. The scatter plot of Bowen ratio for the two days of measurements shown in Figure 7-5. The Bowen ratio is higher in morning hours, this is because the temperature difference

between the surface and the air was higher during those periods. In the afternoon it is getting lower even negative because the air become wormer than the surface and also the temperature difference was minimal.

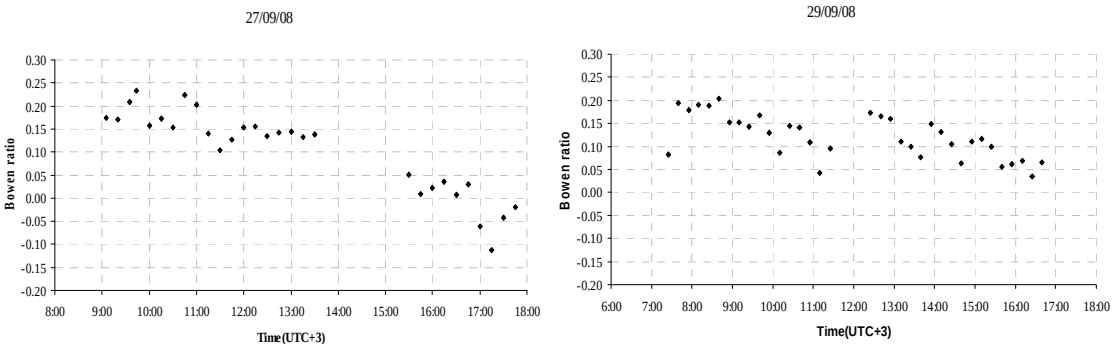

Figure 7-5: Scatter plot of Bowen ratio for day time on September 27th and 29th of 2008.

7.1.3. Turbulent heat flux

The contribution of sensible heat flux in the energy balance of the surface is estimated from eddy covariance measurement as explained in Chapter 6, Section 6.2. From EC data processing and ECPack calculation it can obtain wind speed in three orthogonal directions along with friction velocity, sonic temperature and sensible heat flux. The outputs of ECPack daytime sensible heat flux for 27th September 2008 are presented in the appendix G, Table G-1. The interval files used in the ECPack software are annexed in appendix G_II. The average of vertical wind speed for each interval is close to zero which fulfils one of the assumptions of eddy covariance principles. The diurnal cycle of aerodynamic resistance is calculated using Equation 6-30 from mean wind speed measurements of sonic anemometer. The scatter plot of sensible heat fluxes on 27th of September 2008 shown in Figure 7-6. The calculated sensible heat flux as compared to the net radiation is very low which implies the net radiation is mainly consumed by the latent heat flux and also used to heat up the water as water heat flux.

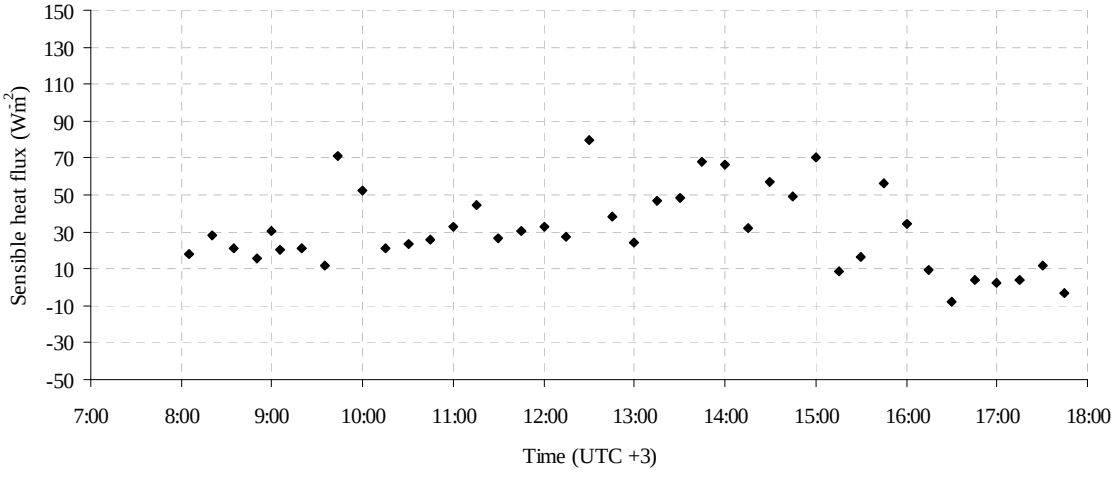

Figure 7-6: Scatter plot of diurnal cycle of sensible heat flux on 27th of September 2008.

The latent heat flux can be estimated directly from EC data measurement. However during the field campaign we didn't collect krypton hygrometer measurements of water vapour density, hence the latent heat flux is estimated from Bowen ratio. The calculated latent heat fluxes are shown in the appendix E, Table E-3 and E-5 for the first and second days respectively.

7.1.4. Water heat flux

The analysis of heat transport in the water bodies requires detailed spatial and temporal temperature data. However these data are lacking for Lake Tana at the required spatial and temporal scale. During field campaign temperature profile measurements on the lake was taken for two days. The first day (27th of September 2008) is shown in Figure 7-8. The figure revealed that temperature variation in all measurement periods hardly vary except at the midday. The temperature of the water body increases from morning to midday and again decreases in the afternoon time and comes to the same morning temperature. Temperature measurements were also taken at a depth of 3 m using diver (see Figure 7-7). The measurements show that water temperature is fairly constant through out the day hence there is no heat storage at lower depth detectable at the daily time scale.

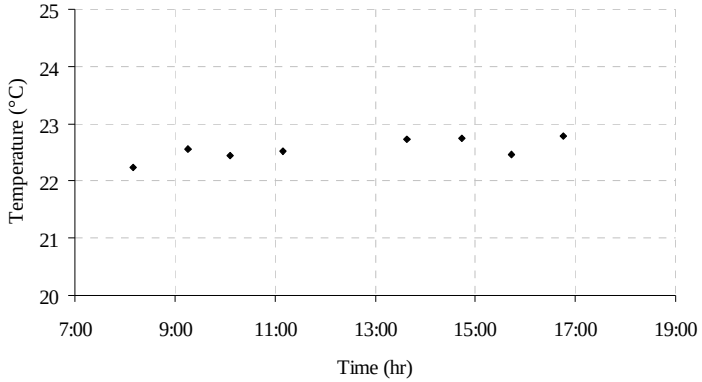

Figure 7-7: Temperature of water at 3 m depth from the surface

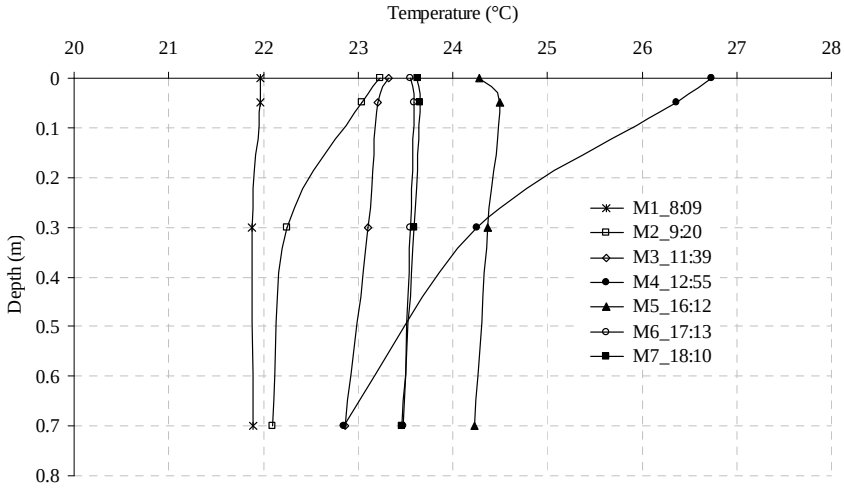

Figure 7-8: Temperature profile at different locations on the lake (refer Figure 4-2 to see the location of sampling points)

Due to the limitations of available data to apply the formula presented in Chapter six (Equation 6-24 and 6-25), it is difficult to calculate the instantaneous water heat flux from temperature profile observation. However since the net radiation, sensible heat flux and Bowen ratio are already calculated, it is possible to estimate the instantaneous water heat flux as a residual of energy balance (see Equation 6-27). The calculated water heat fluxes are plotted on Figure 7-9 and 7-10 for the first and second days respectively. Heating and cooling do occur on an annual scale (Gieske et al., 2008). However the effect is too small to detect on time scale of one day.

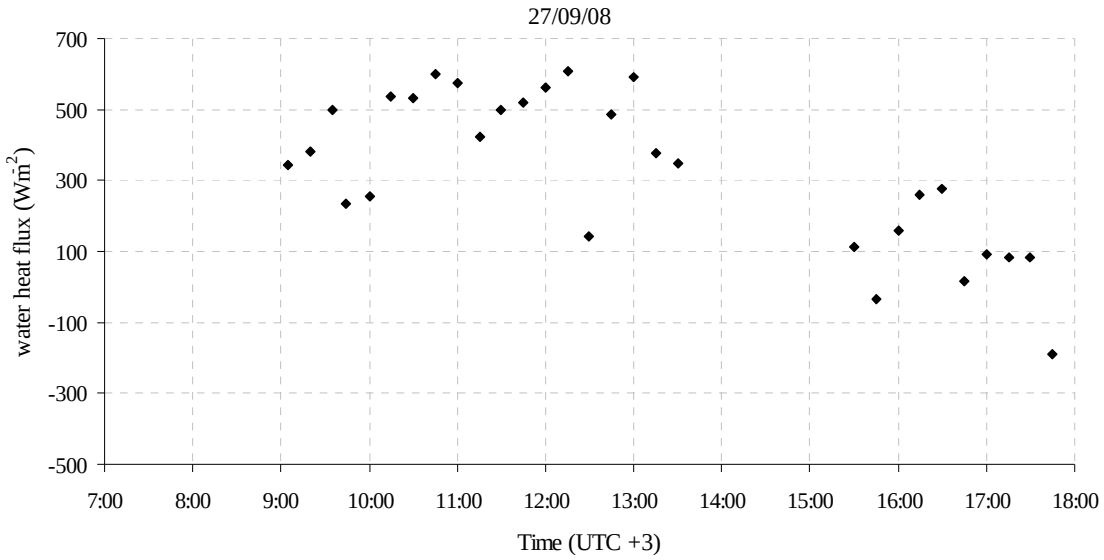

Figure 7-9: Scatter plot of water heat flux on 27th of September 2008

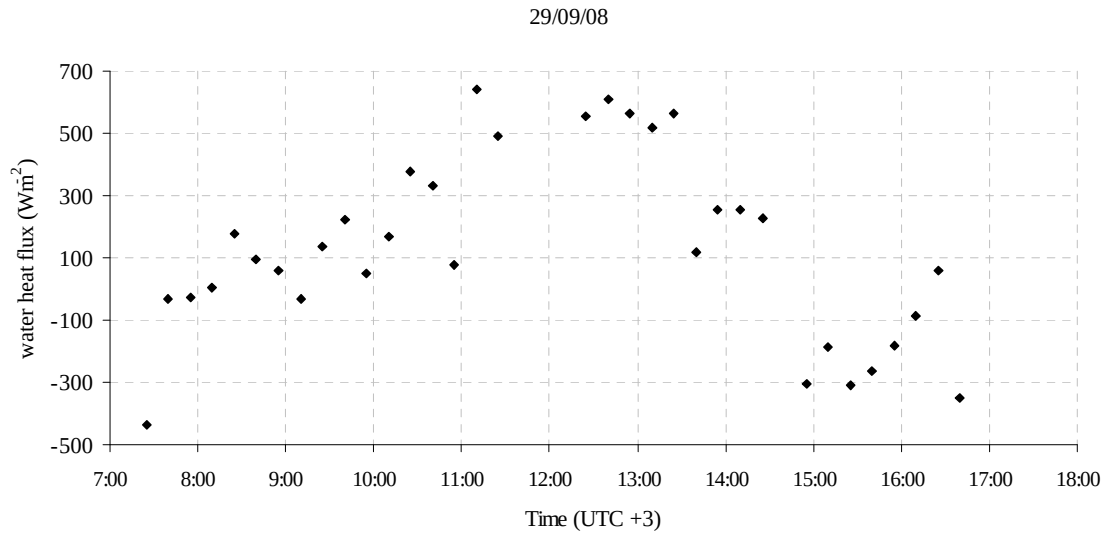

Figure 7-10: Scatter plot of water heat flux on 29th of September 2008.

7.2. Long-term average estimate of daily evaporation

In order to calculate long-term average daily, monthly or seasonal variation of evaporation, time series measurements of meteorological data are required over the lake surface. However there are no direct (over water) meteorological measurements for Lake Tana hence data from the lakeshore station (Bahir Dar) are used. Daily meteorological was collected for the period of 1995 to 2007 and processed for missing and inconsistent data.

The long-term trend of meteorological data at Bahir Dar station shown in Figure 7-11.The incoming solar radiation is the major source of energy for evaporation processes which depends on cloud cover and day of the year. The cloud cover also affects the difference between maximum and minimum temperature in such a way that on a cloudy day (less sunshine hours) it has a lower value than on sunny days (higher sunshine hours).

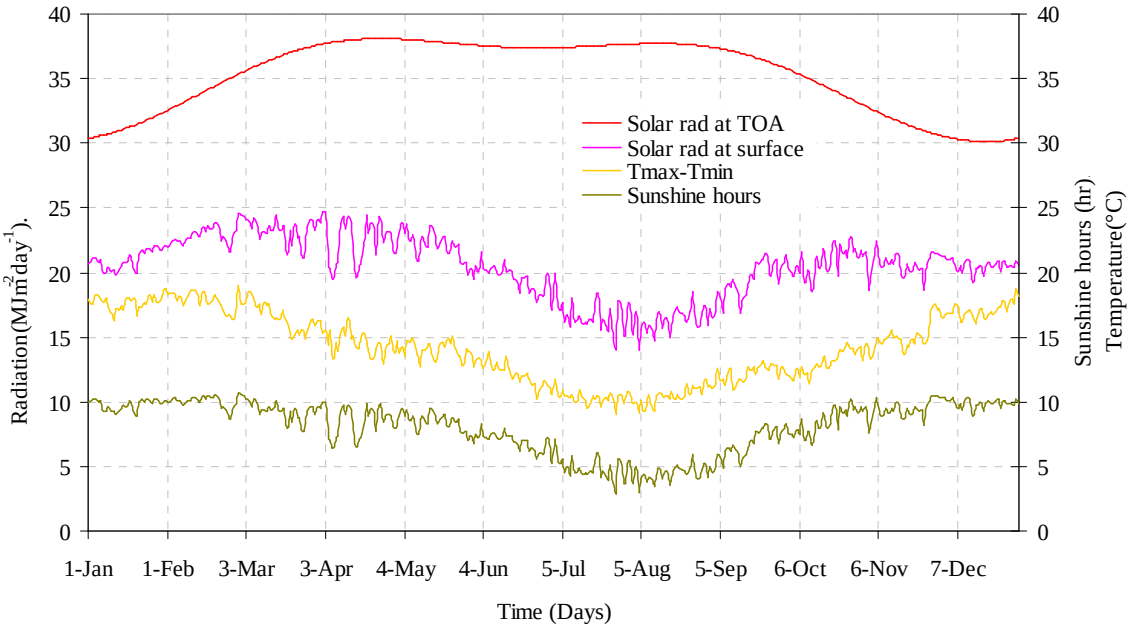

Figure 7-11: Long term average (1995-2007) trend of meteorological data (Bahir Dar station)

In order to calculate the net short wave radiation we need to have the surface albedo. Due to the fact that albedo is one of the most important parameters in the energy balance of the surface hence it is very important to track the spatial as well as temporal variability. However using point observation it is difficult to map the spatial variability. The spatial as well as temporal variability can be derived from satellite observation. In this study I retrieved the annual cycle of albedo from MODIS/Terra surface reflectance products (from October 2007 to September 2008) as explained in Chapter 6, Section 6.1.1.

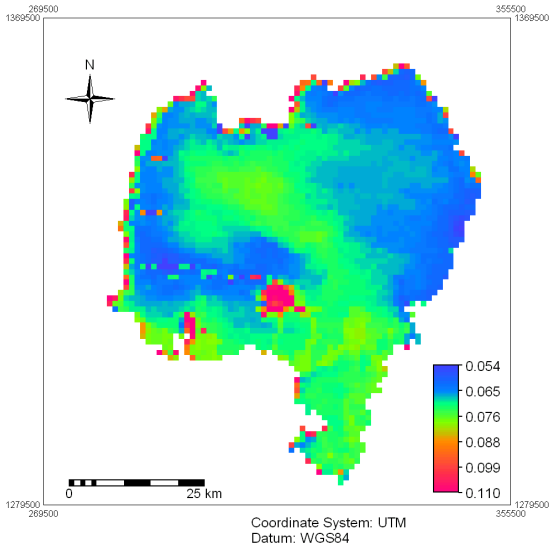

Figure 7-12: Albedo of Lake Tana on October 2007

One interesting observation from the annual cycle of albedo is that there is clear temporal and spatial variability which shows the surface characteristics of the water in the lake. The temporal variability can be explained by the occurrence of rainy season in the area (June-September) is associated with flash flood entering the lake which increase the suspended sediments abruptly and result in a sharp increase on the reflectance (from 0.07 to 0.16) of the water. The average albedo during in situ measurement on 27th of September 2008 as shown in Figure 7-1 is 0.09, which is in the range of the calculated annual cycle of albedo.

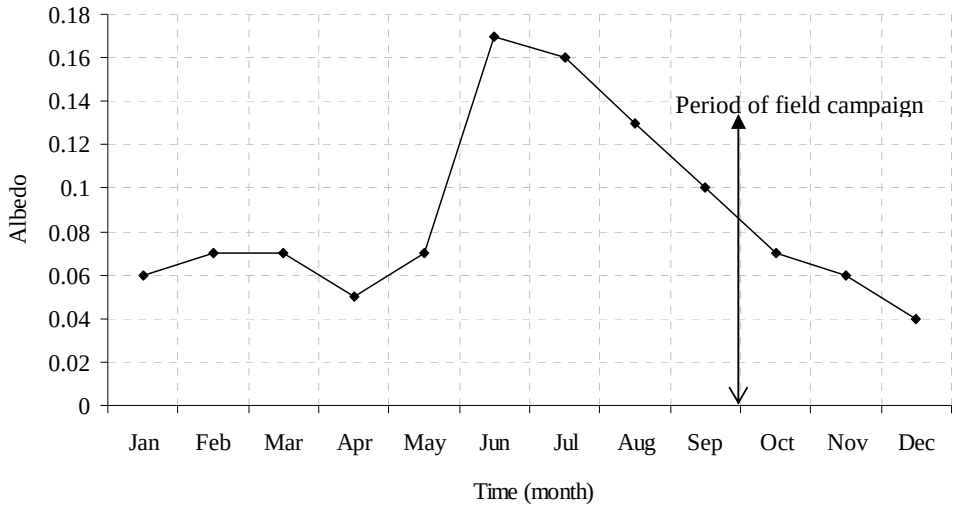

Figure 7-13: Annual cycle of albedo for Lake Tana (2007/2008)

The daily evaporation from long-term average meteorological data for Lake Tana was estimated by four different methods, (Vallet-Coulomb et al., 2001), Penman-Monteith, Bowen ratio energy balance, and Maidment,1993.

Vallet-Coulomb et al. (2001) used the Penman combination approach as described in Chapter six and the Penman's functions of wind speed estimated empirically from wind speed and vapor pressure deficit. In Penman-Monteith (Allen et al., 1998) method, the stomata resistance (r_s) for open water is zero as well as Z_{om} is 0.00137and the aerodynamic resistance calculated using Equation 6-30. The Penman combination formula after Maidment (see Equation 6-11) can also be used for open water evaporation estimates. However this method overestimates evaporation for large lakes by 10-15% (Maidment, 1993) as can be seen from Table 7-1. It might be better suited for evaporation pan and small ponds.

The lake energy balance method is one of the best methods for lake evaporation estimation as inferred by different authors. After simplification of the lake energy balance equation the daily evaporation can be estimated from net radiation and Bowen ratio (refer to Equation 6-6). For a lake surface, the Bowen ratio is generally estimated from measurements of air temperature, humidity, water surface temperature at the required time steps. However since there is no long-term record of surface temperature measurement for Lake Tana, it is difficult to come up with good estimate of Bowen ratio. Researches shown that in a given environment, the Bowen ratio is generally controlled by the water availability of the surface, since this is not a limiting factor in the lake surface; it is possible to assume a value from similar studies of lake evaporation. A constant Bowen ratio of 0.2 for Lake Tana is used for annual evaporation estimation.

Previous studies on Lake Tana (Abeyou, 2008; Kebede et al., 2006) used a constant albedo of 0.06 for annual evaporation estimation, however in this research monthly albedo from MODIS satellite imagery are calculated and used. The variation of using monthly albedo and constant albedo of 0.06 are presented in Table 7-1. The effect of using constant albedo is to over-estimate evaporation during rainy season as shown in Figure 7-14. However according to this research the albedo of the lake during rainy season is higher than 0.06 which reduces evaporation from the lake during those periods.

Table 7-1: Monthly evaporation by different methods

	Method							
	Vallet-Coulomb		Maidment		Penman-Monteith		Energy balance	
Month	monthly α	constant α	monthly α	constant α	monthly α	constant α	monthly α	constant α
Jan	131.87	131.87	164.12	164.12	128.70	128.70	151.66	151.66
feb	138.97	140.94	176.09	178.06	135.39	137.35	154.67	156.93
Mar	160.40	162.45	203.69	205.73	156.30	158.34	174.65	176.95
Apr	160.65	158.70	202.05	200.10	156.80	154.85	172.82	170.66
May	159.61	162.30	195.33	198.01	156.25	158.94	172.68	175.67
Jun	120.81	140.13	143.42	162.73	118.69	138.01	134.12	156.02
Jul	108.60	123.60	124.93	139.93	107.04	122.05	123.47	140.82
Aug	110.93	121.13	125.89	136.09	109.49	119.69	126.56	138.37
Sep	127.93	134.54	145.86	152.48	126.20	132.81	145.15	152.77
Oct	143.97	145.84	169.29	171.16	141.55	143.41	161.46	163.60
Nov	131.32	131.20	159.06	158.94	128.63	128.51	148.74	148.59
Dec	132.31	128.63	162.34	158.66	129.35	125.67	152.09	147.75
Total	1627.37	1681.32	1972.07	2026.02	1594.39	1648.34	1818.08	1879.79

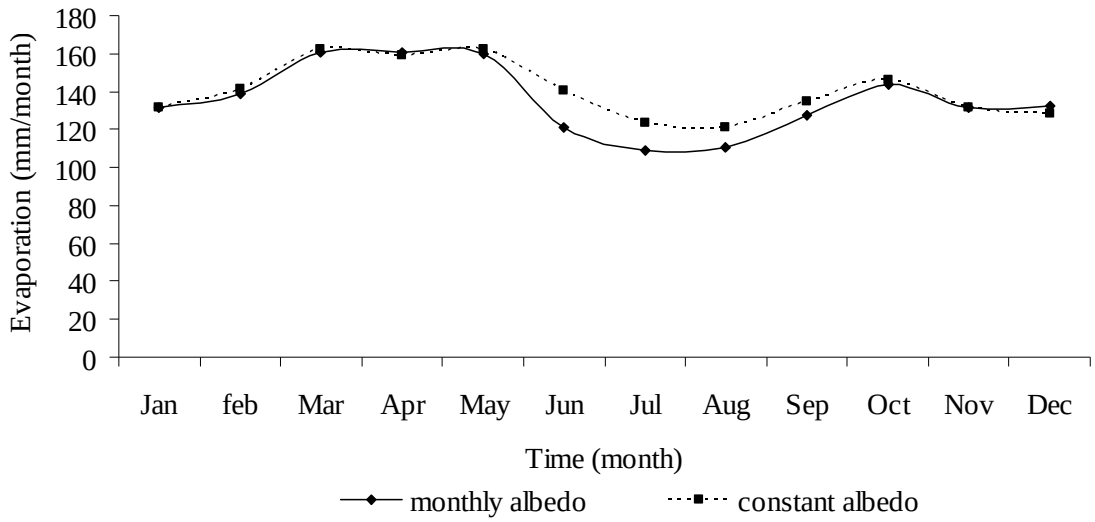

Figure 7-14: Monthly evaporation by Vallet-Coulomb method

7.3. Sensitivity analysis of annual lake evaporation

To understand the significance of different meteorological parameters used in open water evaporation estimation methods a sensitivity analysis has performed. Rigorous uncertainty calculations would be unrealistic because all methods include assumptions and empirical equations and coefficients whose associated errors are difficult or impossible to estimates as well as uncertainties on measured parameters are unknown. However, the consistence of the result can be discussed through sensitivity analysis of the energy and Penman open water methods to their respective input variables: measured data (air temperature (T_air), relative humidity (RH), and wind seed (WS)), short wave radiation (inferred from measurements of daily sunshine duration (SH) and local calibrated parameters) and Bowen ratio.

The influence of individual input variables on evaporation estimates for each method is analyzed by increasing or decreasing of 10% of its value. The analysis shows that both energy balance and Penman are most sensitive to shortwave radiation, which is the energy source of evaporation. The energy balance method is more sensitive to this parameter. The change in evaporation rates induced by a 10 % change of shortwave radiation is 4.96 % and 4.68 % for energy balance and Penman methods respectively. The incoming shortwave radiation uncertainty comes from both the measurement of daily sunshine duration and from the empirical coefficients used in Equation 6-3. Variation in relative humidity influence evaporation rates calculated with Penman method (through the saturation deficit) which is up to 1.28%. Taking into account the fact that the relative humidity data are measured on land based meteorological stations and the uncertainty associated with measurement, its sensitivity to the method is not significant. Uncertainties on wind speed data affect the Penman evaporation rate, but this variable has rather low influence.

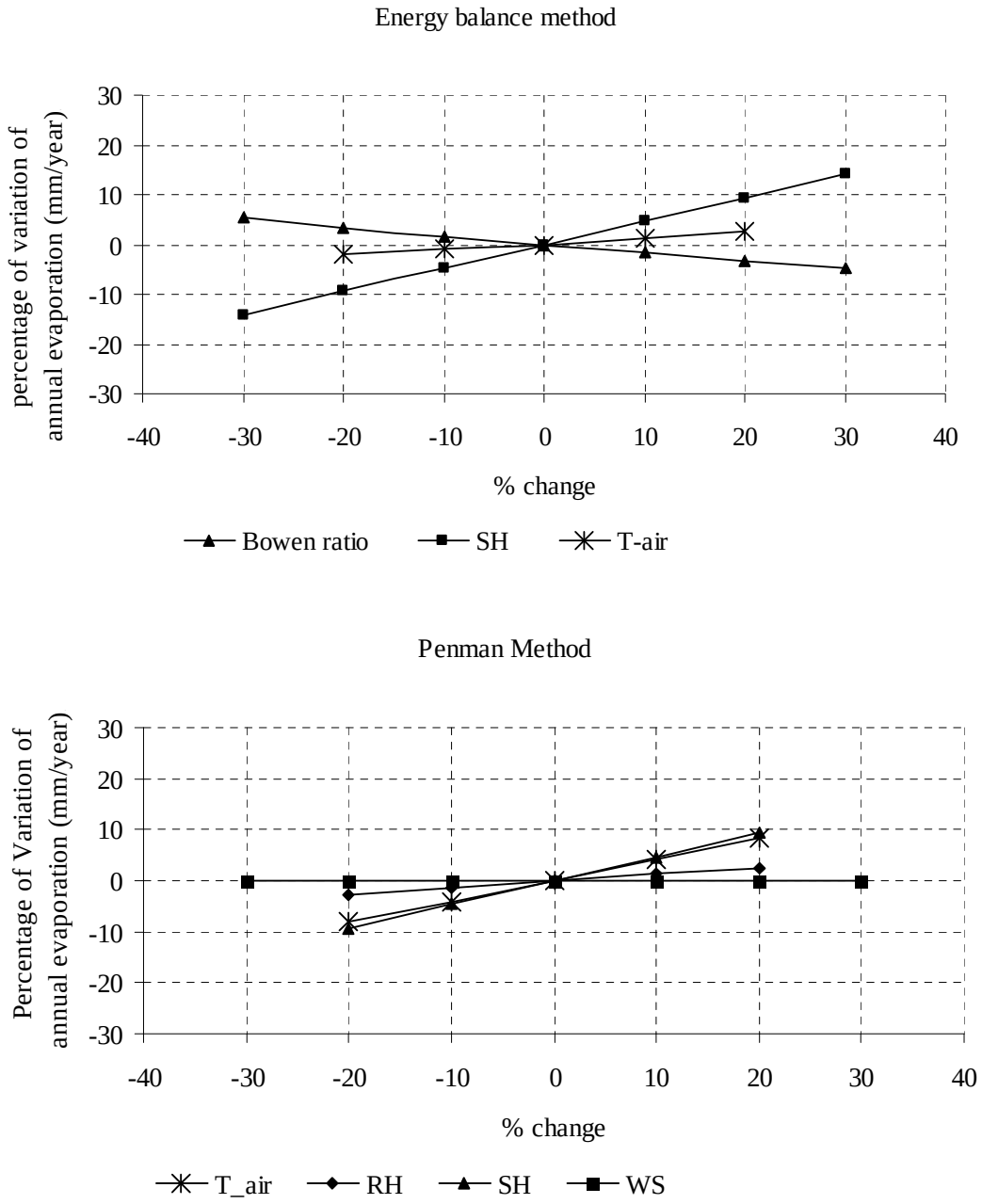

Figure 7-15: Sensitivity analysis of annual lake evaporation using E-B and P-M.

Air temperature is also a variable common to both methods. In the energy balance method, it appears only through the calculation of long-wave radiation (see Equation 6-5) and it doe not significantly influence the evaporation rate (1.2%). In the Penman method it appears, in addition to the calculation of the slope of saturation vapour pressure but also in the vapour pressure deficit and the sensitivity of this method to temperature is relatively large (4.1%). A 10% variation of the Bowen ratio, used in the energy balance method, only slightly changes the annual evaporation estimates (1.7%). However, the Bowen ratio was not measured for the entire period of the year and uncertainty greater than 10 % can be suspected. Assuming that its value ranges reasonably between 0.14 and 0.26 (± 30 %), the associated error in the evaporation rate would be less than 5%.

8. Remote sensing data analysis and result

8.1 Net radiation from MODIS

Net radiation is the difference between the incoming and outgoing radiation fluxes including both long-and shortwave radiation at the surface of the earth. Remote sensing provides an unparalleled spatial and temporal coverage of land surface attributes, thus several studies have attempted to estimate net radiation (or its components) by combining remote sensing observations with surface and atmospheric data. In this study the method described in chapter 6, section 6.3 applied to estimates the net radiation from Terra MODIS satellite.

The earth surface albedo is the most important parameter to estimate short wave radiation. It can be obtained by combining the narrow band spectral reflectance as explained in section 6.1.1. Figure 8-1(left) shows the retrieved albedo map for Lake Tana on 27th of September 2008. From this instantaneous observation the albedo of lake varies between 0.05 and 0.07. However in a very few parts of the lake the albedo values are higher due to cloudy pixels. The net short wave radiation was estimated using Equation 6-22. The solar constant (S_o) of 1367Wm^{-2}, the atmospheric transmittance of in the visible spectrum (C_t) is calculated from the diurnal cycle of in situ measurement of instantaneous incoming solar radiation and extra-terrestrial short wave radiation (see Appendix E, Figure E-6).The atmospheric transmissivity at the time of satellite overpass obtained as 0.77 while the average of the day is 0.8. Higher value of atmospheric transmissivity is due to high elevation of the area. The solar zenith angle obtained from MODIS product or it can be calculated using standard procedure shown in Appendix B.

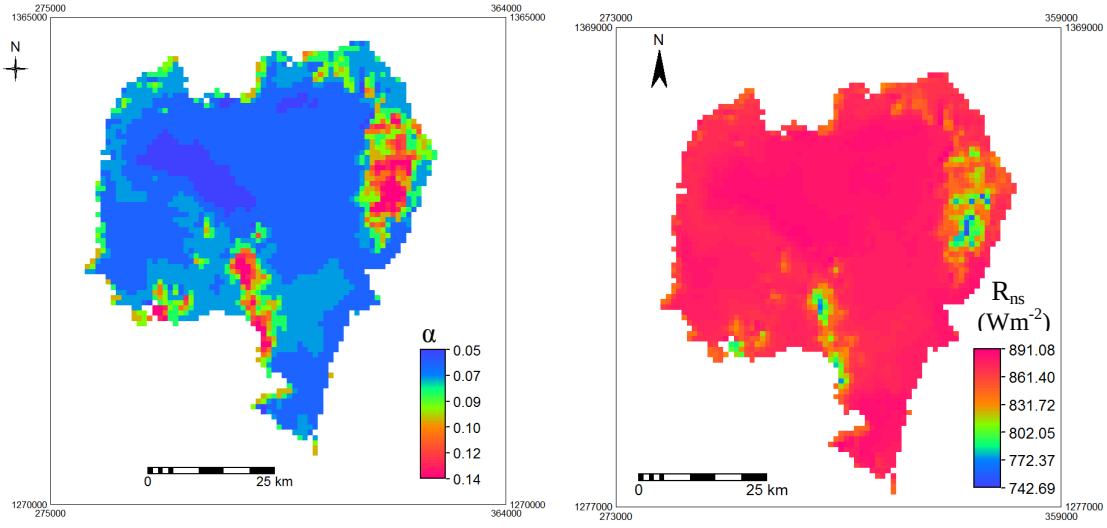

Figure 8-1: Instantaneous albedo (left) and net short wave radiation (Wm^{-2}) (right)

The net long-wave radiation is a balance between the long wave radiation from the atmosphere towards the surface and the long wave radiation emitted from the surface into the atmosphere. However the two components are difficult to separate from each other, which mean they are interdependent. The net long wave radiation can be calculated from the local meteorological observation and remotely sensed data. Therefore to obtain the net long wave radiation, the retrieval of

surface temperature T_S and emissivity ε from remotely sensed data is very important. In this study I make use of an emissivity product from TERRA/MODIS, i.e. narrow band emissivity of band 31 and 32 to calculate the broad band emissivity and further for retrieval of surface temperature. Daily surface temperature product (MOD11A1) of September 27th 2008 is used for computation of net long-wave radiation. The method presented in Chapter 6, Section 6.3 is used for calculating net long wave radiation. The formula requires air temperature, surface emissivity, and vapour pressure of air and surface temperature which can be obtained from in situ measurements. The air temperature during satellite overpass (11:15 local time) is obtained from ground measurement on the lake during field campaign (T_a=295.18 K) and assumed homogenous over the lake. Emissivity of the water is calculated from in situ measurements of outgoing long wave radiation and surface temperature measurements as well as from MODIS narrow band emissivity products (see Appendix E, Table E-1 and Figure E-3)

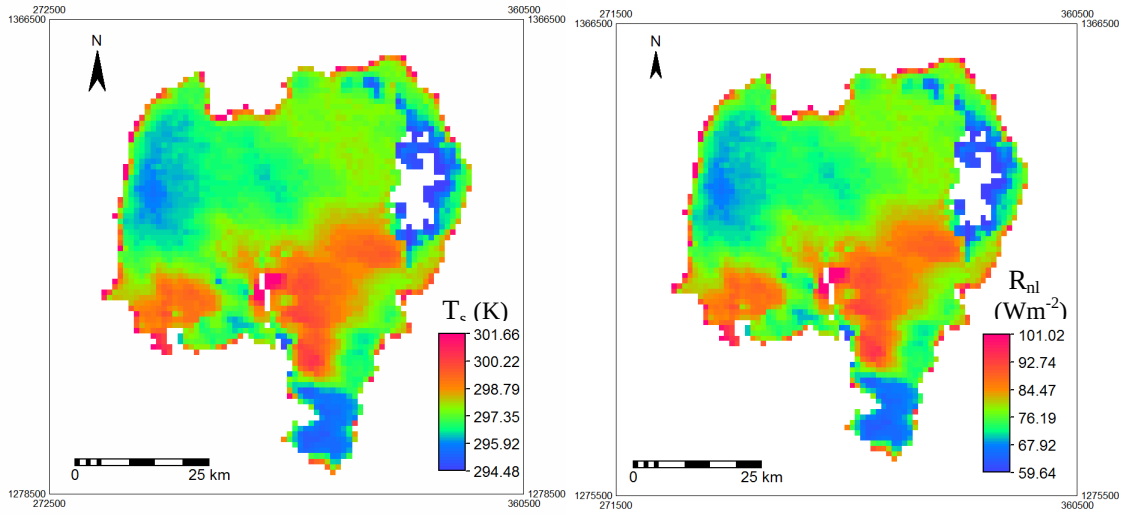

Figure 8-2: Surface temperature (K) (left) and net long-wave radiation (Wm^{-2}) (right)

An area of 4 x 4 pixels has been taken around the point observation of in situ measurements and comparison was made between the results of remote sensing data analysis as shown in Table 8-1. As presented in Figure 7-3 (27th of September 2008) the instantaneous net radiation of in situ measurements during satellite overpass is 777 Wm^{-2}. From remote sensing data analysis the pixel value which corresponds to the in situ measurement is 791 Wm^{-2}.

Table 8-1: Comparison of instantaneous in situ measurements with remote sensing

Paramter	In situ	Remote sensing		Unit
		Mean	STDEV	
Albedo	0.09	0.06	0.00	[ ]
Surface temperature	298	299	0.36	K
Net long-wave radiation	130	87	2.06	Wm^{-2}
Net short-wave radiation	907	877	2.10	Wm^{-2}
Net radiation	777	791	2.82	Wm^{-2}
Sensible heat flux	44	39	3.58	Wm^{-2}
Latent heat flux	315	327	6.22	Wm^{-2}

The comparison of in situ measurement of net long wave radiation with remote sensing data shows some difference. This is because the accuracy of long wave radiation calculated from satellite measurements depends on the accuracy of surface temperature and also empirical constants used in the model.

The sensible heat flux on the lake directly estimated from EC data analysis. The spatial map of sensible heat flux is produced from combination of ground measurements and remote sensing observations. To solve Equation 6-28 the surface temperature retrieved from remote sensing is used. The aerodynamic resistance calculated using Equation 6-30 from wind speed at measurement height and water surface roughness, Z_{om} of 0.00137 is taken.

The latent heat flux calculated from in situ measurements of sensible heat flux and Bowen ratio compared with the residual of energy balance from remote sensing data analysis. The instantaneous water heat flux during satellite overpass from in situ measurements was 423 Wm^{-2} (see Appendix E, Table E-3) used in the energy balance equation to estimate latent heat flux.

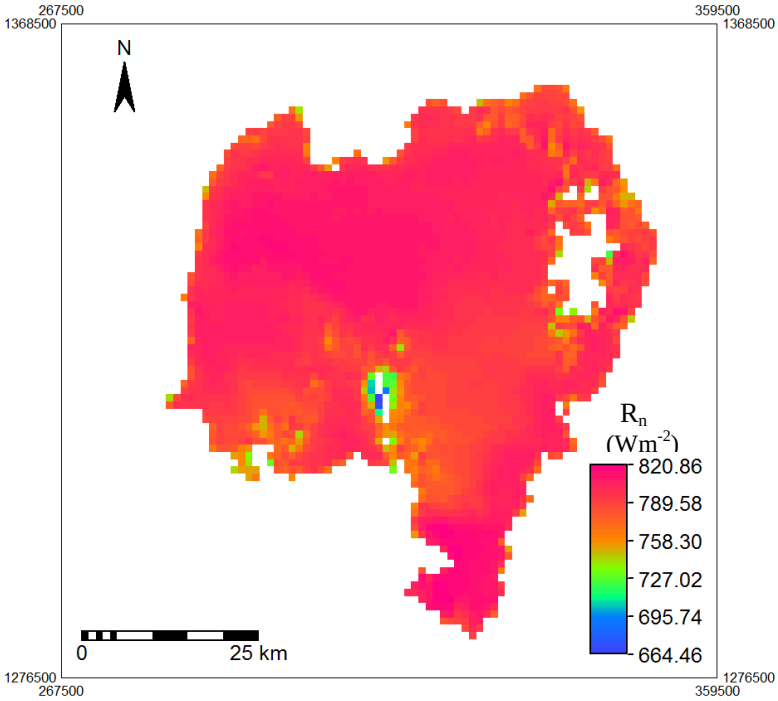

Figure 8-3: Net radiation (Wm^{-2}) on 27th of September 2008 at 11:15 local time

8.2 Daily evaporation from MODIS and in situ measurements

Many agricultural applications and water balance models need daily evaporation estimates instead of instantaneous. To find the daily total evaporation from the instantaneous latent heat flux, the evaporative fraction approach was used. Evaporative fraction is the ratio of energy used for the evaporation processes and the total amount of energy available for evaporation. Therefore in order to

calculate instantaneous evaporative fraction each components of the energy balance has to be determined in advance.

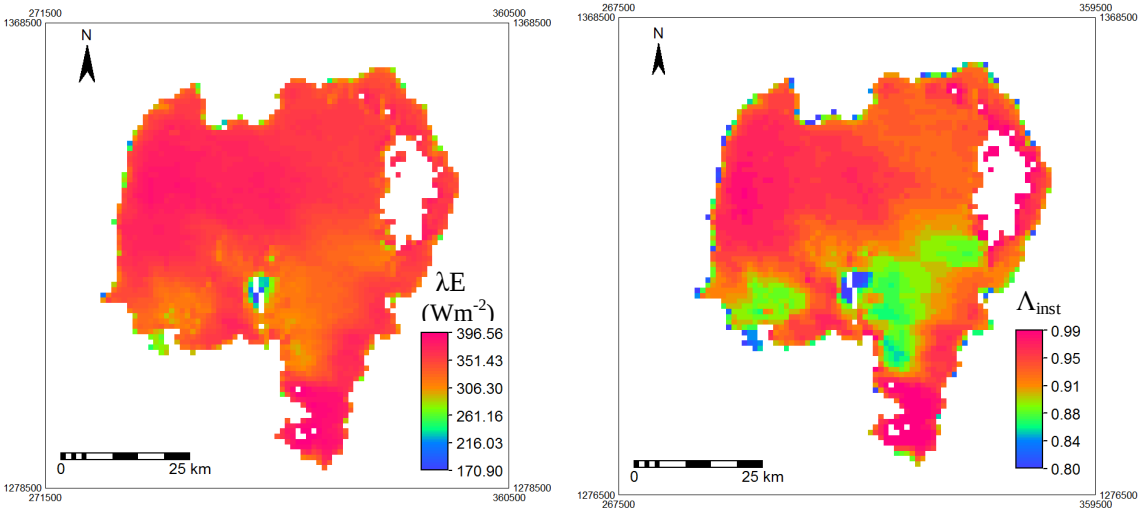

Figure 8-4: Instantaneous latent heat flux (Wm^{-2}) (left) and evaporative fraction (right)

Since the net radiation, sensible heat flux and water heat flux are already estimated. The instantaneous latent heat flux can be calculated as the residual of energy balance as shown in the Figure 8-4 (left). The instantaneous evaporative fraction (Λ_{inst}) shown in figure 8-4 (right) derived from the ratio of energy used for the evaporation processes to the total amount of energy available for evaporation.

The daily (or Λ_{24}) evaporative fraction estimated from the assumption of instantaneous and the integrated daily evaporative fraction holds similar although the sensible and the latent heat fluxes are fluctuating strongly on a daily basis. The daily evaporation, E_{24h} is calculated using equation 6-33 presented in chapter six. The daily net radiation for 27th of September, 2008 calculated from standard meteorological measurements using equation shown in Appendix B.

Figure 8-5 shows the daily evaporation map of Lake Tana calculated using evaporative fraction approach on 27th of September 2008 and its mean and standard deviation are 4.94 mm/day and 0.20 mm/day respectively. The daily evaporation estimated from remote sensing observation can be compared with the daily long term average evaporation calculated by four different methods as presented in table 8-2. The comparison provides an indication of the amount of confidence that can be given to the values of daily evaporation derived from remote sensing.

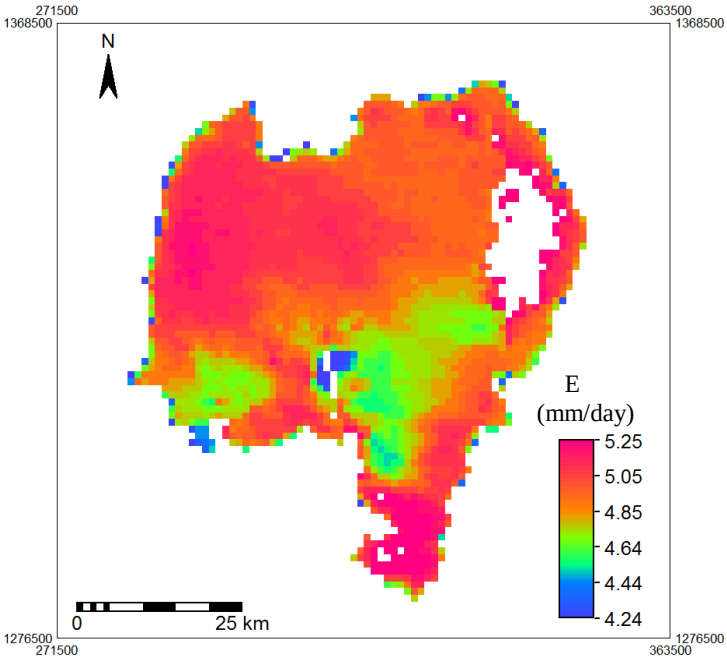

Figure 8-5: Daily evaporation of Lake Tana on 27th of September 2008

Table 8-2: Long-term average evaporation estimates of September 27

Year	Vallet-Coulomb et al. 2001	(Maidment, 1993)	Penman-Monteith	Energy balance method
27-Sep-1995	5.31	5.99	5.24	5.76
27-Sep-1996	4.68	5.34	4.62	5.07
27-Sep-1997	4.67	5.43	4.60	5.01
27-Sep-1998	4.68	5.23	4.63	5.12
27-Sep-1999	5.03	5.72	4.96	5.43
27-Sep-2000	5.13	5.87	5.06	5.52
27-Sep-2001	4.50	5.01	4.46	4.90
27-Sep-2002	4.82	5.41	4.76	5.24
27-Sep-2003	4.55	5.12	4.49	4.90
27-Sep-2004	3.94	4.60	3.87	4.22
27-Sep-2005	4.15	4.74	4.10	4.52
27-Sep-2006	3.83	4.82	3.74	4.16
27-Sep-2007	4.86	5.38	4.81	5.42
27-Sep-2008	4.83	5.44	4.77	5.30
Average	4.63	5.28	4.56	5.02
STDV	0.44	0.42	0.44	0.49

8.3 Diurnal cycle of lake surface temperature

The high temporal resolution of Meteosat second generation satellite images availability (every 15 minute) can be used to track the diurnal cycle of surface temperature. Water temperature has a profound influence on the entire aquatic ecosystems as well as on a wide range of human activities located around water bodies. Lake Tana contains a sufficient large volume and aerial extent of water to exert a considerable influence on local weather patterns. In addition, monitoring of climatologically temperature conditions, temporal and spatial distribution of lake surface temperature can be extremely valuable for different applications. Up to now, there is no area-wide consistent temperature data set for the Lake Tana available. In this study in situ measurement on the lake was collected and used to compare and validate the surface temperature retrieved from remote sensing.

In order to retrieve the surface temperature from MSG/SEVIRI two methods are proposed in this study as described on chapter six, section 6.4.2. All the required thermal channels of brightness temperature were downloaded from ITC data base with repeat interval of 30 minute. However the night time images of the area strongly influenced by clouds, hence the analysis and validation is mainly focused on day time images. The in situ surface temperature measurements of the lake on September 27th 2008 were used to validate the result of remote sensing analysis. Figure 8-6 shows the surface temperature retrieved by using the two methods at a local time of 13:00. Although it is hard to differentiate between them but if we take the pure water pixel on the lake the variation can easy detected and compared with in situ measurements.

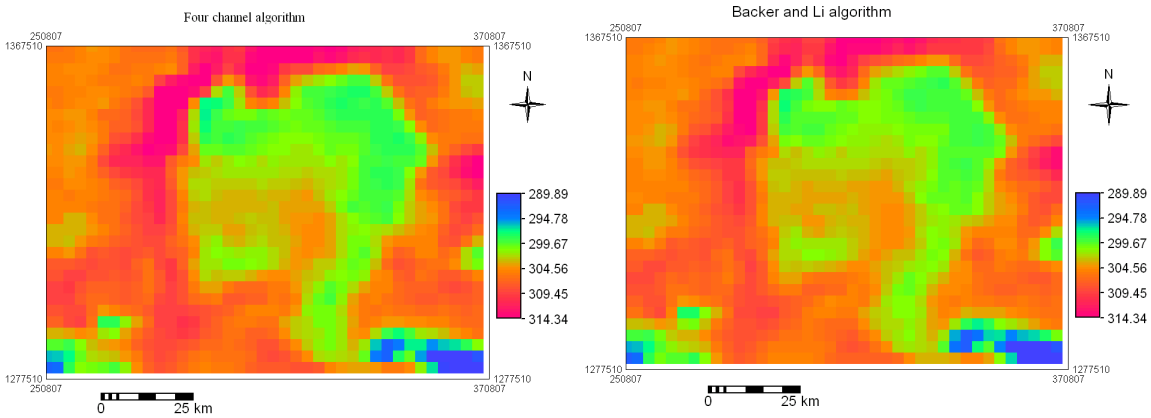

Figure 8-6: Surface temperature calculated by two models on 27/09/08, 13:00 local time.

Figure 8-7 shows the diurnal cycle of lake surface temperature retrieved by the two methods and also in situ measurements. As we can see from the figure the surface temperature increases gradually in the morning and drops sharply in the afternoon. This is due to turbulent mixing of the surface layers as a result of wind on the lake which most of the time occurs late in the afternoon. Validation of the surface temperature with in situ measurements revealed that four channel algorithms of give better result with a root mean square error (RMSE) of 0.57 K as compared with Becker and Li (19900 (split window techniques) having RMSE 0.78 K. The correlation of in situ measurements with remote sensing as in Figure 8-8 also shows four channel algorithm performs well in retrieving the surface temperature of the lake.

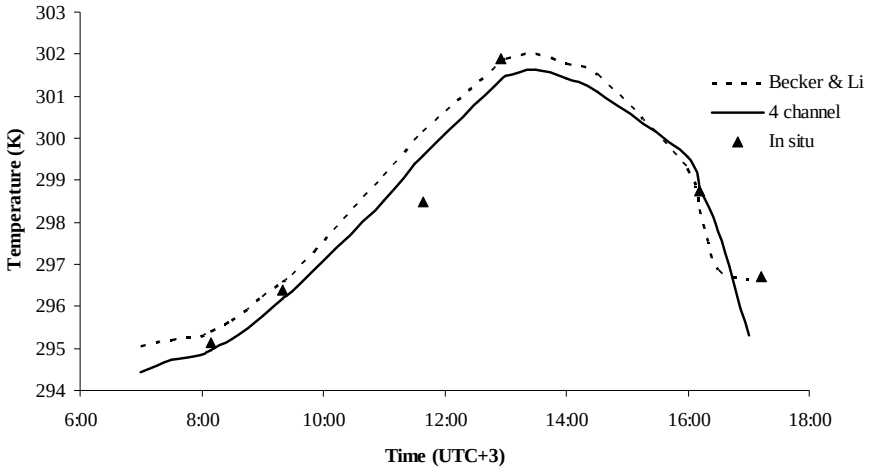

Figure 8-7: The diurnal cycle of lake surface temperature for day time on September 27, 2008

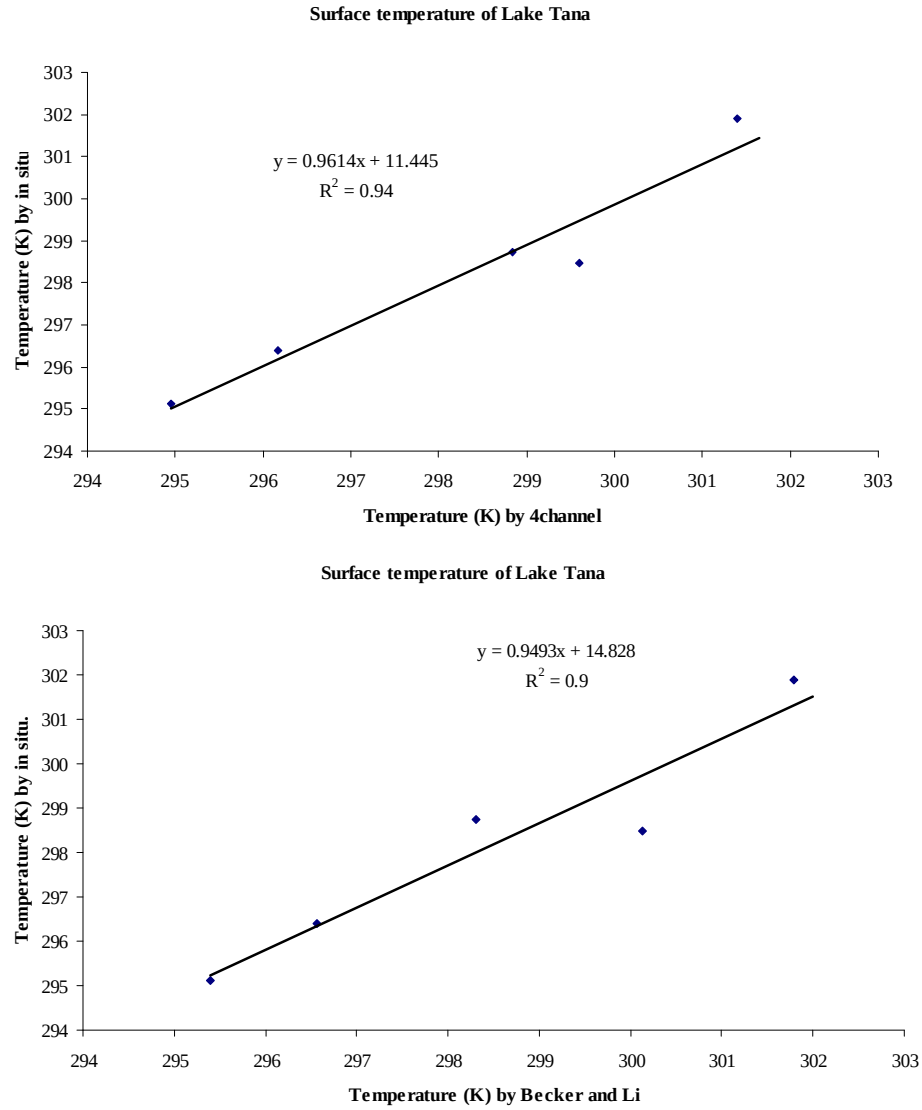

Figure 8-8: Correlation of surface temperature retrieved from MSG with in situ measurements

9. Conclusions and recommendations

9.1. Conclusions

Because of the economic, recreational, and esthetic value of Lake Tana, a firm scientific understanding of the physical, chemical, and biological processes therein is warranted. Many of these processes affect and are affected by atmospheric conditions. Unfortunately, however, direct measurements of all atmospheric variables of importance have not been done at all on the surface of Lake Tana. Examples of such measurements are those of short and long wave radiation, wind speed, direct humidity transport, air temperature above the lake and lake temperature at various depths. The magnitudes of various components of the surface energy balance depend on many factors, including the type of surface and its characteristics, geographic location, time of the year, time of the day and weather.

The incoming solar radiation is the major source of energy for evaporation processes which is modulated by surface albedo to quantify how much solar energy is left on the surface. Hence it is very important to track the spatial as well as temporal variability of albedo. However using point observation it is difficult to map the spatial variability. The spatial as well as temporal variability can be derived from satellite observation. In this study I retrieved the annual cycle of albedo from MODIS/Terra surface reflectance products on a monthly time steps. One interesting observation from the annual cycle of albedo is that there is clear temporal and spatial variability which shows the surface characteristics of the water in the lake. The temporal variability is more pronounced than the spatial variability. The temporal variability can be explained by the occurrence of rainy season in the area (June-September) is associated with flash flood entering the lake which increases the suspended sediments abruptly. Previous studies on Lake Tana have been using a constant albedo of 0.06 for annual evaporation estimation, however in this research monthly albedo from MODIS satellite imagery are calculated and used. The effect of using constant albedo is that it over-estimates evaporation during rainy season.

The result of lake surface data analysis showed that the contribution of sensible heat flux on the energy balance of the lake is in the order of 30 to 50 Wm^{-2} around the noon, which is less than 10% of the net radiation. From instantaneous estimation of energy balance components most of the net radiation goes to heat up the water as water heat flux. Similar studies (Brutsaert, 2005) also confirmed that the water heat flux is at higher order of magnitude for open water bodies than for land surfaces.

For long-term average evaporation calculation, different climatic approaches were applied at a daily time steps for annual evaporation estimates of Lake Tana. The result showed the Penman combination approach after Maidment over-estimates evaporation by 10-15% for large lake. It might be better suited for evaporation pan and small ponds. With continuous and long-term measurement of surface water temperature of the lake the Bowen ratio energy balance method would give reasonable result for lake evaporation estimation.

It was not possible to assign error values to the different evaporation results in a rigorous way. However the influence of individual input variables on evaporation estimates for each climatic method is analyzed by increasing or decreasing of 10% of its value. From this analysis, both energy balance and Penman methods are most sensitive to shortwave radiation, which is the energy source of evaporation. The incoming shortwave radiation uncertainty comes from both the measurement of daily sunshine duration and from the empirical coefficients used. Air temperature is more sensitive to Penman methods than energy balance. Uncertainties on wind speed data affect the Penman evaporation rate, but this variable has rather low influence. The energy balance method is generally considered as a reference method and the result of data analysis show that the method is weakly sensitive to the value of Bowen ratio.

The climatic methods which are used to calculate evaporation are suffering from the difficulty to show the spatial variability at the required scale. However this problem is overcome by the magnificent potential of satellite remote sensing data. Daily evaporation map is calculated using evaporation fraction approach from combination of MODIS/Terra imagery and in situ measurements for a cloud free day of September 27, 2008. The average daily evaporation obtained from this analysis is 4.94 mm/day with a standard deviation of 0.20 mm/day and this value compared with the long term daily evaporation calculated from meteorological data by different methods. The Bowen ratio energy balance method gives fairly closer result as compared with the daily evaporation calculated from evaporative fraction approach.

The spatial and temporal variability of surface temperature of the lake is tracked from MSG/SEVIRI satellite imagery data and validated with in situ measurements. Two methods have been proposed to retrieve the surface temperature. The four channel algorithm gives fairly good result compared with in situ measurements. This algorithm depends on locally calibrated coefficients which can be estimated from radiative transfer model provided that sufficient data set is available to run the radiative transfer model. The diurnal cycle of lake surface temperature shows that the increase in surface temperature is gradual until it reaches to the maximum around the midday and then starts to drops rapidly. This is due to turbulent mixing of the surface layer as a result of wind on the lake which occurs most of the time late in the afternoon.

9.2. Recommendations

To improve the results of open water evaporation estimation from the lake and for further hydrological study of the lake the following recommendations are worth noting:

- Land based meteorological data for estimating evaporation over the lake may not be reliable enough. An independent and long term over water meteorological data is mandatory for better estimates of open water evaporation from the lake.

- The study could re-establish the fact that, the application of remote sending brings a marvellous contribution to estimation of spatial and temporal evaporation. However, direct measurement method for different components of energy balance are always very important, especially in verifying the results of different remote sensing based approaches. In this research, the sonic anemometer data and net radiometer data are vital in this regard.

- Direct measurements of water vapour flux with infrared gas analyzer (open or closed path) may also be useful to establish the latent heat flux directly. However these instruments are very costly.

- Calibration and pre-field work demonstration of some sophisticated equipments is very important to avoid error on data collection during field campaigning. For example the relative humidity sensor which is the most difficult and liable for error at the field measurements.

- Further study on heat content of the lake on daily as well as seasonal basis has to be addressed to improve long term evaporation estimation from the lake.

- The sharp increase in albedo of the lake during the rainy season revealed that there is sedimentation problem on the lake hence detailed scientific research on sedimentation of the lake is very important for sustainable and wise use of the resource.

References

Abeyou, W., 2008. Hydrological balance of Lake Tana upper Blue Nile basin, Ethiopia. MSc Thesis, ITC, Enschede,The Netherlands 94 pp.

Allen, R.G. et al., 1998. FAO Irrigation and Drainage Paper No. 56. Rome: Food and Agriculture Organization of the United Nations.

Allen, R.G. et al., 1996. Chapter 4: Evaporation and transpiration. ASCE Handbook of Hydrology: 125-252.

Anthony, M., Masahiro, T., Dr. Richard , G.A. and William J., K., 2000. Application of the SEBAL Methodology for Estimating Consumptive Use of Water and Stream flow Depletion in the Bear River Basin of Idaho through Remote Sensing.

Ashfaque, A., 1999. Estimation of lake evaporation using meteorological data and remote sensing : a case study of Lake Naivasha, Central rift valley, Kenya. MSc Thesis, ITC, Enschede, The Netherlands, 98 pp.

Assouline, S. and Mahrer, Y., 1993. Evaporation from Lake Kinneret: 1. Eddy Correlation System Measurements and Energy Budget Estimates. Water Resources Research 29(4): 901-910.

Bastiaanssen, W.G.M., Menenti, M., Feddes, R.A. and Holtslag, A.A.M., 1998a. A remote sensing surface energy balance algorithm for land (SEBAL) - 1. Formulation. Journal of Hydrology, 213(1-4): 198-212.

Bastiaanssen, W.G.M. et al., 1998b. A remote sensing surface energy balance algorithm for land (SEBAL) - 2. Validation. Journal of Hydrology, 213(1-4): 213-229.

Becker, F. and Li, Z.-L., 1990. Towards a local split window method over land surfaces. International Journal of Remote Sensing, 11(3): 369 - 393.

Berliand, T.G., 1960. Methods of climatological computation of total incoming solar radiation. Meteorol. Gidrol, 6: 9-12.

Brutsaert, W., 1982. Evaporation Into the Atmosphere: Theory, History, and Applications. Springer.

Brutsaert, W., 2005. Hydrology: an introduction. Cambridge University Press.

Brutsaert, W. and Sugita, M., 1992. Application of self-preservation in the diurnal evolution of the surface energy budget to determine daily evaporation. Journal of Geophysical Research.

Cahoon, J.E., Costello, T.A. and Ferguson, J.A., 1991. Estimating pan evaporation using limited meteorological observations. Agricultural and Forest Meteorology, 55(3-4): 181-190.

Caselles, V. and Sobrino, J., 1989. Determination of frosts in orange groves from NOAA-9 AVHRR data. Remote Sensing of Environment, 29: 135-146.

Chow, V.T., Maidment, D.R. and Mays, L.W., 1988. Applied hydrology. (McGraw-Hill Series in Water Resources and Environmental Engineering). McGraw-Hill, New York etc., 572 pp.

Coll, C., Caselles, V., Sobrino, J.A. and Valor, E., 1994. On The Atmospheric Dependence of The Split-Window Equation For Land Surface Temperature International Journal of Remote Sensing, 15(1): 105-122.

Crago, R.D., 1996. Daytime evaporation from conservation of surface flux ratios. The scaling issue in hydrology. Journal of Hydrology, 178: 241-255.

Delclaux, F., Coudrain, A. and Condom, T., 2007. Evaporation estimation on Lake Titicaca: a synthesis review and modelling. Hydrological Processes, 21(13): 1664-1677.

Dingman, S.L., 2002. Physical hydrology. Prentice Hall, Upper Saddle River, 646 pp.

dos Reis, R.J. and Dias, N.L., 1998. Multi-season lake evaporation: energy-budget estimates and CRLE model assessment with limited meteorological observations. Journal of Hydrology, 208(3-4): 135-147.

Eichinger, W.E. et al., 2003. Lake Evaporation Estimation in Arid Environments, Final Report.

Foken, T. and Wichura, B., 1996. Tools for quality assessment of surface-based flux measurements. Agricultural and Forest Meteorology, 78(1-2): 83-105.

Gianniou, S.K. and Antonopoulos, V.Z., 2007. Evaporation and energy budget in Lake Vegoritis, Greece. Journal of Hydrology, 345(3-4): 212-223.

Gieske, A.S.M., 2006. Analysis of Energy and Co2 Fluxes by Eddy Correlation Measurements at Two Levels Sen2flex Field Campaign (Barrax, Spain, 2006), ESA SEN2FLEX - SENtinel-2 and FLuorescence Experiment Noordwijk ESA-ESTEC, The Netherlands pp. 8.

Gieske, A.S.M. et al., 2005. Processing of MSG-1 / SEVIRI data in the thermal infrared. Algorithm development with the use of the sparc2004 data set. ESA/SPARC2004 Proceedings.

Gieske, A.S.M., Rientjes, T., Alemseged, T.H., Abeyou, W.W. and Getachew, H.A., 2008. Determination of Lake Tana Evaporation by the Combined Use of SEVIRI, AVHRR and IASI, Proceedings of the 2008 EUMETSAT Meteorological Satellite Conference, Sessioin 10, hydrometeorology, Darmstad, Germany, pp. 7.

Granger, R. and Hedstrom, N., 2005. Measuring and Modelling Evaporation from Crean Lake,PANP: Interim report, 2005 field season.

Hostetler, S.W. and Bartlein, P.J., 1990. Simulation of Lake Evaporation With Application to Modeling Lake Level Variations of Harney-Malheur Lake, Oregon. Water Resources Research, 26(10): 2603-2612.

Hurtado, E. and Sobrino, J.A., 2001. Daily net radiation estimated from air temperature and NOAA-AVHRR data: a case study for the Iberian Peninsula. International Journal of Remote Sensing, 22(8): 1521-1533.

Kaba, A., E., 2007. Validation of radar altimetry lake level data and its application in water resource management. MSc Thesis, ITC, Enschede,The Netherlands, 76 pp.

Kaimal, J.C. and Finnigan, J.J., 1994. Atmospheric Boundary Layer Flows: Their Structure and Measurement. Oxford University Press, USA.

Kebede, S., Travi, Y., Alemayehu, T. and Marc, V., 2006. Water balance of Lake Tana and its sensitivity to fluctuations in rainfall, Blue Nile basin, Ethiopia. Journal of Hydrology, 316(1-4): 233-247.

Keijman, J.Q., 1974. The estimation of the energy balance of a lake from simple weather data. Boundary-Layer Meteorology, 7(3): 399-407.

Kerle, N.e. et al., 2004. Principles of remote sensing : an introductory textbook. ITC Educational Textbook Series;2. ITC, Enschede, 250 pp.

Kimura, F. and Shimizu, Y., 1994. Estimation of Sensible and Latent Heat Fluxes from Soil Surface Temperature Using a Linear Air-Land Heat Transfer Model. Journal of Applied Meteorology, 33(4): 477-489.

King, M.D. et al., 1992. Remote sensing of cloud, aerosol, and water vapor properties from the moderate resolution imaging spectrometer (MODIS). Geoscience and Remote Sensing, IEEE Transactions on, 30(1): 2-27.

Liang, S., 2001a. Narrowband to broadband conversions of land surface albedo. I- Algorithms. Remote Sensing of Environment, 76(2): 213-238.

Liang, S.L., 2001b. An optimization algorithm for separating land surface temperature and emissivity from multispectral thermal infrared imagery. IEEE Transactions on Geoscience and Remote Sensing, 39(2): 264-274.

Maidment, D.R., 1993. Handbook of hydrology. McGraw-Hill, New York etc., 650 pp.

Mauder, M. and Foken, T., 2004. Documentation and Instruction Manual of the Eddy Covariance Software Package TK2. Univ., Abt. Mikrometeorologie.

Mobley, C., 1994. Light and Water: Radiative Transfer in Natural Waters, 592pp. Academic Press, Inc, San Diego.

Morandini, G., 1940. Missione di studio al Lago Tana, Vol. 3. Richerche Limnologiche, Parte Prima,Geografia Fisica, Reale Academia d'Italia, Roma, Italia. 319.

Morton, F.I., 1983. Operational Estimates of Lake Evaporation. Journal of Hydrology, 66(1-4).

Oberhuber, J.M., 1988. An Atlas based on the COADS data set: The budgets of heat, buoyancy and turbulent kinetic energy at the surface of the global ocean, Rep. 15. Max-Planck Institut, Hamburg, 20.

Parodi, G.N., 2002. AHVRR hydrological analysis system :Algorithms and theory, version 1.3 : AHAS algorithms and theory, ITC, Enschede.

Pinker, R.T., Frouin, R. and Li, Z., 1995. A review of satellite methods to derive surface shortwave irradiance. Remote Sensing of Environment, 51(1): 108-124.

Price, J.C., 1983. Estimating surface temperatures from satellite thermal infrared data--A simple formulation for the atmospheric effect. Remote Sensing of Environment, 13(4): 353-361.

Rosenberry, D.O., Sturrock, A.M. and Winter, T.C., 1993. Evaluation of The Energy Budget Method of Determining Evaporation at Williams Lake, Minnesota, Using Alternative Instrumentations and Study Approaches Water Resources Research, 29(8): 2473-2483.

Running, S.W. et al., 1994. Terrestrial remote sensing science and algorithms planned for EOS/MODIS. International Journal of Remote Sensing, 15(17): 3587-3620.

Salomonson, V.V., Barnes, W.L., Maymon, P.W., Montgomery, H.E. and Ostrow, H., 1989. MODIS: advanced facility instrument for studies of the Earth as asystem. Geoscience and Remote Sensing, IEEE Transactions on, 27(2): 145-153.

Schotanus, P., Nieuwstadt, F.T.M. and Bruin, H.A.R., 1983. Temperature measurement with a sonic anemometer and its application to heat and moisture fluxes. Boundary-Layer Meteorology, 26(1): 81-93.

Shunlin, L., 2004. Quantitative remote sensing of land surfaces. Wiley Praxis series in Remote Sensing;. Wiley & Sons, Hoboken etc., 534 pp.

SMEC, 2007. Hydrological Study of the Tana-Beles Sub-Basins, Draft Inception Report, Snow Mountains Engineering Corporation, Australia.

Sobrino, J.A., Li, Z.L., Stoll, M.P. and Becker, F., 1996. Multi-channel and multi-angle algorithms for estimating sea and land surface temperature with ATSR data. International Journal of Remote Sensing, 17(11): 2089-2114.

Su, Z., 2002. The Surface Energy Balance System (SEBS) for estimation of turbulent heat fluxes. Hydrology and Earth System Sciences, 6(1): 85-99.

Sun, D. and Pinker, R.T., 2007. Retrieval of surface temperature from the MSG-SEVIRI observations: Part I. Methodology. International Journal of Remote Sensing, 28(23): 5255-5272.

Tasumi, M., 2005. A review of evaporation research on Japanese lakes, Proceedings 2005 EWRI, Anchorage, Alaska, May 15-19.

Temesgen, E., 2009. Estimation of Evapotranspiration from Satellite Remote Sensing and Meteorological Data over the Fogera Flood Plain-Ethiopia. MSc Thesis, ITC, Enschede,The Netherlands 101 pp.

Thom, A.S., 1972. Momentum, mass and heat exchange of vegetation. Quarterly Journal of the Royal Meteorological Society, 98(415): 124-134.

Twine, T.E. et al., 2000. Correcting eddy-covariance flux underestimates over a grassland. Agricultural and Forest Meteorology, 103(3): 279-300.

Vallet-Coulomb, C., Legesse, D., Gasse, F., Travi, Y. and Chernet, T., 2001. Lake evaporation estimates in tropical Africa (Lake Ziway, Ethiopia). Journal of Hydrology, 245(1-4): 1-18.

Vardavas, I.M. and Fountoulakis, A., 1996. Estimation of lake evaporation from standard meteorological measurements: application to four Australian lakes in different climatic regions. Ecological Modelling, 84(1-3): 139-150.

Vassiljev, J., Harrison, S.P. and Haxeltine, A., 1995. Recent lake-level and outflow variations at Lake Viljandi, Estonia: validation of a coupled lake-catchment modelling scheme for climate change studies. Journal of Hydrology, 170(1-4): 63-77.

Vining, R.C. and Blad, B.L., 1992. Estimation of sensible heat flux from remotely sensed canopy temperatures. Journal of Geophysical Research, 97(D17): 18951-18954.

Wan, Z.M. and Dozier, J., 1996. A generalized split-window algorithm for retrieving land-surface temperature from space. IEEE Transactions on Geoscience and Remote Sensing, 34(4): 892-905.

Wang, J., White, K. and Robinson, G.J., 2000. Estimating surface net solar radiation by use of Landsat-5 TM and digital elevation models. International Journal of Remote Sensing, 21(1): 31-43.

WaterWatch, G.F., 2006. Remote Sensing Studies of Tana-Beles sub basins, A Nile basin initiative project, Wageningen, The Netherlands.

Winter, T.C. et al., 2003. Evaporation determined by the energy-budget method for Mirror Lake, New Hampshire. Limnology and Oceanography, 48(3): 995-1009.

Xue, Y. and Cracknell, A.P., 1995. Advanced thermal inertia modelling. International Journal of Remote Sensing, 16(3): 431-446.

Xue, Y., Lawrence, S.P., Llewellyn-Jones, D.T. and Mutlow, C.T., 1998. On the Earth's surface energy exchange determination from ERS satellite ATSR data. Part I: Long-wave radiation. International Journal of Remote Sensing, 19(13): 2561-2583.

Xue, Y., Llewellyn-Jones, D.T., Lawrence, S.P. and Mutlow, C.T., 2000. On the Earth's surface energy exchange determination from ERS satellite ATSR data: Part 2. Short-wave radiation. International Journal of Remote Sensing, 21(18): 3415-3426.

Yin, X.G. and Nicholson, S.E., 1998. The water balance of Lake Victoria. Hydrological Sciences Journal-Journal Des Sciences Hydrologiques, 43(5): 789-811.

Yohannes, D., 2007. Remote Sensing Based Assessment of Water Resource Potential for Lake Tana Basin. MSc Thesis, Addis Ababa University, Addis Ababa, 124 pp.

Annex

Appendix A: List of acronyms

AC	Atmospheric Correction
AVHRR	Advanced Very High Resolution Radiometer
CNR	Net radiometer (Kipp and Zonen, Delft, Holland)
CSAT3	3D-sonic anemometer
DEM	Digital Elevation Model
DN	Digital number
EC	Eddy covariance
EOS	Earth Observation Systems
EUMETSAT	European Organization for the Exploitation of Meteorological Satellites
FAO	Food and Agriculture Organization
GCP	Ground control points
IFOV	Instantaneous Field-of-View
ILWIS	Integrated Land and Water Information System
IR	Infra-red
LST	Land surface temperature
MIR	Mid-infra red
MODIS	Moderate-resolution Imaging Spectroradiometer
MSG	Meteosat Second Generation
NIR	Near Infra-red
NOAA	National Oceanic and Atmospheric Administration
PE	Potential Evapotranspiration
RH	Relative humidity
RMSE	Root Mean Square Error
SEBAL	Surface energy balance algorithm for land
SEBS	Surface Energy Balance Systems
SEVIRI	Spinning Enhanced Visible and Infrared Imager
SMAC	Simplified Method for the Atmospheric Correction
SMEC	Snowy Mountains Engineering Corporation
SRTM	Shuttle Radar Topographic Mission
SWT	Split-window technique
TOA	Top of atmosphere
UTM	Universal Transverse Mercator
VIS	Visible

Appendix B: Standard micro-meterological expressions for evaporation calculation

1. Saturated vapour pressure

$$e_s = 6.11 \exp \frac{17.27 \times (T_a - 273.16)}{(T_a - 273.16) + 237.3}$$

Where

T_a = air temperature at observation height [K]

e_s = saturated vapour pressure [mbar]

2. Actual vapour pressure

$$e_a = e_{s(wet)} - \gamma (T_{dry} - T_{wet}) = RH \times e_s \quad \text{[mbar]}$$

3. Vapour pressure deficit

$$D = e_s - e_a$$

Where,

D = Vapour pressure deficit [mbar]

e_a = actual vapour pressure [mbar]

$e_{s(wet)}$ = saturated vapour pressure at wet bulb temperature [mbar]

T_{dry} = dry bulb temperature [K]

T_{wet} = wet bulb temperature [K]

γ = Psychometric constant [mbarK-1]

RH = Relative humidity [ ]

4. Slope of saturated vapour pressure curve

$$\Delta = 4098 \frac{e_s}{\{(T_a - 273.16) + 237.3\}^2} \quad \text{[mbarK}^{-1}\text{]}$$

5. Vapour density

$$\rho_v = \frac{e_a}{T_a \times 4.61}$$

Where,

ρ_v = actual vapour density [kgm^{-3}]

e_a = actual vapour pressure [mbar]

T_a = air temperature at observation height [K]

6. Dry air density

$$\rho_d = \frac{P - e_a}{T_a \times 2.87}$$

Where

ρ_d = dry air density [kgm^{-3}]

P = Total pressure [mbar]

7. Moist air density

$\rho_a = \rho_d + \rho_v$

Where

ρ_a = moist air density [kg m^{-3}]

8. Total air pressure

$$P = 1004(\frac{293 - 0.0065Z}{293})^{5.26}$$

Where

P = Total pressure [mbar]

Z = Elevation [m]

9. Latent heat of vaporization

$$\lambda = \{2.501 - 0.00326(T - 273.16)\} \times 10^6$$

Where

λ = Latent heat of vaporization [JKg^{-1}]

T = average of surface and air temperature [K]

10. Psychometric constant

$$\gamma = 1630 \frac{P}{\lambda}$$

Where

γ = Psychometric constant [mbar]

P = Total pressure [mbar]

RADIATION

1. Solar declination

$$\delta = 0.409 \sin(0.0172J - 1.39)$$

Where

δ = Solar declination [rad]

J = day number of the year [ ]

Sin = sin function which should be in radian mode

2. Solar distance

$$d_s = 1 + 0.0167 \sin[\frac{2\pi(J - 93.5)}{365}]$$

$$E_0 = 1 + 0.033 \cos(0.0172J)$$

Where

d_s = relative distance between earth and sun [AU]

E_0 = Eccentricity correction factor of the earth [ ]

Cos = cosine function which should be in radian mode

3. Solar hour angle

$$\omega = \arccos(-\tan(lat)\tan\delta)$$

$$\omega_a = \pi(12 - Localtime)/12$$

Where

ω	=	Solar hour angle representing the 24 hour solar radiation [rad]
ω_a	=	Instantaneous Solar hour angle [rad]
Lat	=	latitude [rad]
δ	=	Solar declination [rad]

4. Extra-terrestrial shortwave solar radiation

$$R_a = 435.2 \times E_0 \times (\omega \sin(lat) \sin\delta + \cos(lat)\cos\delta \sin\omega)$$

Where

Ra	=	daily extra-terrestrial short wave solar radiation [Wm^{-2}]

For instantaneous extra-terrestrial short wave solar radiation, R_{ai}

$$\begin{aligned} R_{ai} &= 1367 \times E_0 \times (\sin(lat)\sin\delta + \cos(lat)\cos\delta\cos\omega_a) \\ &= 1367 \times \sin((lat)\sin\delta + \cos(lat)\cos\delta\cos\omega_a)/d_s^2 \\ &= 1367 \times \cos(\phi_{su})/d_s^2 \end{aligned}$$

Where ϕ_{su} = solar zenith angle [rad]

5. Maximum possible sunshine hour

$$N = 7.64\omega$$

Where, N = maximum possible sunshine hours

6. At surface incoming short wave solar radiation

$$K\downarrow = (0.26 + 0.48n/N)R_a$$

Where

$K\downarrow$	=	incoming shortwave solar radiation
R_a	=	Extra-terrestrial short wave solar radiation [Wm^{-2}]
N	=	maximum possible sunshine hours
n	=	actual hours of sunshine [hours]

7. Daily net radiation

$$R_n = (1-\alpha_{24})K_{24}\downarrow -110\frac{K_{24}\downarrow}{R_{24,a}} \qquad [Wm^{-2}]$$

Where α is albedo of the surface [-]

Appendix C: Description of in situ data measured on the field

Table C-1: Instruments used during field work

Instrument	Height above the water	Measurements
CSAT, sonic-anemometer	2.60 m	Wind speed, direction, turbulent quantities
Temperature-humidity Probe	2.60 m	Atmospheric temperature and humidity
Net radiometer, NCR1	2.63m	Incoming and outgoing sort and long wave radiation
Temperature probe (for profile)	0, 5, 30 and 70 cm depths	Lake temperature at various depths.
Infrared gun	-	Radiant temperature of water
EC meter	-	Contact temperature of water
Wind vane	-	Wind speed on the lake

Table C-2: Sampling point on the lake (27/09/08)

Measurements point	Location		Start	end	Remark
	X	Y			
M1	320544.21	1297889.27	6:55	7:14	No measuremnts for temperature, relative humidity and long wave radiation Wind speed measurement was not taken
M2	316418.64	1306139.7	8:14	8:40	
M3	321549.94	1320844.17	10:37	10:56	Wind speed measurement was not taken
M4	314407.02	1314558.34	11:44	12:03	Wind speed measurement was not taken
M5	317125.69	1310633.45	15:13	15:31	
M6	323009.78	1305766.65	16:04	16:20	
M7	323822	1297493.06	17:02	17:18	

Table C-3: Data collected by slow response sensors

Element	Unit	Temporal resolution	Remark
Incoming sort wave radiation (CNR1_Avg(1))	W/m^2	1 min	
Outgoing sort wave radiation (CNR1_Avg(2))	W/m^2	1 min	
Incoming longwave radiation (CNR1_Avg(3))	W/m^2	1 min	
Outgoing longwave radiation (CNR1_Avg(4))	W/m^2	1 min	
Temperature of sensors (PT100_Avg)	°C	1 min	Error from 7:46 to 8:04
Temperature of air (PT1002_Avg)	°C	1 min	
Relative humidity	%	1 min	Error from 7:46 to 8:04

Appendix D: Description of meteorological data

A. Historical data:

i. Meteorological data collected from Ethiopian meteorological agency, Addis Ababa, main office
Station: Bahir Dar
Location: Lat: 1282685.25
Long: 327729.6

Table D-1: Meteorological data at Bahir Dar station

Element	Year	Temporal Scale	Remark
Rainfall	1995-2003	Daily	
T_max	1995-2003	Daily	
T_min	1995-2003	Daily	
Relative humidity	1995-2003	Daily	
Wind speed	1995-2003	Daily	
Sunshine hours	1995-2003	Daily	
Piche evaporation	1986-1993	Daily	

Station: Gondar
Location: Lat: 1387762.74
Long: 328335.91
Table D-2: Meteorological data at Gondar station

Element	Year	Temporal Scale	Remark
Rainfall	1995-2003	Daily	
T_max	1995-2002	Daily	
T_min	1995-2002	Daily	
Relative humidity	1995-1999	Daily	
Wind speed	-	Daily	
Sunshine hours	1985-1991	Daily	
Piche evaporation	1984-1990	Daily	A lot of missing data

ii. Meteorological data collected from Ethiopian meteorological agency, Bahir Dar, Branch office
Station: Bahir Dar
Location: Lat: 1282685.25
Long: 327729.6
Meteorological data at Bahir Dar station

Element	Year	Temporal Scale	Remark
Rainfall	2004-10/09/2008	Daily	
T_max	2004-10/09/2008	Daily	
T_min	2004-10/09/2008	Daily	
Relative humidity	2004-10/09/2008	Daily	
Wind speed	2004-10/09/2008	Daily	
Sunshine hours	2004-10/09/2008	Daily	
Piche evaporation	2002-2006	Daily	

Station: Gondar
Location: Lat: 1387762.74
Long: 328335.91
Meteorological data at Gondar station

Element	Year	Temporal Scale	Remark
Rainfall	2003-10/09/2008	Daily	
T_max	2003-10/09/2008	Daily	
T_min	2003-10/09/2008	Daily	
Relative humidity	2004-10/09/2008	Daily	
Wind speed	2004-10/09/2008	Daily	
Sunshine hours	2004-10/09/2008	Daily	
Piche evaporation	2001-2004	Daily	

B. Automatic weather data

Location: Woreta
Lat: 357392.85,
Long: 1316517.70
Starting date: 23/06/2008
Last date: 29/09/2008 (up to the end of the field work)

Table D-3: Weather data collected at Woreta station

Element	Unit	Temporal resolution	Remark
Air temperature	°C	5 min	
Relative humidity	%	5 min	
Pressure	mbar	5 min	
Wind speed	m/s	5 min	
Guest speed	m/s	5 min	
Wind direction	angle(∅)	5 min	
Water content at ---cm	m^3/m^3	5 min	
Water content at ---cm	m^3/m^3	5 min	
Water content at ---cm	m^3/m^3	5 min	
Solar radiation	W/m^2	5 min	
Temperature at 5 cm	°C	5 min	
Temperature at 10 cm	°C	5 min	
Temperature at 20 cm	°C	5 min	

Appendix E: In situ data analysis

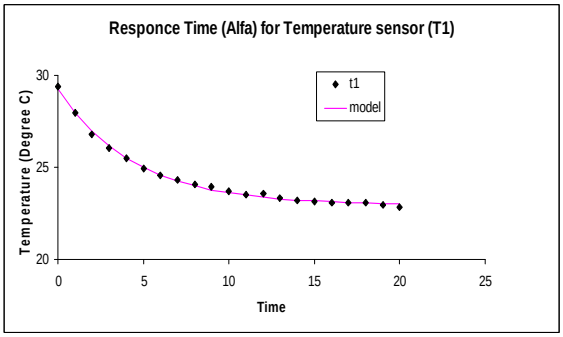

a

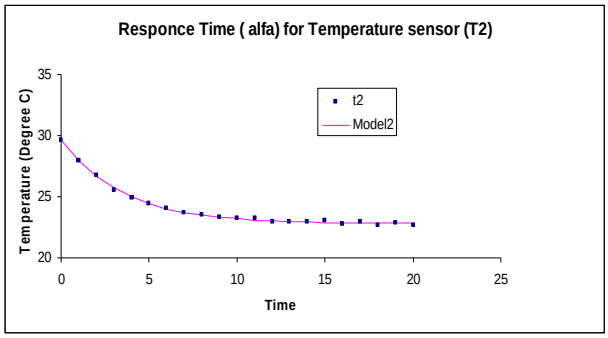

b

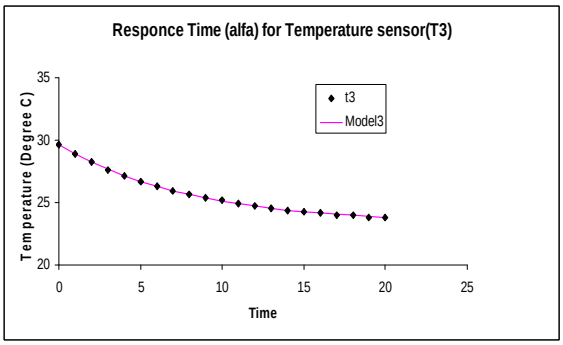

c

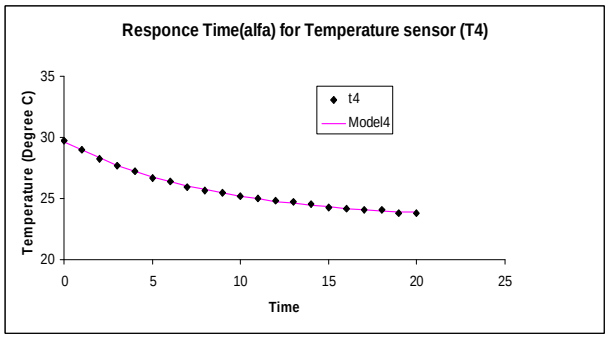

d

Figure E-1: Measured and modelled temperature during calibration of temperature probes

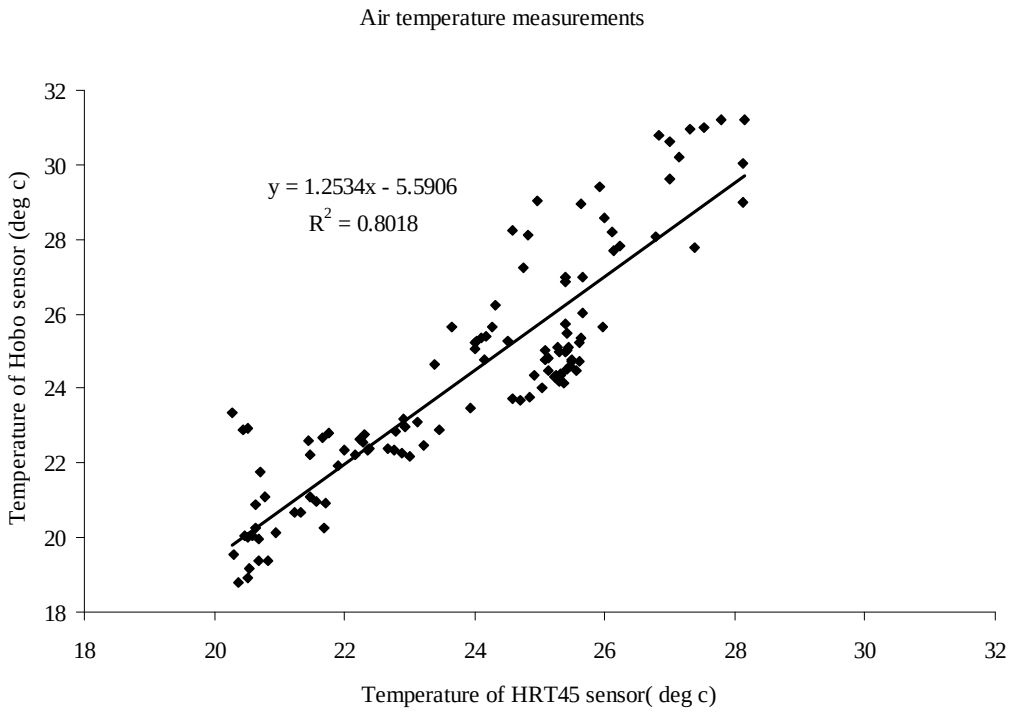

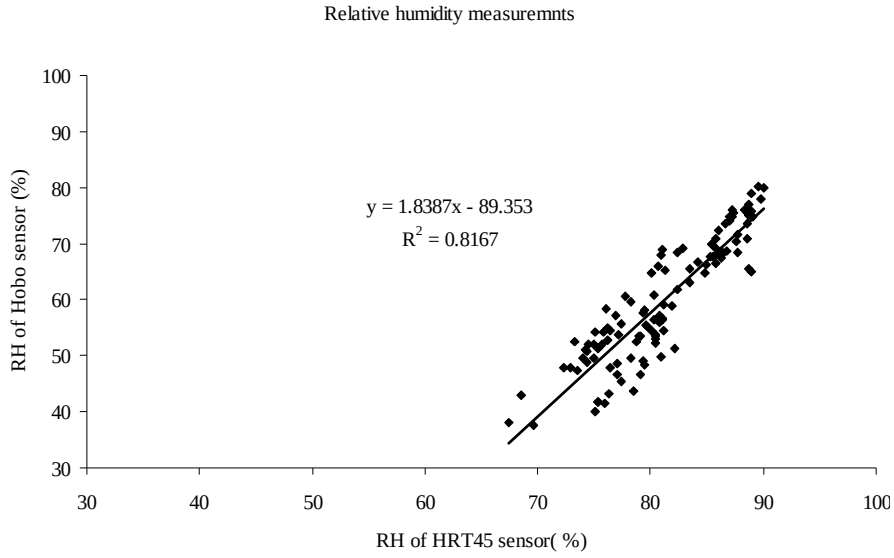

Figure E-2: Comparison air temperature and relative humidity measurements by different sensors

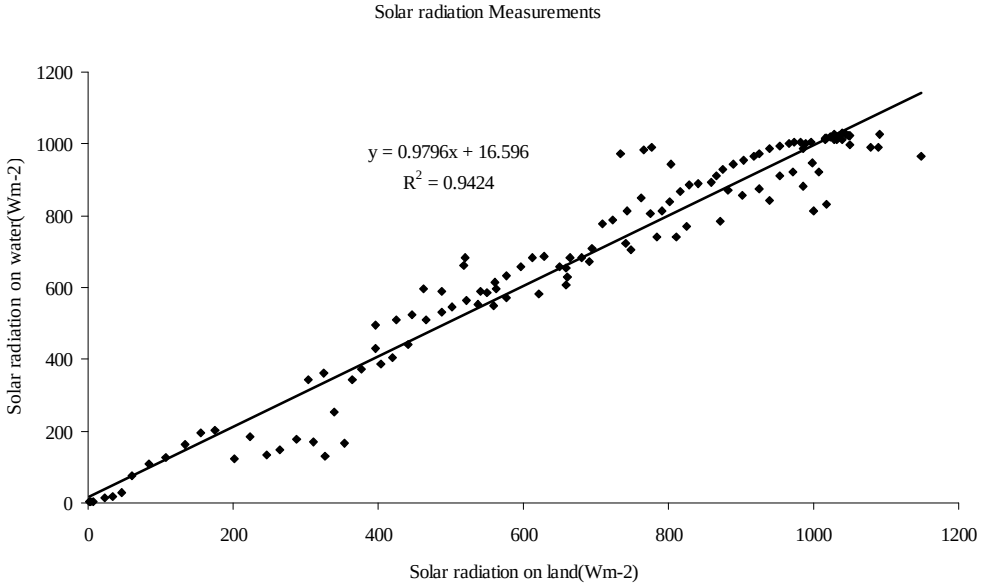

Figure E-3: Correlation of solar radiation measured on land and water surface (27/09/08)

Table E-1: Emissivity of the water from infrared gun and long wave radiation measurements (September 27th , 2008)

Local time [hr]	Radiant temperature [K]	outgoing longwave radiation W/m^2	Emissivity
8:09	295.00	no data	
9:27	298.29	442.19	0.99
11:46	302.42	461.67	0.97
12:53	303.71	475.10	0.98
16:22	300.55	453.01	0.98
17:12	298.73	443.85	0.98
18:10	298.60	445.41	0.99
Average			0.98

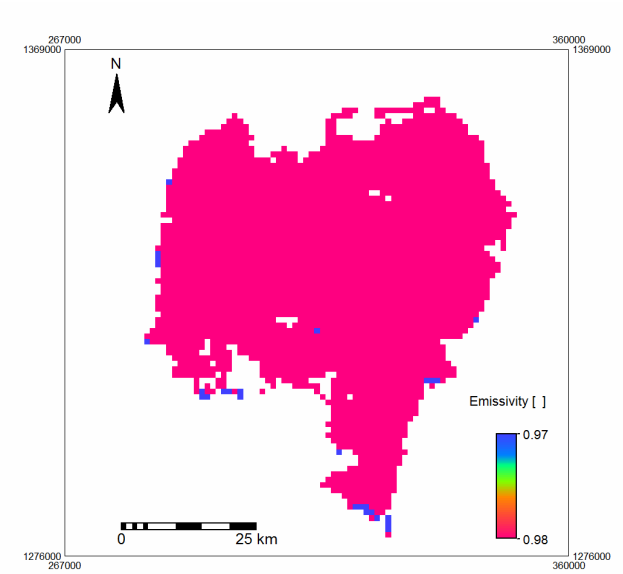

Figure E-4: Emissivity of Lake Tana on 27/09/08 at 11:15 local time (TERRA/MODIS)

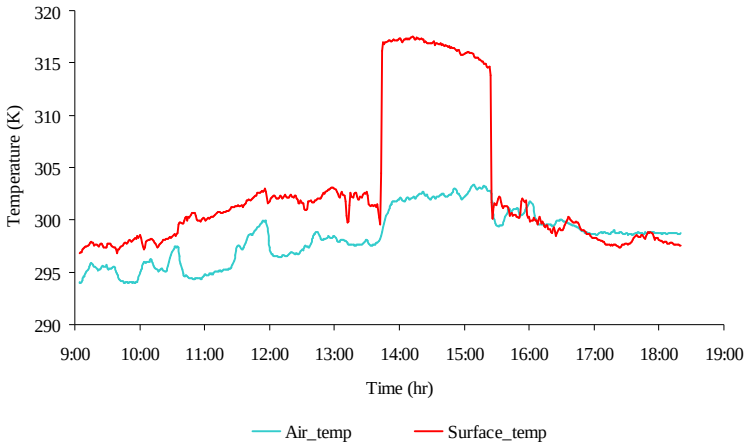

Figure E-5: Air and surface temperature measurements on the lake on 27/09/08

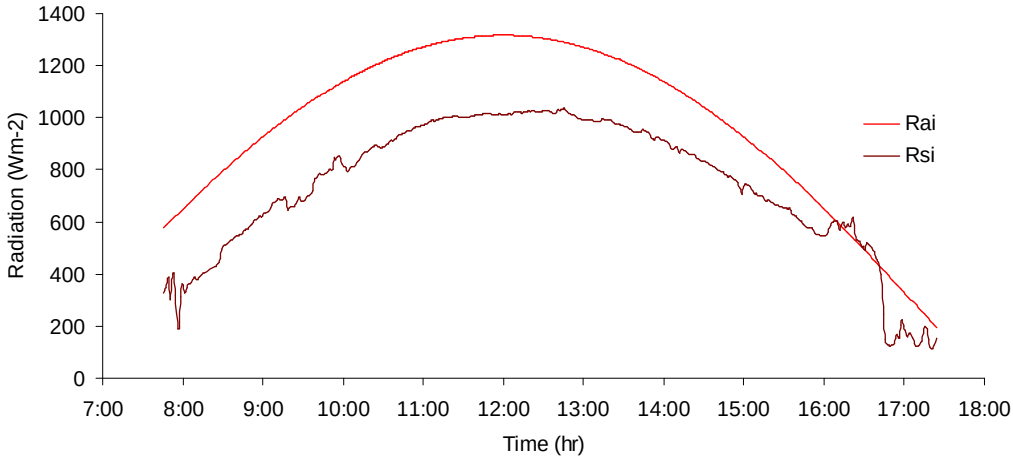

Figure E-6: Incoming short wave (R_{si}) and extra-terrestrial (R_{ai}) radiation on 27/09/08

Table E-2: Surface and atmospheric variable measured on the lake (27/09/08)

Local Time	Wind speed	T_air	T_water	RH	Saturated vap. pressure	Actual vap. pressure	Slope of sat. vap pressure
[hr]	[m/s]	[K]	[K]	[%]	[mbar]	[mbar]	($mbarK^{-1}$)
9:05	1.25	295.08	297.50	86.62	30.46	22.80	1.39
9:20	2.06	295.39	297.59	87.41	30.62	23.45	1.43
9:35	2.55	294.52	297.46	88.86	30.38	22.61	1.38
9:44	0.51	294.01	297.98	89.11	31.36	21.97	1.35
10:00	2.25	295.76	297.94	85.85	31.28	23.55	1.43
10:15	2.47	295.45	297.96	86.28	31.30	23.22	1.41
10:30	4.17	296.13	298.35	85.47	32.05	23.97	1.45
10:45	4.13	294.40	298.59	87.56	32.52	22.10	1.36
11:00	2.36	294.89	298.77	85.82	32.86	22.33	1.36
11:15	3.07	295.18	298.15	75.32	31.66	19.94	1.22
11:30	2.79	297.87	299.60	80.74	34.52	25.14	1.50
11:45	3.17	297.34	300.45	75.03	36.28	22.63	1.36
12:00	3.44	296.63	300.76	76.30	36.94	22.06	1.33
12:15	0.63	296.76	301.11	76.02	37.70	22.15	1.33
12:30	0.88	297.86	301.55	75.51	38.69	23.50	1.40
12:45	1.25	298.31	302.62	75.96	41.14	24.29	1.45
13:00	3.34	298.00	302.41	75.69	40.65	23.75	1.42
13:15	4.55	297.69	301.35	74.76	38.24	23.03	1.38
13:30	0.19	297.73	301.60	75.20	38.80	23.23	1.39
15:30	0.65	300.12	301.32	70.44	38.16	25.06	1.47
15:45	1.47	300.91	27.75	70.49	37.17	26.26	1.53
16:00	2.86	300.31	27.15	71.32	35.13	25.66	1.50
16:15	0.70	299.65	26.49	72.05	33.44	24.93	1.47
16:30	0.52	299.63	26.47	72.61	34.78	25.10	1.48
16:45	2.65	298.86	25.70	74.24	33.06	24.52	1.45
17:00	2.85	298.72	25.56	75.87	31.31	24.85	1.47
17:15	3.62	298.78	25.62	75.36	30.59	24.78	1.47
17:30	2.25	298.69	25.53	75.29	31.64	24.62	1.46
17:45	2.49	298.77	25.61	74.44	32.29	24.46	1.45

Table E-3: Calculation of different components of energy balance from in situ data (27/09/08)

Local Time	Latent heat of vaporatzation	P_atm	Psychometric constant	Bowen-Ratio (β)	sensible heat flux	Latent heat flux	Net Radiation	Water heat flux
[hr]	[Jkg^{-1}]	[mbar]	($mbarK^{-1}$)	[ ]	[Wm^{-2}]	[Wm^{-2}]	[Wm^{-2}]	[Wm^{-2}]
9:05	2441590.76	823.38	0.55	0.18	20.22	115.42	480.01	344.38
9:20	2441373.94	823.35	0.55	0.17	21.27	125.08	525.44	379.08
9:35	2441690.24	823.55	0.55	0.21	12.06	57.68	570.11	500.38
9:44	2440424.63	823.55	0.55	0.23	70.90	302.63	607.62	234.09
10:00	2440526.58	823.42	0.55	0.16	52.26	332.94	642.05	256.85
10:15	2440490.10	823.28	0.55	0.17	21.44	124.36	680.21	534.42
10:30	2439538.11	823.18	0.55	0.15	23.41	152.88	707.32	531.02
10:45	2438958.74	823.12	0.55	0.22	25.39	113.84	739.81	600.58
11:00	2438534.25	823.02	0.55	0.20	33.07	162.13	767.69	572.48
11:15	2440034.64	822.72	0.55	0.14	44.22	315.01	782.15	422.92
11:30	2436532.22	822.45	0.55	0.10	26.85	259.56	785.20	498.79
11:45	2434504.84	822.15	0.55	0.13	30.70	242.34	790.74	517.70
12:00	2433756.92	821.85	0.55	0.15	33.03	214.77	810.17	562.37
12:15	2432926.20	821.65	0.55	0.15	27.65	178.45	812.82	606.71
12:30	2431852.55	821.35	0.55	0.13	79.68	590.47	810.76	140.61
12:45	2429301.35	821.12	0.55	0.14	38.00	268.38	791.65	485.27
13:00	2429801.64	820.98	0.55	0.14	23.97	165.70	782.36	592.69
13:15	2432340.06	820.82	0.55	0.13	47.15	353.17	778.25	377.93
13:30	2431739.54	820.48	0.55	0.14	48.55	352.78	749.92	348.59
15:30	2432420.29	819.18	0.55	0.05	16.17	314.76	445.53	114.60
15:45	2433507.33	819.12	0.55	0.01	56.60	366.65	390.30	-32.95
16:00	2435817.89	819.15	0.55	0.02	34.63	225.66	417.60	157.31
16:15	2437823.41	819.05	0.55	0.04	9.11	61.91	428.94	257.92
16:30	2436231.95	818.95	0.55	0.01	-7.87	-47.11	320.23	275.22
16:45	2438282.15	819.12	0.55	0.03	3.18	32.26	50.22	14.78
17:00	2440480.23	819.12	0.55	-0.06	2.63	-42.61	52.84	92.82
17:15	2441417.78	819.18	0.55	-0.11	4.12	-36.94	49.39	82.20
17:30	2440064.75	819.18	0.55	-0.04	11.62	-71.13	24.45	83.97
17:45	2439242.97	819.18	0.55	-0.02	-3.07	163.83	-26.67	-187.43

Table E-4: Surface and atmospheric variable measured on the lake (29/09/08)

Local Time	Wind speed	T_air	T_water	RH	Saturated vap. pressure	Actual vap. pressure	Slope of sat. vap pressure
[hr]	[m/s]	[K]	[K]	[%]	[mbar]	[mbar]	(mbarK-1)
7:25	1.85	293.66	294.13	89.15	24.84	21.51	1.33
7:40	2.00	293.73	295.72	89.49	27.36	21.68	1.34
7:55	0.64	293.83	295.67	88.50	27.29	21.58	1.33
8:10	0.55	293.57	295.62	88.46	27.19	21.22	1.31
8:25	3.72	293.79	295.80	88.62	27.50	21.55	1.33
8:40	3.11	293.84	296.33	88.48	28.40	21.59	1.33
8:55	1.37	294.92	296.69	86.50	29.02	22.55	1.38
9:10	0.87	294.72	296.47	86.34	28.64	22.23	1.36
9:25	1.94	294.90	296.39	87.05	28.49	22.66	1.38
9:40	2.51	294.51	296.44	87.17	28.58	22.15	1.36
9:55	1.40	295.40	296.84	85.94	29.27	23.06	1.40
10:10	1.91	295.98	296.86	84.58	29.31	23.51	1.42
10:25	3.10	295.66	297.52	85.54	30.51	23.32	1.42
10:40	2.92	295.90	297.91	84.21	31.22	23.30	1.41
10:55	0.86	296.47	298.07	81.51	31.51	23.34	1.41
11:10	0.49	298.62	299.20	79.37	33.70	25.85	1.53
11:25	1.12	297.80	299.32	80.68	33.94	25.03	1.49
12:25	4.08	297.33	302.64	80.43	41.20	24.25	1.45
12:40	3.80	297.21	301.92	79.38	39.53	23.76	1.43
12:55	3.67	297.47	301.66	80.31	38.94	24.43	1.46
13:10	2.83	298.64	300.89	79.47	37.22	25.90	1.54
13:25	1.69	298.64	300.38	80.93	36.12	26.38	1.57
13:40	1.08	299.07	300.32	80.44	36.01	26.90	1.59
13:55	2.52	297.87	301.21	81.77	37.91	25.47	1.52
14:10	2.51	298.48	302.13	76.31	40.01	24.64	1.46
14:25	1.25	299.43	302.57	71.35	41.02	24.38	1.44
14:40	0.76	300.84	302.48	71.13	40.82	26.40	1.54
14:55	2.66	298.89	301.82	74.50	39.29	24.66	1.46
15:10	2.92	298.32	301.22	75.31	37.95	24.09	1.43
15:25	1.89	298.36	300.50	76.37	36.38	24.49	1.46
15:40	1.94	298.64	299.67	74.45	34.65	24.28	1.44
15:55	2.23	298.67	299.84	74.57	35.01	24.36	1.45
16:10	3.96	298.43	299.66	76.41	34.63	24.60	1.46
16:25	3.61	298.34	298.82	78.66	32.96	25.20	1.50
16:40	5.05	296.56	297.36	80.99	30.22	23.32	1.41

Table E-5: Calculation of different components of energy balance from in situ data (29/09/08)

Local Time	Latent heat of vaporatzation	P_atm	Psychometric constant	Bowen-Ratio (β)	sensible heat flux	Latent heat flux	Net Radiation	Water heat flux
[hr]	[Jkg-1]	[mbar]	(mbarK-1)	[ ]	[Wm-2]	[Wm-2]	[Wm-2]	[Wm-2]
7:25	2449666.80	822.65	0.55	0.08	32.75	400.37	-1.11	-434.23
7:40	2445857.66	822.75	0.55	0.19	25.43	130.64	125.69	-30.37
7:55	2445968.80	822.75	0.55	0.18	37.92	211.49	222.10	-27.31
8:10	2446106.45	822.78	0.55	0.19	49.62	260.55	313.85	3.69
8:25	2445664.76	822.78	0.55	0.19	15.28	81.29	275.52	178.95
8:40	2444388.98	822.95	0.55	0.20	18.32	90.38	205.94	97.25
8:55	2443526.05	823.05	0.55	0.15	55.82	366.92	479.97	57.22
9:10	2444046.93	823.08	0.55	0.15	36.31	238.28	242.16	-32.42
9:25	2444254.42	823.22	0.55	0.14	16.42	115.42	268.34	136.50
9:40	2444130.40	823.25	0.55	0.17	13.93	83.26	318.18	220.99
9:55	2443179.12	823.22	0.55	0.13	26.58	205.38	280.07	48.10
10:10	2443123.44	823.25	0.55	0.09	17.59	205.10	392.89	170.20
10:25	2441525.86	823.25	0.55	0.14	17.25	119.41	512.83	376.17
10:40	2440596.12	823.08	0.55	0.14	18.75	132.69	484.03	332.59
10:55	2440220.91	822.95	0.55	0.11	50.93	466.85	595.68	77.90
11:10	2437512.33	822.72	0.55	0.04	7.60	180.04	830.62	642.98
11:25	2437219.67	822.52	0.55	0.10	15.79	165.86	670.36	488.71
12:25	2429239.20	821.48	0.55	0.17	36.00	207.32	796.36	553.05
12:40	2430964.20	821.32	0.55	0.17	24.58	148.38	783.02	610.06
12:55	2431590.88	821.05	0.55	0.16	30.16	188.60	781.24	562.48
13:10	2433445.63	820.75	0.55	0.11	26.00	234.63	778.82	518.19
13:25	2434680.83	820.52	0.55	0.10	20.36	204.48	788.69	563.86
13:40	2434811.10	820.52	0.55	0.08	46.16	596.91	761.09	118.02
13:55	2432691.77	820.48	0.55	0.15	59.26	399.32	711.36	252.78
14:10	2430464.55	820.82	0.55	0.13	40.61	307.96	603.53	254.96
14:25	2429420.20	820.52	0.55	0.10	36.32	347.12	609.02	225.58
14:40	2429624.16	820.52	0.55	0.06	95.20	1497.59	488.06	-1104.73
14:55	2431211.31	820.08	0.55	0.11	41.83	376.71	115.54	-303.00
15:10	2432653.91	819.92	0.55	0.12	22.72	195.55	33.97	-184.30
15:25	2434385.30	819.95	0.55	0.10	31.40	314.01	37.20	-308.20
15:40	2436381.86	820.02	0.55	0.06	17.84	321.29	73.60	-265.52
15:55	2435958.28	819.72	0.55	0.06	14.56	236.10	67.61	-183.05
16:10	2436398.48	819.55	0.55	0.07	11.19	162.62	88.00	-85.81
16:25	2438411.55	819.65	0.55	0.04	3.04	85.15	147.99	59.80
16:40	2441910.94	819.85	0.55	0.07	25.80	391.30	66.48	-350.62

Appendix F: Daily evaporation estimation by different methods

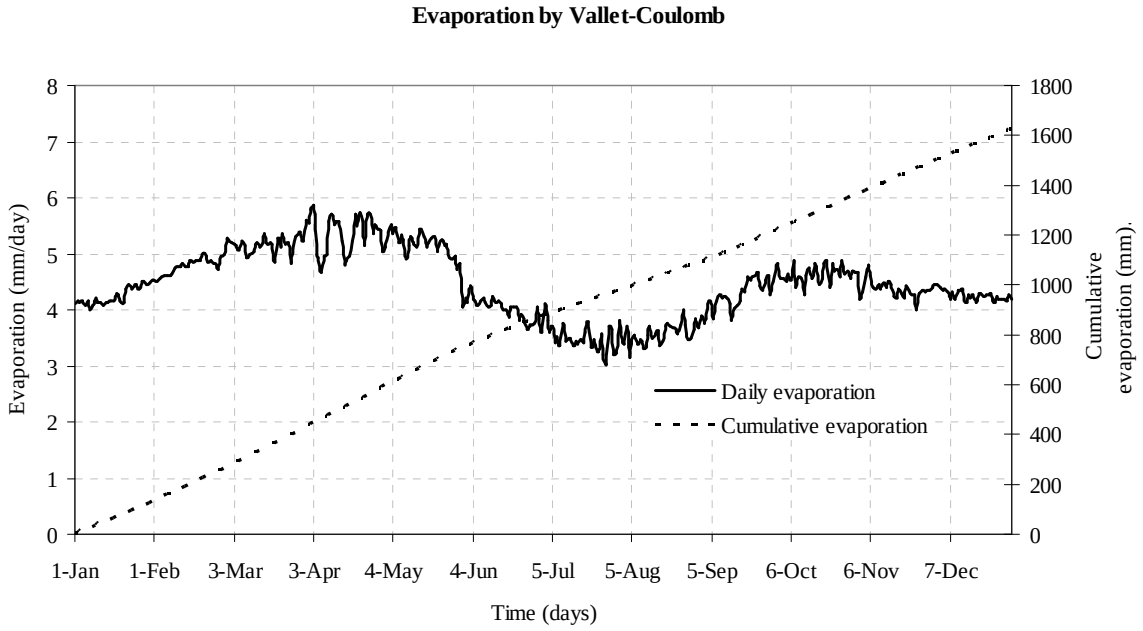

(a)

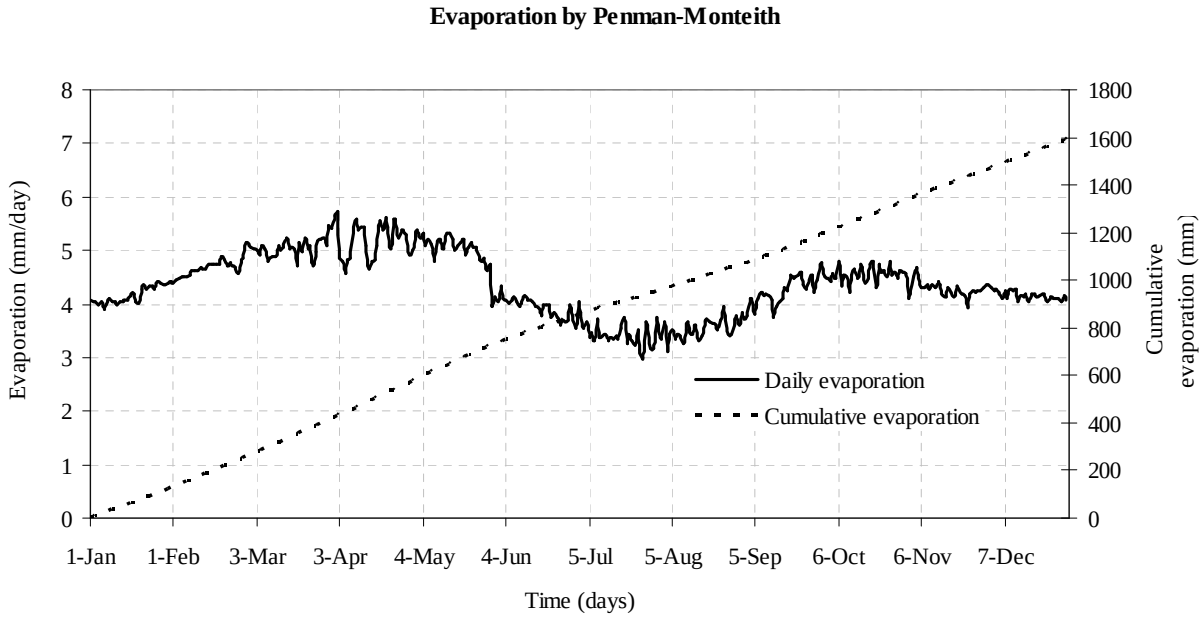

(b)

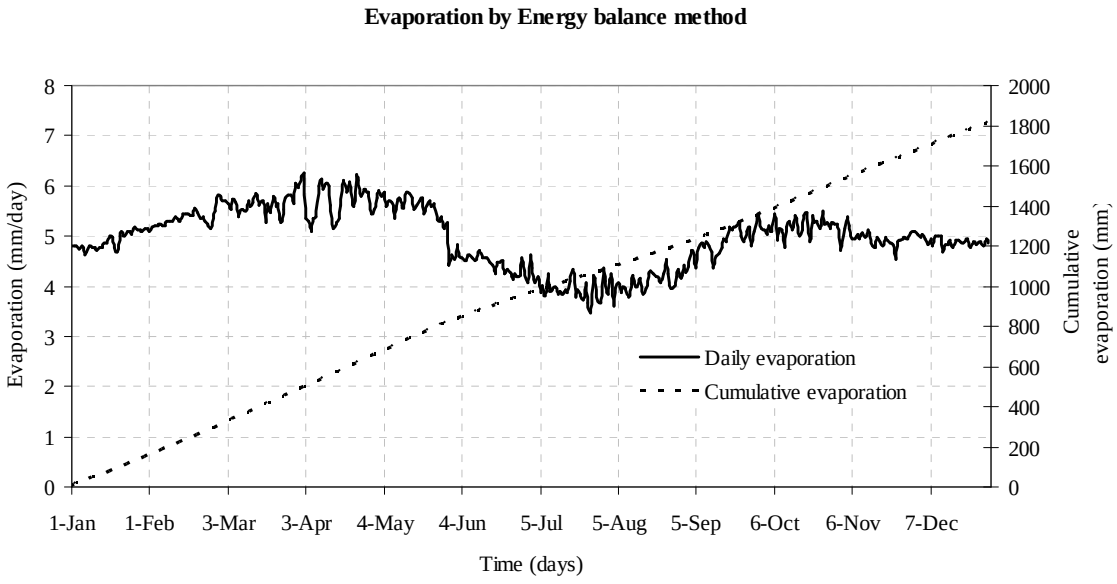

(c)

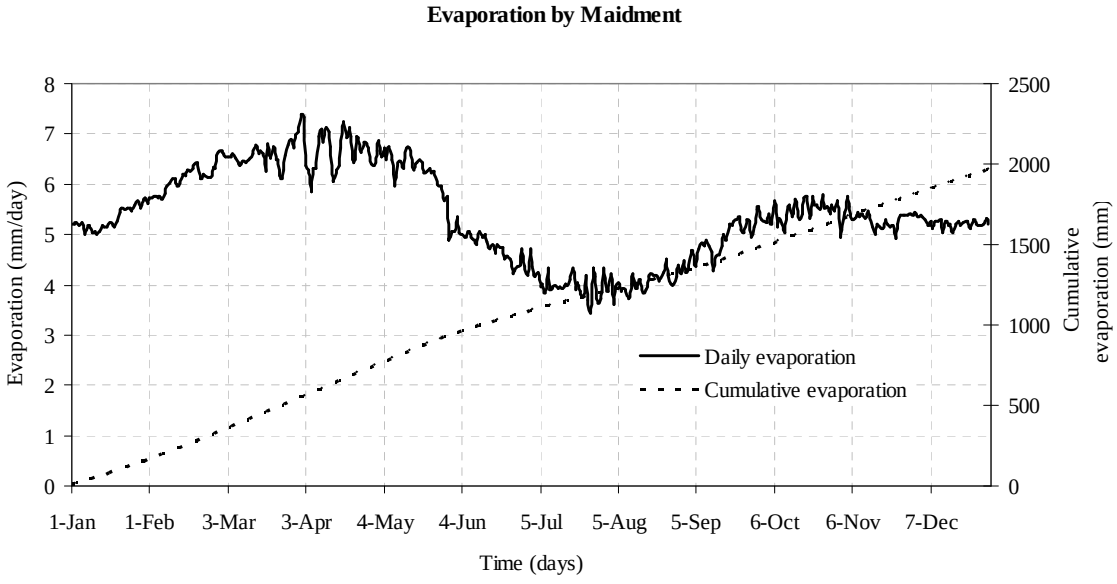

(d)

Figure F-1: Long-term daily average evaporation of Lake Tana by different approach

Appendix G: Eddy flux data analysis

Appendix G_I: Steps to calculate the eddy covariance fluxes

The following steps are used to calculate the eddy covariance fluxes in ECPack software

1. Create the file ‘convert.bat’
2. Run ‘convert’ in the dos prompt
3. Create the file ‘intTana.txt’
4. Run ‘ec_ncdf < confTana.con’
5. Open the flux file and check the data

Step 1.
The data first have to be converted from TOB or TOA format (the format that the datalogger uses) to NetCDF format (the format that the software uses). This is carried out with the program ‘csi2ncdf.exe’. You can write a short file, called ‘convert.bat’, in which you specify the name of the raw data file (from the logger), and the name of the output file (the NetCDF file). There is already an example ‘convert.bat’, all you need to do is to change the names of the input and output file, and save it.

Step 2.
The next step is to run the conversion. You can either to this by double clicking on the file ‘convert.bat’. If this does not work, you do the following:

- In Windows, go to START, Run…, and type in: ‘command’, enter
- Navigate to the directory where the software is, in this case: ‘d:\’ enter, cd Ethiopia\software’
- Type in: ‘convert’, enter

Now the output file should appear in the data.

Step 3
Next the fluxes are calculated with ECPack. This starts with creating an interval file. In the interval file, you specify the time intervals over which you calculate the fluxes. This can be half-hourly or 10 minute intervals, or any other interval you like (half hourly and 10-min are usually ok, shorter or longer time steps are not recommended).

The interval file starts with a blank line, followed by two lines with the following columns:

1. Day of the year of the start of the interval
2. Hour of the day of the start of the interval
3. Minutes of the hour of the start of the interval
4. Day of the year of the end of the interval
5. Hour of the day of the end of the interval
6. Minutes of the hour of the day of the end of the interval
7. water vapour density in kg m-3 from a slow sensor
8. Atmospheric pressure in Pa
9. Name of the NetCDF data file where the data are in

10. Name of a file for intermediate output

The vapour density and atmospheric pressure you get from the meteo data.

Other files that can be changed:

ParamT: here you can specify which corrections you want to apply
ConfTana: here you specify where the data are, and where the parameter files are

Appendix G_II: Interval files used in ECPack software for day1

```
271 07 04 271 07 20  .0151 82285 EC080927a.nc intermed.dat
271 07 20 271 07 35  .0148 82285 EC080927a.nc intermed.dat
271 07 35 271 07 50  .0167 82305 EC080927a.nc intermed.dat
271 07 50 271 08 05  .0170 82322 EC080927a.nc intermed.dat
271 08 05 271 08 20  .0172 82328 EC080927a.nc intermed.dat
271 08 20 271 08 35  .0177 82338 EC080927a.nc intermed.dat
271 08 35 271 08 44  .0170 82335 EC080927a.nc intermed.dat
271 08 44 271 09 00  .0165 82355 EC080927b.nc intermed.dat
271 09 00 271 09 15  .0177 82355 EC080927b.nc intermed.dat
271 09 15 271 09 30  .0175 82342 EC080927b.nc intermed.dat
271 09 30 271 09 45  .0181 82328 EC080927b.nc intermed.dat
271 09 45 271 10 00  .0166 82318 EC080927b.nc intermed.dat
271 10 00 271 10 15  .0168 82312 EC080927b.nc intermed.dat
271 10 15 271 10 30  .0172 82302 EC080927b.nc intermed.dat
271 10 30 271 10 45  .0182 82272 EC080927b.nc intermed.dat
271 10 45 271 11 00  .0192 82245 EC080927b.nc intermed.dat
271 11 00 271 11 15  .0166 82215 EC080927b.nc intermed.dat
271 11 15 271 11 30  .0167 82185 EC080927b.nc intermed.dat
271 11 30 271 11 45  .0177 82165 EC080927b.nc intermed.dat
271 11 45 271 12 00  .0183 82135 EC080927b.nc intermed.dat
271 12 00 271 12 15  .0179 82112 EC080927b.nc intermed.dat
271 12 15 271 12 30  .0173 82098 EC080927b.nc intermed.dat
271 12 30 271 12 45  .0175 82082 EC080927b.nc intermed.dat
271 12 45 271 13 00  .0176 82048 EC080927b.nc intermed.dat
271 13 00 271 13 15  .0174 82018 EC080927b.nc intermed.dat
271 13 15 271 13 30  .0171 82002 EC080927b.nc intermed.dat
271 13 30 271 13 45  .0175 81982 EC080927b.nc intermed.dat
271 13 45 271 14 00  .0178 81968 EC080927b.nc intermed.dat
271 14 00 271 14 15  .0181 81945 EC080927b.nc intermed.dat
271 14 15 271 14 30  .0180 81948 EC080927b.nc intermed.dat
271 14 30 271 14 45  .0189 81932 EC080927b.nc intermed.dat
271 14 45 271 15 00  .0198 81918 EC080927b.nc intermed.dat
271 15 00 271 15 15  .0193 81912 EC080927b.nc intermed.dat
271 15 15 271 15 30  .0188 81915 EC080927b.nc intermed.dat
271 15 30 271 15 45  .0189 81905 EC080927b.nc intermed.dat
271 15 45 271 16 00  .0185 81895 EC080927b.nc intermed.dat
271 16 00 271 16 15  .0187 81912 EC080927b.nc intermed.dat
271 16 15 271 16 30  .0187 81912 EC080927b.nc intermed.dat
271 16 30 271 16 45  .0186 81918 EC080927b.nc intermed.dat
271 16 45 271 17 00  .0184 81918 EC080927b.nc intermed.dat
271 17 00 271 17 20  .0183 81918 EC080927b.nc intermed.dat
```

Appendix G_III: Interval files used in ECPack software for day2

```
274 06 25 274 06 40  .0162 82265 EC080930.nc intermed.dat
274 06 40 274 06 55  .0163 82275 EC080930.nc intermed.dat
274 06 55 274 07 10  .0162 82275 EC080930.nc intermed.dat
274 07 10 274 07 25  .0160 82278 EC080930.nc intermed.dat
274 07 25 274 07 40  .0162 82278 EC080930.nc intermed.dat
274 07 40 274 07 55  .0162 82295 EC080930.nc intermed.dat
274 07 55 274 08 10  .0170 82305 EC080930.nc intermed.dat
274 08 10 274 08 25  .0167 82308 EC080930.nc intermed.dat
274 08 25 274 08 40  .0171 82322 EC080930.nc intermed.dat
274 08 40 274 08 55  .0167 82325 EC080930.nc intermed.dat
274 08 55 274 09 10  .0174 82322 EC080930.nc intermed.dat
274 09 10 274 09 25  .0177 82325 EC080930.nc intermed.dat
274 09 25 274 09 40  .0176 82325 EC080930.nc intermed.dat
274 09 40 274 09 55  .0175 82308 EC080930.nc intermed.dat
274 09 55 274 10 10  .0176 82295 EC080930.nc intermed.dat
274 10 10 274 10 25  .0195 82272 EC080930.nc intermed.dat
274 10 25 274 10 40  .0189 82252 EC080930.nc intermed.dat
274 10 40 274 10 55  .0183 82232 EC080930.nc intermed.dat
274 10 55 274 11 10  .0177 82218 EC080930.nc intermed.dat
274 11 10 274 11 25  .0175 82185 EC080930.nc intermed.dat
274 11 25 274 11 40  .0183 82148 EC080930.nc intermed.dat
274 11 40 274 11 55  .0179 82132 EC080930.nc intermed.dat
274 11 55 274 12 10  .0184 82105 EC080930.nc intermed.dat
274 12 10 274 12 25  .0195 82075 EC080930.nc intermed.dat
274 12 25 274 12 40  .0199 82052 EC080930.nc intermed.dat
274 12 40 274 12 55  .0203 82052 EC080930.nc intermed.dat
274 12 55 274 13 10  .0192 82048 EC080930.nc intermed.dat
274 13 10 274 13 25  .0186 82082 EC080930.nc intermed.dat
274 13 25 274 13 40  .0184 82052 EC080930.nc intermed.dat
274 13 40 274 13 55  .0199 82052 EC080930.nc intermed.dat
274 13 55 274 14 10  .0186 82008 EC080930.nc intermed.dat
274 14 10 274 14 25  .0181 81992 EC080930.nc intermed.dat
274 14 25 274 14 40  .0185 81995 EC080930.nc intermed.dat
274 14 40 274 14 55  .0183 82002 EC080930.nc intermed.dat
274 14 55 274 15 10  .0184 81972 EC080930.nc intermed.dat
274 15 10 274 15 25  .0185 81955 EC080930.nc intermed.dat
274 15 25 274 15 40  .0190 81965 EC080930.nc intermed.dat
274 15 40 274 15 55  .0176 81985 EC080930.nc intermed.dat
```

Table G-1: Output of ECPack for sensible heat flux calculation on 27th of September 2008

Interval	Local Time	Horizontal wind speed		Vertical wind speed	Friction velocity	Aerodynamic resistance	Sonic temperature	Covariance of Tson and w	Sensible heat flux
		Mean(u)	Mean(v)	Mean(w)	Ustar	r_{ah}	Mean(Tson)	Cov(Tson*w)	Hsonic
No.	Hr	[m/s]	[m/s]	[m/s]	[m/s]	(s/m)	[K]	[Kms^{-1}]	[Wm^{-2}]
1	8:05	0.84	-1.79E-17	-3.52E-16	3.86	403.74	294.87	1.86E-02	18.04
2	8:20	1.56	1.69E-15	1.22E-16	2.92	216.95	294.99	2.90E-02	28.07
3	8:35	4.14	-2.03E-16	3.17E-17	1.42	81.92	294.49	2.15E-02	20.80
4	8:50	3.74	1.03E-15	2.69E-17	1.04	90.59	294.66	1.62E-02	15.71
5	9:00	0.33	1.16E-16	5.54E-17	3.01	145.66	295.32	3.13E-02	30.22
6	9:05	1.25	4.48E-16	1.77E-16	2.33	272.21	295.12	2.09E-02	20.22
7	9:20	2.06	-2.17E-16	1.57E-16	8.33	164.46	295.47	2.20E-02	21.27
8	9:35	2.55	1.08E-15	1.74E-17	2.75	132.91	295.42	1.25E-02	12.06
9	9:44	0.51	5.04E-16	2.67E-16	7.65	659.43	295.89	7.35E-02	70.90
10	10:00	0.25	2.36E-16	-2.20E-17	5.98	150.95	296.12	5.42E-02	52.26
11	10:15	2.47	-1.63E-15	-1.59E-16	2.02	137.09	295.57	2.22E-02	21.44
12	10:30	4.17	7.00E-16	-2.28E-18	1.56	81.21	295.71	2.43E-02	23.41
13	10:45	4.13	3.69E-15	4.21E-16	1.50	82.04	295.95	2.63E-02	25.39
14	11:00	2.36	9.80E-15	1.07E-15	2.27	143.88	296.35	3.44E-02	33.07
15	11:15	0.57	5.45E-17	-1.74E-18	5.91	119.55	296.46	4.60E-02	44.22
16	11:30	0.79	1.20E-15	2.43E-17	3.29	121.56	296.69	2.80E-02	26.85
17	11:45	3.17	8.65E-16	1.08E-16	2.17	106.84	297.00	3.20E-02	30.70
18	12:00	3.44	4.22E-15	4.87E-16	2.24	98.40	297.42	3.45E-02	33.03
19	12:15	0.63	2.78E-16	-5.47E-17	5.67	538.57	298.10	2.90E-02	27.65
20	12:30	0.88	-4.16E-16	-8.84E-17	9.32	385.28	298.61	8.36E-02	79.68
21	12:45	1.25	5.04E-17	5.19E-17	8.88	272.17	299.24	1.35E-01	128.14
22	13:00	3.34	4.82E-16	2.88E-16	1.94	101.62	298.54	2.52E-02	23.97
23	13:15	4.55	3.95E-15	3.81E-16	6.40	74.47	298.81	4.95E-02	47.15
24	13:30	0.19	-7.72E-17	-5.53E-17	13.13	1786.35	300.23	5.13E-02	48.55
25	13:45	0.15	2.51E-16	1.24E-16	14.84	2284.41	300.17	7.21E-02	68.29
26	14:00	0.33	1.55E-16	-1.69E-16	9.12	1027.12	300.23	7.00E-02	66.24
27	14:15	0.41	6.78E-16	-1.94E-16	5.33	817.84	300.33	3.37E-02	31.84
28	14:30	0.33	7.12E-17	4.20E-17	8.12	1038.96	300.57	6.01E-02	56.77
29	14:45	0.22	3.98E-17	9.34E-18	12.44	1551.87	301.02	5.21E-02	49.14
30	15:00	0.89	-1.31E-16	4.00E-17	11.37	382.87	301.24	7.45E-02	70.24
31	15:15	1.32	9.73E-16	1.81E-16	1.32	256.46	300.14	9.10E-03	8.60
32	15:30	0.65	1.86E-16	6.54E-17	2.18	518.06	300.30	1.71E-02	16.17
33	15:45	1.47	2.88E-15	-3.97E-17	3.95	230.38	300.45	6.00E-02	56.60
34	16:00	2.86	1.10E-15	2.30E-16	3.84	118.67	300.22	3.67E-02	34.63
35	16:15	0.70	1.29E-15	-3.89E-17	3.58	486.74	301.07	9.68E-03	9.11
36	16:30	0.52	1.05E-16	-5.20E-17	2.00	654.77	300.79	-8.35E-03	-7.87
37	16:45	2.65	-4.70E-16	-8.95E-18	1.85	128.11	300.19	4.43E-03	4.18
38	17:00	2.85	-4.67E-16	-1.83E-16	1.43	118.89	300.17	2.78E-03	2.63
39	17:15	3.62	3.14E-16	-4.93E-17	0.86	93.60	300.42	4.37E-03	4.12
40	17:30	2.25	8.08E-16	5.08E-16	1.20	150.78	300.58	1.23E-02	11.62
41	17:45	2.49	6.20E-15	1.34E-15	0.71	135.91	300.58	-3.26E-03	-3.07

Appendix H: Albedo map from MODIS surface reflectance product

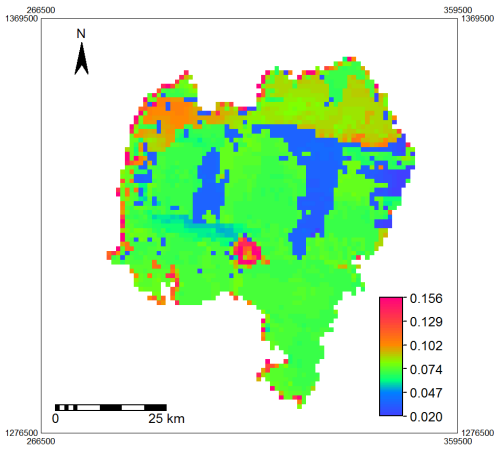

Albedo of March, 2008

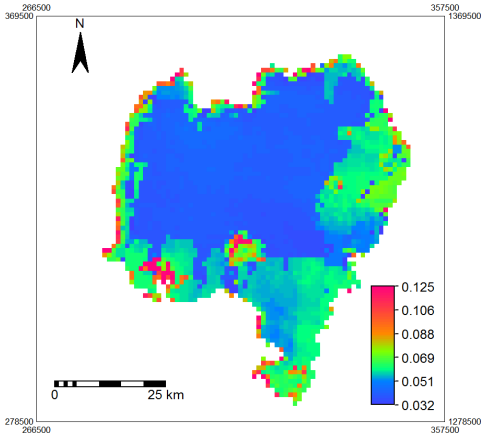

Albedo of April, 2008

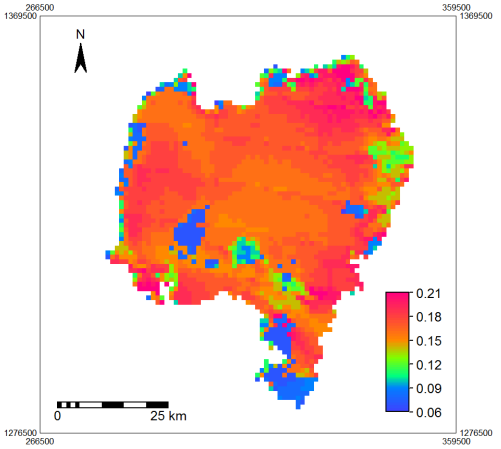

Albedo of July, 2008

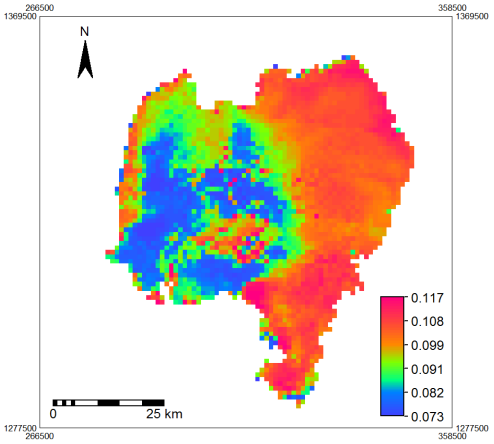

Albedo of September, 2008

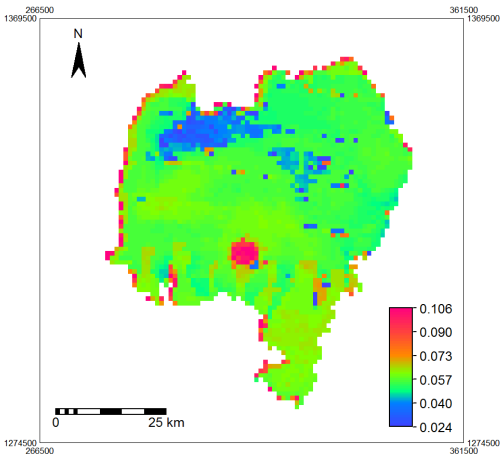

Albedo of November, 2007

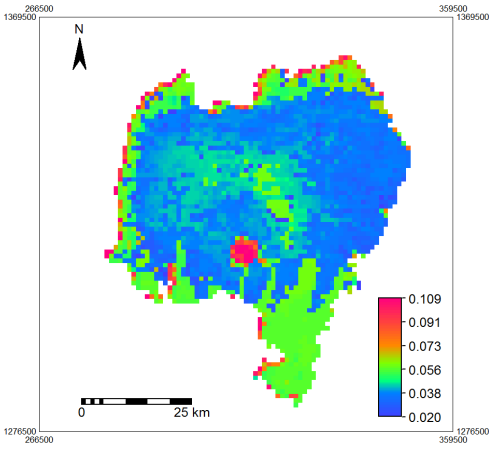

Albedo of December, 2007

Appendix I: ILWIS script for zenith angle calculation from MSG

Rem: Calculate satellite, sun zenith angle and sun elevation / illumination condition, for MSG projection
Rem: The output georeference should be available, first import using the data retriever the required MSG images

Rem: Call external batch file, called generate angles.bat

! generateangles.bat

Copy satzen*.* msgzen
Copy sunzen*.* solzen
msgzen:=map('msgzen',genras,Convert,378,0,Real,4,SwapBytes)
solzen:=map('solzen',genras,Convert,378,0,Real,4,SwapBytes)
setgrf msgzen.mpr angle
setgrf solzen.mpr angle
msg_zenres.mpr{dom=value.dom;vr=-1000:1000:0.001}:= MapResample(msgzen.mpr,%1,bicubic)
calc msg_zenres.mpr
sec_msgzen.mpr{dom=value.dom;vr=0:10:0.001}:=(1/(cos(degrad(msg_zenres))))
calc sec_msgzen.mpr
sol_zenres.mpr{dom=value.dom;vr=-1000:1000:0.001}:= MapResample(solzen.mpr,%1,bicubic)
calc sol_zenres.mpr
sec_solzen.mpr{dom=value.dom;vr=0:10:0.001}:=(1/(cos(degrad(sol_zenres))))
calc cos_solzen.mpr
sun_elev.mpr{dom=value.dom;vr=-1000:1000:0.001}:=90-sol_zenres
calc sun_elev.mpr

Rem: Definition of illumination condition thresholds according to Meteo France
illum_cond%2.mpr{dom=illum_cond} :=iff(sun_elev<-3,"night",iff(sun_elev<10,"twillight","day"))
calc illum_cond%2.mpr

Rem: delete obsolete and temporary maps

rem del msg_zenres.mpr -force
rem del sol_zenres.mpr -force
rem del sec_solzen.mpr -force
rem del sun_elev.mpr -force
rem del msgzen.mpr -force
rem del solzen.mpr -force

closeall

Appendix J: ILWIS script for daily evaporation calculation

albedo_sebs.mpr{dom=value.dom;vr=0:1:0.01}:=MapAlbedo(band1_smac.mpr,band2_smac.mpr,
modis,band3_smac.mpr,band4_smac.mpr,band5_smac.mpr,band7_smac.mpr)

RS_net.mpr{dom=value.dom;vr=0:1200:0.01}:=(1-albedo_sebs)*1367*0.75*cos(sza*3.14/180)

Rem: sza is the solar zenith angle obtained from modis product

Rl_net.mpr{dom=value.dom;vr=0:300:0.01}:=0.98*0.0000000567*295.18^4*(0.39-
0.05*SQRT(2648)/100)+4*0.988*0.0000000567*(295.18^3)*(lst_corr1-295.18)

R_net.mpr{dom=value.dom;vr=0:1000:0.01}:=RS_net2-Rl_net

Rem: RS_net2 is the resampled map of RS_net

H_flux.mpr{dom=value.dom;vr=0:200:0.01}:=1.2*1004*(lst_corr1-295.18)/120

L_flux.mpr{dom=value.dom;vr=0:500:0.01}:=R_net-H_flux-422.92

Rem: L_flux=R_net-H_flux-G, where G is 422.92

Evap_frac.mpr{dom=value.dom;vr=0:1:0.01}:=l_flux/(R_net-422.92)

Rem: evap_fraction= L_flux/(R_net-G)

Rem: Daily evaporation is calcualted from evaporative fraction and daily net radiation

Daily_E.mpr{dom=value.dom;vr=0:7:0.01}:=(8.64*10^7*Evap_frac*150.3424)/(2.45*10^6*1000)

Appendix K: ILWIS script for surface temperature retrieval from MSG data

Four channel algorithm

Rem: Four channel algorithms can be used to calculate surface temperature form MSG thermal bands.
Rem: The formula used to calculate for day time surface temperature is given by: a0+ a1*T_10.8+a2*(T_10.8-T_12) +a3*(T_3.9-T_8.7) +a4*(T_10.8-T_12)^2+a5*(secteta_sat-1) +a6*T_3.9*cos(teta_sol).
Rem: the regression coefficients are depending on the land cover type.

```
T_day_4c_0300:=-29.2629+1.1054*t_200809270300_ir_108+2.2502*(t_200809270300_ir_108-
t_200809270300_ir_120)+0.1322*(t_200809270300_ir_039-
t_200809270300_ir_087)+0.1889*(t_200809270300_ir_108-
t_200809270300_ir_120)^2+464.1204*(sec_Tmsgzen1-1)+5.701*10^-5*(1/sec_solzen1)
T_day_4c_0330:=-29.2629+1.1054*t_200809270330_ir_108+2.2502*(t_200809270330_ir_108-
t_200809270330_ir_120)+0.1322*(t_200809270330_ir_039-
t_200809270330_ir_087)+0.1889*(t_200809270330_ir_108-
t_200809270330_ir_120)^2+464.1204*(sec_Tmsgzen2-1)+5.701*10^-5*(1/sec_solzen2)
T_day_4c_0400:=-29.2629+1.1054*t_200809270400_ir_108+2.2502*(t_200809270400_ir_108-
t_200809270400_ir_120)+0.1322*(t_200809270400_ir_039-
t_200809270400_ir_087)+0.1889*(t_200809270400_ir_108-
t_200809270400_ir_120)^2+464.1204*(sec_Tmsgzen3-1)+5.701*10^-5*(1/sec_solzen3)
T_day_4c_0430:=-29.2629+1.1054*t_200809270430_ir_108+2.2502*(t_200809270430_ir_108-
t_200809270430_ir_120)+0.1322*(t_200809270430_ir_039-
t_200809270430_ir_087)+0.1889*(t_200809270430_ir_108-
t_200809270430_ir_120)^2+464.1204*(sec_Tmsgzen4-1)+5.701*10^-5*(1/sec_solzen4)
T_day_4c_0500:=-29.2629+1.1054*t_200809270500_ir_108+2.2502*(t_200809270500_ir_108-
t_200809270500_ir_120)+0.1322*(t_200809270500_ir_039-
t_200809270500_ir_087)+0.1889*(t_200809270500_ir_108-
t_200809270500_ir_120)^2+464.1204*(sec_Tmsgzen5-1)+5.701*10^-5*(1/sec_solzen5)
T_day_4c_0530:=-29.2629+1.1054*t_200809270530_ir_108+2.2502*(t_200809270530_ir_108-
t_200809270530_ir_120)+0.1322*(t_200809270530_ir_039-
t_200809270530_ir_087)+0.1889*(t_200809270530_ir_108-
t_200809270530_ir_120)^2+464.1204*(sec_Tmsgzen6-1)+5.701*10^-5*(1/sec_solzen6)
T_day_4c_0600:=-29.2629+1.1054*t_200809270600_ir_108+2.2502*(t_200809270600_ir_108-
t_200809270600_ir_120)+0.1322*(t_200809270600_ir_039-
t_200809270600_ir_087)+0.1889*(t_200809270600_ir_108-
t_200809270600_ir_120)^2+464.1204*(sec_Tmsgzen7-1)+5.701*10^-5*(1/sec_solzen7)
T_day_4c_0630:=-29.2629+1.1054*t_200809270630_ir_108+2.2502*(t_200809270630_ir_108-
t_200809270630_ir_120)+0.1322*(t_200809270630_ir_039-
t_200809270630_ir_087)+0.1889*(t_200809270630_ir_108-
t_200809270630_ir_120)^2+464.1204*(sec_Tmsgzen8-1)+5.701*10^-5*(1/sec_solzen8)
T_day_4c_0800:=-29.2629+1.1054*t_200809270800_ir_108+2.2502*(t_200809270800_ir_108-
t_200809270800_ir_120)+0.1322*(t_200809270800_ir_039-
t_200809270800_ir_087)+0.1889*(t_200809270800_ir_108-
t_200809270800_ir_120)^2+464.1204*(sec_Tmsgzen9-1)+5.701*10^-5*(1/sec_solzen9)
T_day_4c_0830:=-29.2629+1.1054*t_200809270830_ir_108+2.2502*(t_200809270830_ir_108-
t_200809270830_ir_120)+0.1322*(t_200809270830_ir_039-
t_200809270830_ir_087)+0.1889*(t_200809270830_ir_108-
t_200809270830_ir_120)^2+464.1204*(sec_Tmsgzen10-1)+5.701*10^-5*(1/sec_solzen10)
```

T_day_4c_1000:=-29.2629+1.1054*t_200809271000_ir_108+2.2502*(t_200809271000_ir_108-t_200809271000_ir_120)+0.1322*(t_200809271000_ir_039-t_200809271000_ir_087)+0.1889*(t_200809271000_ir_108-t_200809271000_ir_120)^2+464.1204*(sec_Tmsgzen11-1)+5.701*10^-5*(1/sec_solzen11)
T_day_4c_1030:=-29.2629+1.1054*t_200809271030_ir_108+2.2502*(t_200809271030_ir_108-t_200809271030_ir_120)+0.1322*(t_200809271030_ir_039-t_200809271030_ir_087)+0.1889*(t_200809271030_ir_108-t_200809271030_ir_120)^2+464.1204*(sec_Tmsgzen12-1)+5.701*10^-5*(1/sec_solzen12)
T_day_4c_1100:=-29.2629+1.1054*t_200809271100_ir_108+2.2502*(t_200809271100_ir_108-t_200809271100_ir_120)+0.1322*(t_200809271100_ir_039-t_200809271100_ir_087)+0.1889*(t_200809271100_ir_108-t_200809271100_ir_120)^2+464.1204*(sec_Tmsgzen13-1)+5.701*10^-5*(1/sec_solzen13)
T_day_4c_1130:=-29.2629+1.1054*t_200809271130_ir_108+2.2502*(t_200809271130_ir_108-t_200809271130_ir_120)+0.1322*(t_200809271130_ir_039-t_200809271130_ir_087)+0.1889*(t_200809271130_ir_108-t_200809271130_ir_120)^2+464.1204*(sec_Tmsgzen14-1)+5.701*10^-5*(1/sec_solzen14)
T_day_4c_1300:=-29.2629+1.1054*t_200809271300_ir_108+2.2502*(t_200809271300_ir_108-t_200809271300_ir_120)+0.1322*(t_200809271300_ir_039-t_200809271300_ir_087)+0.1889*(t_200809271300_ir_108-t_200809271300_ir_120)^2+464.1204*(sec_Tmsgzen15-1)+5.701*10^-5*(1/sec_solzen15)
T_day_4c_1330:=-29.2629+1.1054*t_200809271330_ir_108+2.2502*(t_200809271330_ir_108-t_200809271330_ir_120)+0.1322*(t_200809271330_ir_039-t_200809271330_ir_087)+0.1889*(t_200809271330_ir_108-t_200809271330_ir_120)^2+464.1204*(sec_Tmsgzen16-1)+5.701*10^-5*(1/sec_solzen16)
T_day_4c_1400:=-29.2629+1.1054*t_200809271400_ir_108+2.2502*(t_200809271400_ir_108-t_200809271400_ir_120)+0.1322*(t_200809271400_ir_039-t_200809271400_ir_087)+0.1889*(t_200809271400_ir_108-t_200809271400_ir_120)^2+464.1204*(sec_Tmsgzen17-1)+5.701*10^-5*(1/sec_solzen17)

Split-window techniques algorithm (Becker and Li)

Rem: split window algorithm can be used to calculate surface temperature form MSG thermal bands of 9 and 10
Rem: Tday_1300:=3.672206*T0004_band_15+-2.66902*T0005_band_15+1.274

Tday_B_0300.mpr{dom=VALUE.dom;vr=273.0:350.0:0.1} = 3.672206*t_200809270300_ir_108+-2.66902*t_200809270300_ir_120+1.274
Tday_B_0330.mpr{dom=VALUE.dom;vr=273.0:350.0:0.1} = 3.672206*t_200809270330_ir_108+-2.66902*t_200809270330_ir_120+1.274
Tday_B_0400.mpr{dom=VALUE.dom;vr=273.0:350.0:0.1} = 3.672206*t_200809270400_ir_108+-2.66902*t_200809270400_ir_120+1.274
Tday_B_0430.mpr{dom=VALUE.dom;vr=273.0:350.0:0.1} = 3.672206*t_200809270430_ir_108+-2.66902*t_200809270430_ir_120+1.274
Tday_B_0500.mpr{dom=VALUE.dom;vr=273.0:350.0:0.1} = 3.672206*t_200809270500_ir_108+-2.66902*t_200809270500_ir_120+1.274

Tday_B_0530.mpr{dom=VALUE.dom;vr=273.0:350.0:0.1} = 3.672206*t_200809270530_ir_108+-2.66902*t_200809270530_ir_120+1.274

Tday_B_0600.mpr{dom=VALUE.dom;vr=273.0:350.0:0.1} = 3.672206*t_200809270600_ir_108+-2.66902*t_200809270600_ir_120+1.274
Tday_B_0630.mpr{dom=VALUE.dom;vr=273.0:350.0:0.1} = 3.672206*t_200809270500_ir_108+-2.66902*t_200809270630_ir_120+1.274

Rem:Tday_B_0700.mpr{dom=VALUE.dom;vr=273.0:350.0:0.1} = 3.672206*t_200809270700_ir_108+-2.66902*t_200809270700_ir_120+1.274
Rem: Tday_B_0730.mpr{dom=VALUE.dom;vr=273.0:350.0:0.1} = 3.672206*t_200809270730_ir_108+-2.66902*t_200809270730_ir_120+1.274

Tday_B_0800.mpr{dom=VALUE.dom;vr=273.0:350.0:0.1} = 3.672206*t_200809270800_ir_108+-2.66902*t_200809270800_ir_120+1.274
Tday_B_0830.mpr{dom=VALUE.dom;vr=273.0:350.0:0.1} = 3.672206*t_200809270830_ir_108+-2.66902*t_200809270830_ir_120+1.274

Rem:Tday_B_0900.mpr{dom=VALUE.dom;vr=273.0:350.0:0.1} = 3.672206*t_200809270900_ir_108+-2.66902*t_200809270900_ir_120+1.274
Rem: Tday_B_0930.mpr{dom=VALUE.dom;vr=273.0:350.0:0.1} = 3.672206*t_200809270930_ir_108+-2.66902*t_200809270930_ir_120+1.274

Tday_B_1000.mpr{dom=VALUE.dom;vr=273.0:350.0:0.1} = 3.672206*t_200809271000_ir_108+-2.66902*t_200809271000_ir_120+1.274
Tday_B_1030.mpr{dom=VALUE.dom;vr=273.0:350.0:0.1} = 3.672206*t_200809271030_ir_108+-2.66902*t_200809271030_ir_120+1.274
Tday_B_1100.mpr{dom=VALUE.dom;vr=273.0:350.0:0.1} = 3.672206*t_200809271100_ir_108+-2.66902*t_200809271100_ir_120+1.274
Tday_B_1130.mpr{dom=VALUE.dom;vr=273.0:350.0:0.1} = 3.672206*t_200809271130_ir_108+-2.66902*t_200809271130_ir_120+1.274

Rem: Tday_B_1200.mpr{dom=VALUE.dom;vr=273.0:350.0:0.1} = 3.672206*t_200809271200_ir_108+ -2.66902*t_200809271200_ir_120+1.274
Rem: Tday_B_1230.mpr{dom=VALUE.dom;vr=273.0:350.0:0.1} = 3.672206*t_200809271230_ir_108+-2.66902*t_200809271230_ir_120+1.274

Tday_B_1300.mpr{dom=VALUE.dom;vr=273.0:350.0:0.1} = 3.672206*t_200809271300_ir_108+-2.66902*t_200809271300_ir_120+1.274
Tday_B_1330.mpr{dom=VALUE.dom;vr=273.0:350.0:0.1} = 3.672206*t_200809271330_ir_108+-2.66902*t_200809271330_ir_120+1.274
Tday_B_1400.mpr{dom=VALUE.dom;vr=273.0:350.0:0.1} = 3.672206*t_200809271400_ir_108+-2.66902*t_200809271400_ir_120+1.274

Rem:Tday_B_1430.mpr{dom=VALUE.dom;vr=273.0:350.0:0.1} = 3.672206*t_200809271430_ir_108+-2.66902*t_200809271430_ir_120+1.274